Aus dem Adolf-Butenandt-Institut
Lehrstuhl Molekularbiologie im Biomedizinischen Centrum
Institut der Ludwig-Maximilians-Universität München
Vorstand: Prof. Dr. rer. nat. Peter B. Becker

In vivo functional dissection of CHRAC/ACF and DOMINO chromatin regulators

Dissertation
Zum Erwerb des Doktorgrades der Naturwissenschaften
an der Medizinischen Fakultät der
Ludwig-Maximilians-Universität zu München

vorgelegt von
Alessandro Scacchetti
aus Mirandola (Italien)
2020

Betreuer: Prof. Dr. rer. nat. Peter B. Becker

Zweitgutachter: Prof. Dr. rer. nat. Klaus Förstemann

Dekan: Prof. Dr. med. dent. Reinhard Hickel

Tag der mündlichen Prüfung: 11.11.2020

Eidesstattliche Versicherung

Scacchetti, Alessandro

Ich erkläre hiermit an Eides statt, dass ich die vorliegende Dissertation mit dem Thema

„in vivo functional dissection of CHRAC/ACF and DOMINO chromatin regulators"

selbständig verfasst, mich außer der angegebenen keiner weiteren Hilfsmittel bedient und alle Erkenntnisse, die aus dem Schrifttum ganz oder annähernd übernommen sind, als solche kenntlich gemacht und nach ihrer Herkunft unter Bezeichnung der Fundstelle einzeln nachgewiesen habe.

Ich erkläre des Weitern, dass die hier vorliegende Dissertation nicht in der gleichen oder in ähnlicher Form bei einer anderen Stelle zur Erlangung eines akademischen Grades eingereicht wurde.

München, 11.05.2020

_____

Ort, Datum

Alessandro Scacchetti

_____

Unterschrift Doktorandin/Doktorand

a Laura,
musa e amore della mia vita.

Table of Contents

Preface

In this thesis, I will present and discuss my work on the two nucleosome remodeling complexes CHRAC/ACF and DOMINO. My personal interest in transcription and its regulation defined the common ground between them. As entirely different projects developed chronologically for the two remodelers, I decided to follow their history and present them separately and sequentially. For convenience, I will share their introduction as many features are shared between these remodeling complexes.

List of publications

Scacchetti, A., Schauer, T., Reim, A., Apostolou, Z., Sparr, AC, Krause, S., Heun, P., Wierer, M., and Becker, PB (2020). Drosophila SWR1 and NuA4 complexes are defined by DOMINO isoforms. *biorXiv*. (accepted for publication at *eLife*)

Scacchetti, A., Brueckner, L., Jain, D., Schauer, T., Zhang, X., Schnorrer, F., van Steensel, B., Straub, T., and Becker, PB (2018). CHRAC / ACF contribute to the repressive ground state of chromatin. *Life Science Alliance*.

Summary

The chromatin accessibility complex (CHRAC) and the ATP-utilizing chromatin assembly and remodeling factor (ACF) are chromatin remodeling complexes that slide nucleosomes to generate regularity along the chromatin fiber. Both complexes contain, beside the catalytic subunit ISWI, the regulatory subunit ACF1. Their molecular mechanisms of nucleosome remodeling have been extensively studied *in vitro*, but the relevance of ACF1-induced nucleosome regularity for genome integrity and gene expression in *a* physiological context are still unclear. We first investigated the role of *Drosophila melanogaster* CHRAC/ACF on transcription by two orthogonal strategies. By targeting ACF1 to thousands of reporter genes integrated in several unique locations in the genome, we scored a context-dependent repressive effect, particularly on lowly transcribed reporters in repressive chromatin environment. Our complementary analysis of single-embryo transcriptomes in a new *Acf* knock-out strain revealed that only lowly transcribed genes are activated by the loss of ACF1, mirroring our results obtained with the targeting system. Interestingly, *Acf*-deficient embryos appear to lose physiological nucleosome regularity, especially in domains that are transcriptionally silent. We concluded that CHRAC/ACF participate in the establishment of an inactive ground state of the genome via chromatin organization. Additionally, we tried to assess whether ACF-containing remodeling complexes participate in DNA damage response. We didn't score any major difference in sensitivity to DNA damaging agents in *Acf* knock-out embryos, nor any change in phosphorylated histone H2A.V variant dynamics. This suggests a minor involvement of CHRAC/ACF in embryonic response to DNA damage.

Deposition of histone H2A.Z variant and histone acetylation are key features of active transcription. The DOMINO (DOM) chromatin regulator of *D. melanogaster* is thought to combine both activities in a single, multi-subunit complex. Here we show that two splice variants of the central ATPase subunit, DOM-A and DOM-B, define two physically distinct protein complexes. Both are necessary for maintaining physiological gene expression, but their contribution to transcriptional regulation is different. The DOM-B complex acts as a "bona-fide" nucleosome remodeler and, similarly to the yeast SWR1 complex, incorporates H2A.V (the fly ortholog of H2A.Z) in an ATP-dependent manner along the whole genome. The DOM-A complex, instead, doesn't use its ATPase activity to remodel nucleosomes, but rather exploits the histone acetyltransferase activity of its partner TIP60 to primarily target lysine 12 of histone H4 in an ATP-independent manner - similar to the yeast NuA4 complex. Our work highlights an interesting example of how two evolutionary strategies lead to similar functional separation. In humans and yeast, the distinction between histone acetyltransferase complexes and H2A.Z remodelers arise from gene duplication and paralog specification. The

same diversity, in *Drosophila* and possibly other insects, is achieved by alternative splicing of a single gene.

Zusammenfassung

Der Chromatin Accessibility Complex (CHRAC) und der ATP-abhängige Chromatin Assembly and Remodeling Factor (ACF) haben die ATPase ISWI sowie die charakteristische Untereinheit ACF1 gemeinsam. Diese Enzyme katalysieren die gut untersuchte „nucleosome sliding" Reaktion *in vitro*, aber deren Einfluss auf die Genexpression oder die Mechanismen der DNA-Schadensantwort ist unklar. Zuerst untersuchten wir den Einfluss von *Drosophila melanogaster* CHRAC / ACF auf die Transkription mithilfe komplementärer „gain- and loss-of-function" Ansätze. Das „Targeting" von ACF1 an mehrere Reportergene, die an verschiedenen genomischen Loci inseriert wurden, führte zur kontextabhängigen Inaktivierung schwach transkribierter Reportergene in repressivem Chromatin. Dementsprechend zeigte die Transkriptomanalyse von einzelnen Embryos eines Acf-Knockout-Allels, dass nur schwach exprimierte Gene in Abwesenheit von ACF1 dereprimiert werden. Weiterhin weisen die Nukleosomenarrays von Acf-defizientem Chromatin einen Verlust der physiologischen Regularität auf, insbesondere in transkriptionell inaktiven Domänen. Unsere Ergebnisse zeigen, dass Remodellingfaktoren, welche ACF1 beinhalten, Chromatinstruktur organisieren können und hierbei zu einem inaktivem Grundzustand des Genoms beitragen. Anschließend haben wir versucht, die Funktion von CHRAC / ACF in der DNA-Schadensantwort zu definieren. Wir haben weder einen wesentlichen Unterschied in der Sensitivität gegenüber DNA-schädigenden Substanzen in Acf-Knock-out-Embryonen noch eine Änderung der Dynamik der phosphorylierten Histonvariante H2A.V festgestellt. Dies deutet auf eine geringfügige Beteiligung von CHRAC / ACF an den Mechanismen der DNA-Schadensantwort in Embryonen hin.

Die Acetylierung von Histonen sowie der Einbau der Histonvariante H2A.Z sind Kennzeichen aktiver Transkription. In *Drosophila* wird vermutet, dass der Chromatin-Remodeling-Komplex DOMINO beide Aktivitäten mittels eines unbekannten Mechanismus vereint. Wir zeigen, dass zwei Isoformen von DOMINO, DOM-A und DOM-B, zwei unterschiedliche Komplexe mit mehreren Untereinheiten spezifizieren. Beide Komplexe sind für die Transkriptionsregulation notwendig, jedoch über unterschiedliche Mechanismen. Der DOM-B-Komplex inkorporiert in Abhängigkeit von ATP genomweit die Variante H2A.V (das Fliegen-Ortholog von H2A.Z), wie es für den SWR1-Komplex aus Hefe bekannt ist. Der DOM-A-Komplex fungiert stattdessen als ATP-unabhängiger Histon-Acetyltransferase-

Komplex ähnlich dem NuA4-Komplex in Hefe, der Lysin 12 von Histon H4 acetyliert. Unsere Arbeit zeigt, wie unterschiedliche evolutionäre Strategien zu einer ähnlichen Trennung funktionaler Prozesse führen. In Hefe sowie im Menschen entstanden Nukleosomen-Remodelling- und Histon-Acetyltransferase-Komplexe aus Genduplikation und Spezifikation von Paralogen. In *Drosophila* entsteht dieselbe Diversität durch alternatives Spleißen eines einzelnen Gens.

1. INTRODUCTION

1.1 Hello compaction!

It is well established, nowadays, that genetic information is the code of life. Not all organisms are complex in the same way, some are more and some are less, and the complexity of genetic information follows accordingly. Inside cells, information is stored in a 4-letter code format in long polymers of DNA. Perhaps not surprising, the more information stored, the longer the polymers become. At a certain point during evolution, the need for more and more "storage" clashed with the size of cells and organisms had to develop efficient ways to compact these long DNA molecules in the small space of a nucleus. It is not surprising that most of living organisms employ a certain level of DNA compaction.

1.2 Modes of compaction across living domains

If we consider the linear size of human DNA and the average nucleus diameter, the long DNA molecules have to be compacted around 10 thousand-fold to fit in. How is this compaction achieved in living domains?

In prokaryotes, such as bacteria, DNA is not confined in the nucleus but still retains some degree of compaction. While still not completely clear, it has been proposed that DNA condensation might be mediated by supercoiling, binding to architectural proteins, segregative phase separation or, likely, a combination thereof (1-3).

A nuclear structure is also absent in archaea. Contrary to prokaryotes, however, DNA compaction seems to be mediated mostly by electrostatic protein-DNA interactions. In archaea, DNA is wrapped around homo- or hetero-dimers of histone-fold (HF)-containing proteins (see below) in units of around 70-90 base pairs (bp) (4). Curiously, archaeal HF-containing proteins can associate, when exogenously expressed, with prokaryotic genomes *in vivo* to form archaeal-like compacted DNA structures, with only very mild phenotypic effects (5). This suggest an advantageous switch to protein-based DNA compaction strategy during evolution. In fact, eukaryotes rely on DNA-protein interactions for compaction too. In the eukaryotic nucleus, stretches of 147 base-pairs (bp) of DNA are wrapped in 1.65 turns of left-handed superhelix around an octameric protein core to form structures called nucleosome core particles. DNA connecting adjacent nucleosomes is called linker, which together with the nucleosome core particle define a fundamental unit: the nucleosome. The repetition of such units along the genome originates a "beads-on-a-string" like structure known as chromatin (6). The octamer at the core of nucleosome core particles is formed by two copies of four types of histones: H2A, H2B, H3 and H4. Histones are small proteins (11-

17 kDa), with a stereotypical structure named "histone fold" consisting of 3 α-helices (important for dimerization and non-specific DNA interactions) separated by flexible loops (7) (**Figure 1.1**). Histones make extensive hydrophilic contacts with DNA, rendering the nucleosome a rather stable structure (8-10).

Figure 1.1 Crystal structure of the nucleosome core particle. View from down (left) or perpendicular to (right) the superhelical axis. Histone proteins are labeled with different colors. Figure adapted from (7). Reprinted with permission from Springer Nature.

In addition, each histone possesses an N-terminal tail not necessarily engaged with DNA interaction but rather utilized as a regulatory surface (discussed below). It has been estimated that around 80% of the eukaryotic genome is covered by nucleosomes (11). Another histone protein is very important for chromatin organization: the linker histone H1 (12). Compared to the other core histone proteins, H1 has a different structure composed of N- and C-terminal flexible domains separated by a central winged helix fold domain (13). The linker histone binds the DNA, both on and between nucleosomes, through electrostatic interactions (14). Compared to the core histones, the physiological functions of H1 are still largely unclear. The linker histone has been historically connected to transcriptional repression (15, 16), although it may also participate in gene activation (17). These opposite findings may be explained by the fact that histone H1 is post-transcriptionally modified *in vivo*, so its effects on gene regulation may be dependent on the combination of modifications (18). H1 has also been implicated in cell cycle regulation (19-21).

### 1.3 Chromatin organization beyond the nucleosome

Wrapping DNA around nucleosomes compacts the genome around 2-fold, which is a much lower degree of compaction compared to what observed in living cells. There must be, therefore, additional layers of genome condensation. Based on initial observations *in vitro*, it

was proposed that linear chromatin folds into 30 nm fibers (22, 23). To date, however, no evidence of a 30 nm-like chromatin structure has been found in eukaryotic nuclei (6, 24). A recent study showed, instead, that yeast nucleosomes tend to fold in α-tetrahedron and β-rhombus structures along the fiber (25). In human cells, nucleosomes appear to organize in trimeric structures (26). This may suggest a conserved tendency of chromatin fiber to organize in secondary structures, different than the theorized 30 nm fiber. At a higher level, a novel, electron microscopy-based method revealed that mammalian chromatin is organized in 5- to 24- nanometer domains without a defined geometry *in vivo* (27). High order organization of the nucleosome fiber, regardless of its modes, not only provides the necessary compaction for DNA to fit in the nucleus but also creates an additional layer of regulation of chromatin.

1.4 The classical types of chromatin

In the 1920's, pioneering work from Emil Heitz [reviewed in (28)] defined two types of chromatin based on differential staining of chromosomal territories and post-mitotic behavior: euchromatin (post-mitotic de-condensation) and heterochromatin (no post-mitotic de-condensation). Later on, with the advancements of electron microscopy techniques in the 1960's and 1970's, these alternative structures could be observed in nuclei from various cell types (29, 30) and even as a "band-like" pattern along the giant *D. melanogaster* polytene chromosomes (31). The intense staining of heterochromatin indicated a densely compacted structure, in which genes are probably absent or inactive as proposed by Heitz himself. In fact, early characterization of satellite DNA showed that repetitive elements are generally silent and tend to localize in heterochromatin (32, 33). The lighter staining of euchromatin, on the other hand, suggested a higher gene activity due to a more relaxed organization. Heterochromatin could be classically distinguished into two different types (**Figure 1.2**). Constitutive heterochromatin is generally present at centromere and telomeres, mostly covering repetitive sequences, and it is characterized by specific epigenetic marks such as DNA methylation and H3K9 di- and tri-methylation (histone modifications will be discussed in more detailed in the paragraph 1.9), and by the presence of the HP1 protein [reviewed in (34, 35)]. This type of heterochromatin is not only is characterized by low transcriptional activity, but actively represses transcription – with notable exceptions such as in fission yeast, where transcription is required for establishment and maintenance of heterochromatic domains (36). The position-effect variegation (PEV) of *D. melanogaster* beautifully illustrate the repressive potential of constitutive heterochromatin: a chromosomal inversion places the gene encoding for the red eye color next to the pericentric domain of the X-chromosome resulting in a red/white variegated phenotype due to the random inactivation of such gene (37). Facultative heterochromatin, instead, is more dynamic and could transition into an

euchromatin-like state under specific circumstances, such as stress or cell differentiation [reviewed in (38)]. This latter type of heterochromatin is generally marked by H3K27 tri-methylation and it is controlled by the Polycomb/Trithorax system in most animals (39).
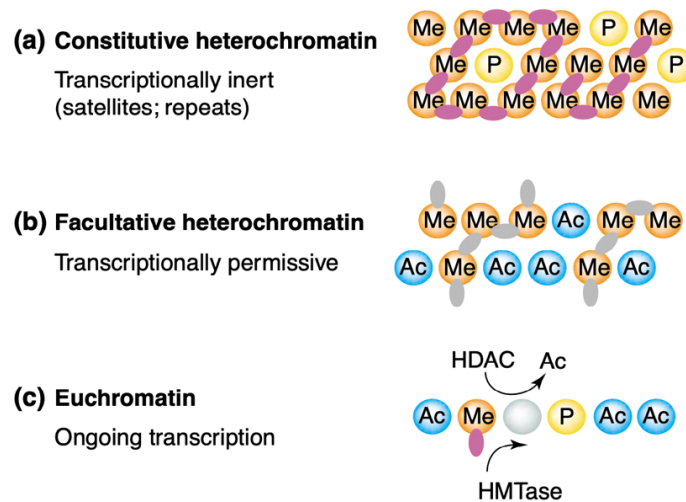
Figure 2.2 Schematic illustration of the classical types of chromatin. Constitutive and facultative heterochromatic regions are both generally compact and transcriptionally silent, but facultative heterochromatin can be permissive to transcription under certain circumstances (see main text). Euchromatin is, instead, loose and transcriptionally active. Me, Ac and P indicate histone methylation, acetylation and phosphorylation respectively. HDAC: histone de-acetylases. HMT: histone methyltransferases. Purple and grey ellipses indicate chromatin proteins. Figure adapted from (35) and reprinted with permission from Elsevier.

The definition of euchromatin is looser but it generally comprises transcriptionally active regions of the genome. The presence of specific histone marks, such as H3K4 and H3K36 methylation, H3S10 phosphorylation, and more importantly histone acetylation, make heterochromatic regions an "easy-access" substrate to many proteins that facilitate transcription (35) (**Figure 1.2**).

1.5 Accessing information in a packed genome
Information contained in the genome is usually read by molecular machineries that need direct access to free DNA, hence the wrapping around nucleosomes and possibly further compaction is rather a big informational barrier. Indeed, It has been estimated that only 2-3% of the eukaryotic genome is accessible at any given time (40). It is important to keep in mind, however, that chromatin accessibility is not always correlated with accessibility of information. For example, it appears that some factors (e.g.: pioneering transcription factors, discussed below) are able to read DNA sequences directly on the surface of nucleosomes (41-43). Therefore, the fraction of "readable" genome might indeed be higher than the 2-3% aforementioned. Regardless of the actual proportion of accessible/readable DNA, information stored in DNA sequences has to be available when needed in order to ensure proper

execution of biological processes, from transcription and replication to complex phenomena like development and differentiation. Furthermore, occluding inappropriate information usage through inaccessibility is also very important to avoid aberrant developmental programs. How are these genomic stretches rendered accessible/inaccessible? It is conceivable to think that different mechanisms and molecular machines operate for a common goal: altering the proprieties of nucleosomes and, ultimately, chromatin.

1.6 Regulation of gene expression by transcription factors

Transcription factors are proteins which function is to read the information contained in the DNA sequence and transmit it to the cell via the form of gene expression programs. Through the establishment of complex networks, transcription factors play a pivotal role in cell cycle (44), cell differentiation (45), stress response (46) and, ultimately, development (47). Following the discovery of the first eukaryotic transcription factors (48-50), these proteins were defined as DNA binders which regulate transcription, either positively or negatively, via direct or indirect modulation of RNA polymerases activity (51). There are several families of transcription factors, classified based on the structure of their DNA binding domain, as well as their mode of recognition of the DNA substrate [reviewed in (52)]. In order to recognize specific DNA sequences, transcription factors need to access "free" DNA. As most of the eukaryotic genome is in the form of chromatin, transcription factors are often in direct competition with nucleosomes for DNA binding. Therefore, accessory proteins (further described in the next paragraphs) are required to "remodel" or "modify" the chromatin in order to expose, or occlude, transcription factor binding sites (53, 54). This cooperation goes also in a different direction: transcription factors can recruit chromatin remodelers/modifiers to alter the chromatin structure, facilitating or impeding transcription of chromatinized DNA by RNA polymerases (55, 56). A notable exception is represented by a specific class of transcription factors, the pioneering transcription factors, that possess the ability to bind nucleosomal DNA (41, 42, 57-59). As recently shown for SOX2, SOX11 and OCT4, pioneering factors have to ability to weaken DNA – octamer core interactions (60, 61), exposing stretches of free DNA and potentially allowing other non-pioneering transcription factors to bind.

1.7 ATP-dependent nucleosome remodelers

Nucleosome remodelers (henceforth referred interchangeably also as chromatin remodelers or remodelers) are ATP-dependent enzymes that operate on chromatin by changing the contacts between histones and DNA. All part of the Snf2 helicase family (superfamily S2), nucleosome remodelers are usually multi-subunit enzymes divided in 4 main subfamilies,

depending on the presence and arrangement of domains in the core ATPase subunit: SWI/SNF, ISWI, INO80/SWR1 and NuRD/Mi-2/CHD (62, 63) (**Figure 1.3**).
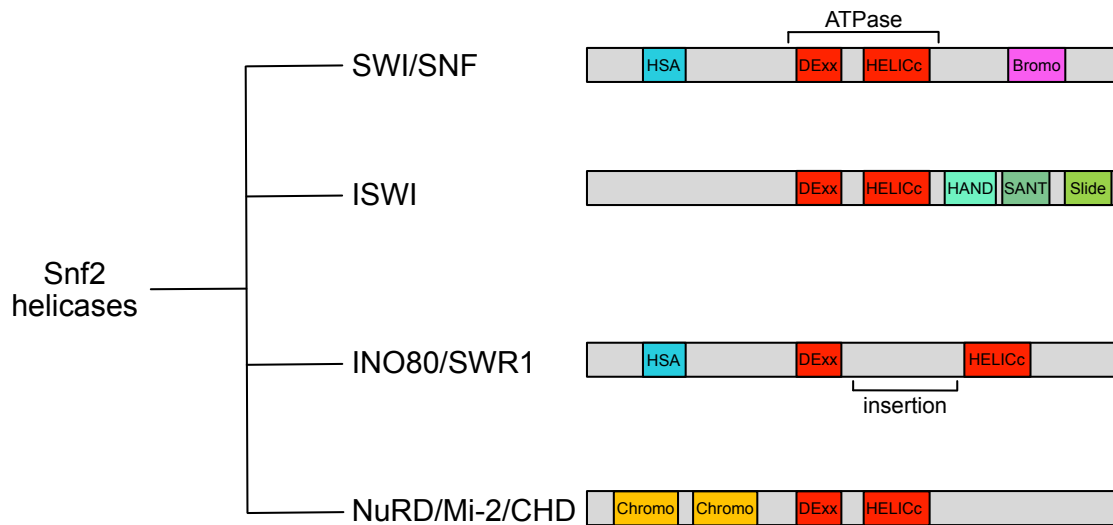
Figure 1.3 Schematic representation of the different families of nucleosome remodelers. The ATPase domain is fromed by DExx and HELICc separated by a short (SWI/SNF, ISWI, NuRD/Mi-2/CHD) or a long (INO80/SWR1) insertion. Additional domains characterize the different families. The SWI/SNF family contains an HAS and a Bromodomain. The ISWI family has a C-terminal HAND-SANT-Slide domain. The INO80/SWR1 also contains an HAS domain. The NuRD/Mi-2/CHD family has an N-terminal tandem Chromodomain.

Nucleosome remodelers can contact nucleosomes in several ways, for example through domains that interact with DNA (e.g. HSA, HAND-SANT-Slide domains) or domains that can bind histones (Bromo- and Chromo-domain). As a general principle, the engagement of the nucleosome core particle by their ATPase domain, and subsequent ATP hydrolysis, causes nucleosome destabilization. These events lead to various consequences that differ between the family of remodelers [reviewed in (62)] (**Figure 1.4**). In the case of the SWI/SNF family, remodeling causes eviction of the histone octamer, freeing the DNA previously wrapped around it (64). ISWI, CHD1 and INO80 remodelers, instead, slide the DNA along the histone octamer altering the relative position of a given sequence relative to the nucleosome (65-69). The INO80/SWR1 family destabilizes nucleosome to incorporate/exchange or evict variants of histone proteins(70, 71). Finally, the ISWI family has also been implicated in nucleosome assembly, a process which requires the cooperation between remodelers and histone chaperones (72, 73).
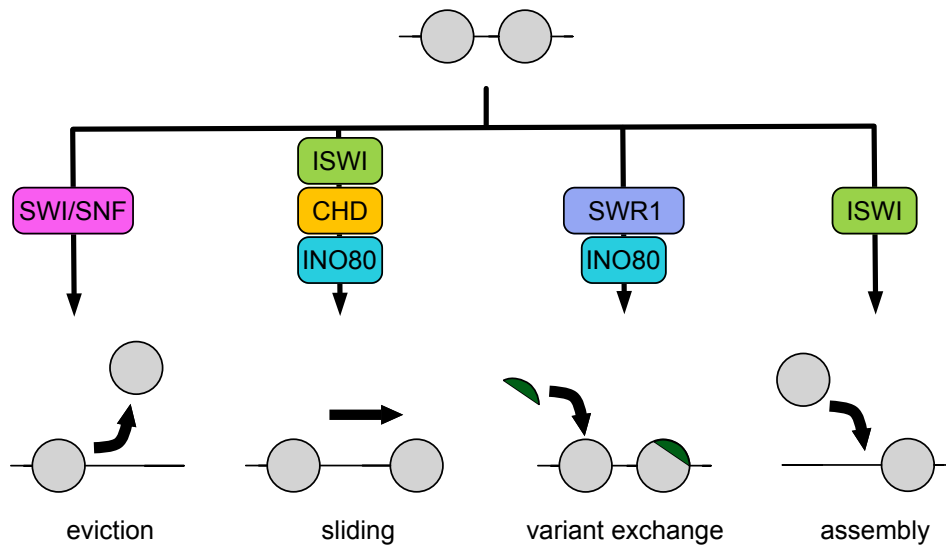
Figure 1.4 Mechanisms of action of nucleosome remodelers. The SWI/SNF family evicts nucleosome from chromatin, while ISWI, NuRD/Mi-2/CHD (CHD), and INO80 slide nucleosomes without disrupting the fiber. INO80/SWR1 family exchange canonical histone with variants. The ISWI family also participates in chromatin assembly.

While the mechanisms of these enzymes are quite well studied and described *in vitro*, the physiological consequences of their nucleosome remodeling are, to date, not entirely understood. Furthermore, it is still unclear how the activity of these remodelers is regulated *in vivo*.

1.8 The ISWI-type remodelers CHRAC and ACF

ISWI-type remodelers are multi-subunits nucleosome sliding complexes. In *Drosophila melanogaster*, the core ATPase ISWI is incorporated in six known remodeling complexes (CHRAC, ACF, RSF, NURF, ToRC and NoRC) (62) **(Figure 1.5)**. The different accessory subunits dictate and regulate the sliding activity of ISWI. For example, on *in vitro* reconstituted chromatin, the NURF and ACF complexes slide nucleosomes in opposite directions despite the common ISWI motor (74-77). Interestingly, ISWI complexes possess also a so-called *spacing* activity derived from their sliding capabilities: when provided to "uneven" nucleosomal arrays, they equalize the space between nucleosomes, even in the presence of H1 (78, 79).

The 'Chromatin Accessibility Complex' (CHRAC) and 'ATP-utilizing chromatin assembly and remodeling factor' (ACF) are highly related complexes originally purified from *Drosophila* embryo extracts (80, 81). Both CHRAC and ACF originate by the association of ISWI, and a large subunit, ACF1. CHRAC contains two additional histone-fold-like subunits, CHRAC-14 and CHRAC-16 (82), but its nucleosome sliding activity *in vitro* is essentially similar to ACF

(83). Since ISWI is present in several other nucleosome remodelers (62), ACF1 serves as the signature regulatory subunit for the two complexes.
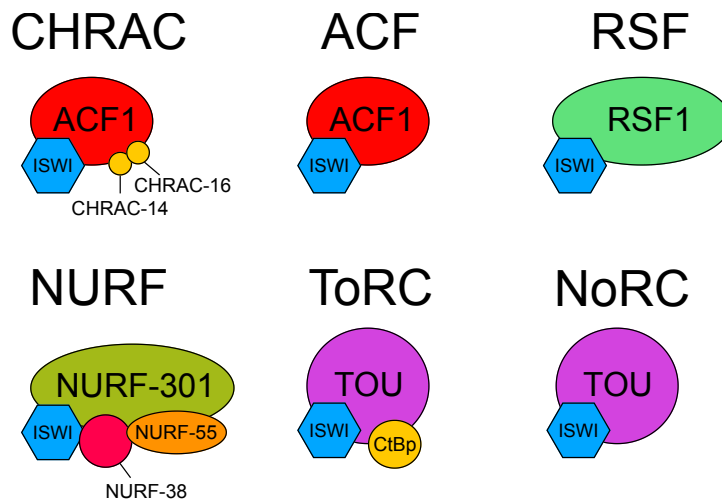
Figure 1.5 The main ISWI-containing complexes in *D. melanogaster* identified and characterized to date. While all catalyze nucleosome sliding, the presence of different accessory subunits, together with ISWI, diversifies the outcome of their reaction.

The mechanisms and dynamics of CHRAC/ACF remodeling have been extensively studied in vitro. ISWI and ACF1 bind nucleosomes by making contacts with both the nucleosome core particle and the linker DNA. Nucleosome and ATP binding/hydrolysis cycles generate conformational changes in the remodeler, which in turn cause nucleosomes sliding by disrupting histone-DNA interactions (66, 68, 84-89).

Despite the evolutionary conservation of these factors from yeast to mammals, their physiological function is poorly understood. In *D. melanogaster,* CHRAC/ACF have been implicated in developmental processes like embryogenesis and oogenesis, in which mutations of ACF1 causes a variety of phenotypic defects (90, 91). ACF1 seems also to contribute to general chromatin organization, cell cycle regulation, Polycomb silencing and heterochromatin formation (92). In mammals, mutations in the ACF1 ortholog BAZ1A cause spermatogenesis defects (93), alteration in neuronal development (94) and impairment in behavioral stress response (95).

By sliding nucleosomes, CHRAC/ACF may affect transcription through different mechanisms (54). Remodeling could alter nucleosome positioning at promoters, exposing or occluding transcription factor binding sites. For example, the yeast ortholog of CHRAC/ACF, the Isw2 complex, slides nucleosomes towards the nucleosome free region (NFR) of promoters (53, 96, 97). In fact, ACF1 seems to be directly involved in the repression of wingless target genes in *Drosophila* (98), as well as in the regulation of specific transcriptional programs during mouse spermatogenesis (93). On the other hand, CHRAC/ACF may globally influence

transcription through their nucleosome assembly and spacing activities. By generating regularity along the chromatin fiber, these nucleosome sliders may generally reduce the level of accessible DNA (6, 80, 84, 99). *Acf* mutants, in flies, show global loss of nucleosome regularity as assessed by Micrococcal nuclease digestion and gel electrophoresis (92). CHRAC/ACF have been indeed implicated in the establishment of repressive, silent heterochromatic domains (90, 100). The phenotypic defects observed during oogenesis in *Acf* mutants (91) may be explained by both mechanisms.

The *Drosophila* CHRAC/ACF may also be involved in DNA repair processes. When a DNA damaging even occurs, several machineries have to access the lesion in order to restore the damage (101). As most of the genome is covered with nucleosomes, it is conceivable that remodeler may be involved in freeing the broken DNA from nucleosomes or restoring chromatin after DNA is repaired (101, 102). Human CHRAC/ACF complexes are recruited to dsDNA breaks and cells depleted of ISWI (SNF2H) or ACF1 (BAZ1A) seem to be more sensitive to DNA damage (103-106). Flies carrying a mutation in the CHRAC-14 subunit of CHRAC complex also appear to be sensitized to DNA damaging agents (107).

To date, whether in the context of transcription or DNA damage response, the molecular consequences of a complete loss of *Drosophila* ACF1 (and thus the remodeling complexes it defines) are still unknown.

1.9 Histone variants

Many families of ATP-dependent remodelers change the properties of chromatin without altering the composition of the nucleosome particles. Some, instead, change the nucleosome octameric core by replacing canonical histone with histone variants (108). Besides differences found in the primary sequence, canonical histone and variants are primarily distinguished by the regulation of their genes. Canonical histone genes are present in multiple clustered copies, their mRNA lack poly-adenylation and are synthesized only during the S-phase of the cell cycle (109). This ensures that enough histones are present to assemble chromatin on the newly synthesized DNA. Such a tight regulation is of high importance, as ectopic expression of canonical histones is toxic to the cells (110, 111). Histone variant genes, on the other hand, have introns, their mRNA is poly-adenylated, and are expressed at lower levels but throughout the cell cycle (112). The degree of conservation of canonical histones across eukaryotes is higher than for histone variants. However, some universal histone variants are present in almost all eukaryotes: H2A.Z, H2A.X, H3.3 and CENP-A (113). The role of these histone variants is to furnish nucleosomes with special features. For example, nucleosomes containing the H3 variant CENP-A have a structure that differ only slightly from the canonical nucleosomes (114) but that guarantees specific recognition by centromeric proteins. Indeed, CENP-A is important for centromere

establishment and maintenance (115). Another H3 variant, H3.3, appears to destabilize nucleosomes (116) but its function is still not clear. It has been speculated that H3.3 replenishes nucleosomes outside of S-phase (117). H3.3 has been implicated in positive regulation of transcription but it also enriches silent domains such as telomeric and pericentromeric heterochromatin (118, 119). Amongst the H2A variants, H2A.X is the most similar to its canonical counterpart (around 80% identical). However, this relatively small difference is key and makes this variant an important player involved in genome integrity (120). The C-terminus of H2A.X contains a conserved serine within a SQ[E/D]Φ motif, which is phosphorylated upon DNA damage by ATM/ATR and DNA-PK kinases (121). The phosphorylated variant, called γH2A.X, spreads over megabases from the site of DNA break and becomes a platform for recruitment of repair factors (122). Another prominent H2A variant, H2A.Z, will be discussed in the next section.

1.10 The histone variant H2A.Z / H2A.V

H2A.Z is one of the most conserved H2A variants throughout evolution and accounts for ~5-10% of the total H2A-type histones in vertebrate (123, 124) and flies (125). H2A.Z is around 50-60% identical to H2A (depending on the species) (**Figure 1.6A**), and the differences are found along the entire sequences. In *Drosophila,* H2A.Z is the only H2A variant encoded in the genome and it is historically referred to as H2A.V (126). Phylogenetic analysis showed extensive homology between H2A.V and the H2A.Z of yeast and mammals (**Figure 1.6B**) (127).

Figure 1.6 A. Comparison between *D. melanogaster* H2A and the variant H2A.V. Domains in the canonical histone are depicted under the sequence alignment. The C-terminal SQ[E/D]Φ motif is highlighted in red. **B.** Multiple sequence alignment of H2A.V and H2A.Z from human (hs), frog (xl), budding yeast (sc) and worm (ce). Figure adapted from (127). Reprinted with permission from Springer Nature.

One feature distinguishes this fly variant from other species. At the C-terminus, H2A.V possesses a SQ[E/D]Φ motif identical to the one found in H2A.X variants (**Figure 1.6A,B**) as

mentioned previously. H2A.V is then a "chimera", a fusion between two different histone variants. On the one hand, H2A.V is primarily enriched in active promoters and enhancers as in its function as H2A.Z, and it is generally thought to be important for activation of transcription (128-132). On the other hand, H2A.V is phosphorylated upon DNA damage (γH2A.V) and, just like H2A.X, it is important for DNA damage response (133, 134). While flies lacking H2A.V can't survive, deletion of just the C-terminal part containing the SQ[E/D]Φ motif doesn't affect viability (135). The same deletion, however, sensitizes larvae to DNA damaging agents like x-rays (136). H2A.V has also been implicated in heterochromatin formation and Polycomb silencing, although only a few, isolated studies focused on such aspects (90, 137). Interestingly, it appears that deletion of ACF1 causes H2A.V variegation and heterochromatin defect (90), suggesting a potential relationship between a nucleosome slider and a histone variant that may be discussed later in the Appendix section.

1.11 SWR1 in yeast and flies

In *Saccharomyces cerevisiae*, the introduction of H2A.Z into chromatin is dependent on the SWR1 complex (SWR1.C), a multi-subunit ATP-dependent chromatin remodeler with the INO80-type ATPase Swr1 at its core (138-142). Years of biochemistry (138, 141, 143, 144) and a recent cryo-EM structure (70) elucidated the mechanism of histone exchange by the yeast SWR1.C (**Figure 1.7**). The complex engages the nucleosome through the interaction of the catalytic subunit Swr1 and the nucleosomal DNA to prime the histone exchange. This interaction causes the DNA to be "peeled" off the nucleosome by ~ 2.5 turns and translocated by 1 bp, causing a distortion of the DNA. Subsequent ATP hydrolysis stimulates the exchange of the SHL2-proximal H2A-H2B dimer with H2A.Z-H2B. The exchange reaction in a nucleosome happens sequentially in a step-wise manner, with one H2A-H2B dimer exchanged after the other (143). It seems that the SWR1.C deposits H2A.Z specifically at promoters of active genes *in vivo* because it is attracted by wide nucleosome free regions (NFRs) and histone acetylation, both consequence of high transcription (141).
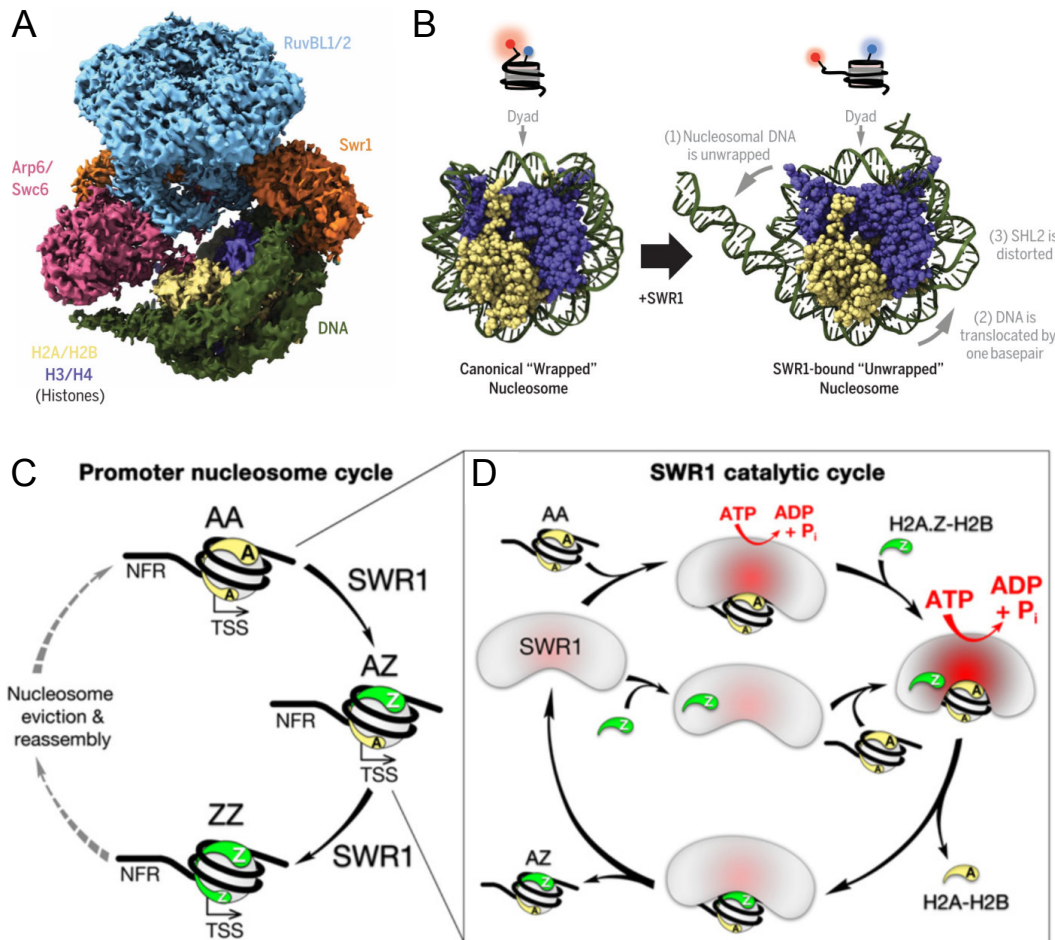
Figure 1.7 A.Reconstruction of SWR1.C structure in complex with a nucleosome from CryoEM data. The different SWR1.C subunits, as well as histones and DNA are color coded. **B.** Effects on SWR1.C binding to the nucleosomes. Detailed mechanism is explained in the main text. **C.** Stepwise incorporation of H2A.Z at promoter by SWR1.C. **D.** Catalytic cycle of SWR1.C. The complex binds stochastically a nucleosome containing two H2A-H2B dimers. Binding stimulates ATP hydrolysis which, in turn, leads to incorporation of one H2A.Z-H2B dimers concomitant with the eviction of one H2A-H2B dimer. The decreasing affinity for H2A.Z-H2B leads to dissociation of SWR1.C, leaving a heterotypic nucleosome. Another SWR1.C stochastically binds the other side of the nucleosome repeating the incorporation cycle and leaving a homotypic H2A.Z nucleosome behind.
A) and B*)* are adapted from (70) and reprinted with permission from AAAS. C) and D*)* are adapted from (143) and reprinted with permission from Elsevier.

In humans, two genes were found to be paralogs of Swr1, EP400 and SRCAP, with some evidence suggesting them to be responsible for H2A.Z incorporation (145, 146). In *Drosophila melanogaster*, only one gene encodes for the homolog of the yeast Swr1: *domino* (*dom*) (147). *dom* was discovered in 1997 after a screen for genes responsible for proliferation and hematopoietic disorders and got its name from the stereotypical larval phenotype consisting of necrotic lymph glands (two black spots on the anterior part of the fly larvae) (148). The first biochemical characterization revealed the presence of a multi-subunit complex composed of 15 proteins associated to the DOM ATPase (133). While, many of the subunits identified are homologs of the ones found in the yeast SWR1.C, additional

interactors were described. Surprisingly, these latter ones were identified as the homologous components of a distinct yeast complex, the Nucleosome Acetyltransferase of H4 (NuA4.C) (133). Unlike SWR1.C, the NuA4.C is not an ATP-dependent chromatin remodeler but rather an acetyltransferase complex with histone H4 N-terminal tail as its primary target (139, 149-151). Thus, the DOM complex (DOM.C) appears to be a chimera, a fusion between two yeast complexes with distinct biochemical activities. Coordination between these two reactions seem to be essential for the function of the DOM.C during DNA repair (133). Based on the current model of action, upon dsDNA breaks and phosphorylation of γH2A.V, DOM.C is recruited to the damaged sites. Once there, the histone acetyltransferase subunit TIP60 of DOM.C acetylates lysine 5 of γH2A.V (histone acetylation will be discussed in the next chapter). This double-modified variant (acetylated and phosphorylated) is then recognized as an exchange substrate for the SWR1.C-like module of DOM.C and replaced by an unmodified H2A.V to clear out the phosphorylation signal from chromatin. This is in contrast with the model mechanism of phosphorylation removal from the mammalian γH2A.X, which requires a phosphatase (152-155). Genetic characterization of DOM.C subunits revealed interesting phenotypes: defects in neuroblasts polarity and maintenance (156), improper E2F expression and enhanced cell proliferation (157), defects in wing development (158) and defects in Polycomb silencing and suppression of position-effect variegation (PEV) (159). To date two key aspects of DOM biology are still unclear. First, it is unknown if DOM.C is responsible for H2A.V incorporation into chromatin under physiological conditions. Second, if the acetyltransferase activity of the complex is relevant besides specific conditions such as DNA damage response.

It has been known since its discovery that the *dom* transcripts are alternatively spliced to generate two major isoforms, DOM-A and DOM-B (147). Is has been previously shown that these two splice variants are non-redundant and both essential for fly development. In other words, one isoform can't compensate for the absence of the other. The same study identified isoform-specific developmental phenotypes with little overlap (160). This suggests that the activity of the DOM.C might be regulated, at least partially, by the specific presence of one or the other, or both isoforms at its core.

1.12 Post translational modification of histone tails

ATP dependent chromatin remodelers act at the core of nucleosomes, but they are not the only enzymes capable of altering the proprieties chromatin. As previously mentioned, histone proteins are characterized by flexible N-terminal "tail" domains of various length that protrude from the nucleosome core. While they are not required for assembly of nucleosome particles (161-163), they are essential *in vivo* (164). This suggests that they are very important hotspots for chromatin regulation. What is then the role of the histone tails in nucleosome

and chromatin regulation? Early on, it was noted that histones extracted from cells are chemically modified, specifically acetylated and methylated (165, 166). Acetylated histones weaken the inhibitory effects of nucleosomes on *in vitro* transcription reactions and are associated with actively transcribed genes *in vivo* (167). Only after the discovery of the first acetyltransferases targeting histone tails and their link to transcriptional modulation (168-170), it became clear that histone post-translational modifications (PTMs) have functional relevance for regulation of nuclear processes. Since these early discoveries a zoo of PTMs have been documented (171, 172), the most prominent being acetylation, methylation, phosphorylation and ubiquitylation **(Figure 1.8)**.
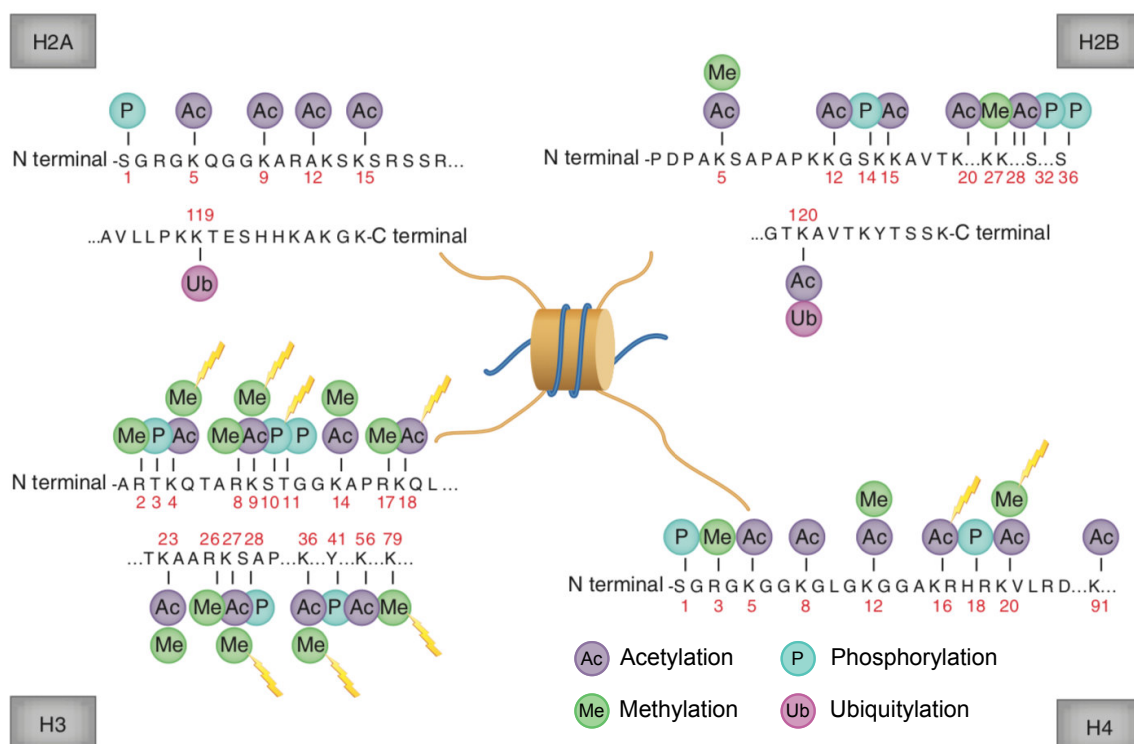
Figure 1.8 Most represented histone modification found in the N-terminal tails of canonical histones. Modified residues are highlighted in red. Figure adapted from (172). Reprinted with permission from Springer Nature.

The current model proposes that the combination of histone PTMs introduced in one or several histone tails by specific enzymes ("writers") forms a code that is read by other proteins ("readers") to instructs downstream effectors (173-175). Additional proteins are responsible to erase of this code ("erasers"). The combination of histone modifications, and their context, appears to be an important regulatory aspect of gene expression (176), DNA repair (177) and heterochromatin formation/maintenance (178). The latter is a quite a stereotypical example of functional reader-writer cooperation, especially well described in fission yeast (179). To establish a heterochromatin domain, a specific histone methyltransferase is recruited and "writes" di- or tri-methylation on lysine 9 of histone H3

(H3K9me2/3). This modified residue is "read" by a chromodomain-containing protein, which in turns recruit or stabilizes effectors responsible for heterochromatin maintenance. To date, many writers, readers and erasers for diverse histone modifications have been identified and characterized (180) **(Figure 1.9)**.
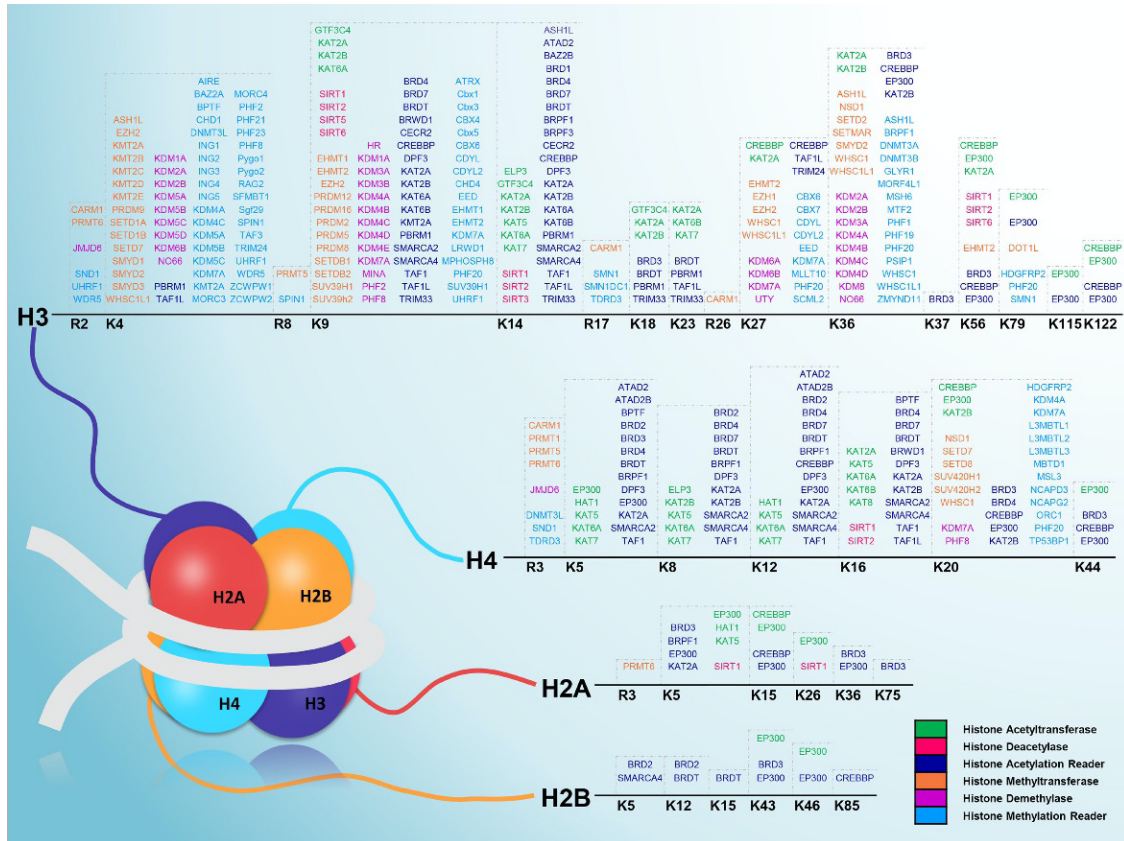
Figure 1.9 A catalog of major mammalian histone modification writers, readers and erasers targeting canonical histones. Figure from (180). Reprinted with permission from Oxford University Press.

1.13 Histone acetylation

One of the first discovered and perhaps one of the most characterized of all the possible PTMs, histone acetylation is a central factor of chromatin regulation. The reaction is relatively simple, consisting of the covalent attachment of an acetyl group (derived from acetyl-CoA) to the ε-amino group of a lysine residue. Acetylation reduces the charge of histones by "quenching" the positive charge of the amino groups, potentially reducing the strength of interaction between histones and DNA. Indeed, hyper-acetylated chromatin is more flexible and accessible to DNaseI *in vitro* (181, 182). Histone acetyltransferases (HATs) are the enzymes responsible for the deposition of acetylation on chromatin. There are at least 5 main families of HATs, classified based on the sequence/structure of the catalytic domain (**Figure 1.10**) (183). Their opponents, the histone deacetylases (HDACs) function as erasers

to remove acetyl groups from modified histones (184). It has been shown *in vivo* that a basal, low level of acetylation is present across the genome, likely due to the concerted and non-specific action of HATs and HDACs (185).

Before knowing the product of their catalytic activity, HATs and HDACs were genetically identified as transcriptional activators (186) and repressors (184, 187, 188), respectively.

Major HAT subfamilies	Prominent members	Key structural and biochemical properties
HAT1	yHat1	Member of the GNAT family
		Amino- and carboxy-terminal segments used for histone substrate binding
		Requires the yHat2 regulatory subunit for maximal catalytic activity
Gcn5/PCAF	yGcn5	Member of the GNAT family
	hGCN5	Uses a ternary complex catalytic mechanism
	hPCAF	Amino- and carboxy-terminal segments used for histone substrate binding
MYST	yEsa1	Uses a ping-pong catalytic mechanism
	ySas2	Requires autoacetylation of a specific lysine at the active site for cognate histone acetylation
	ySas3	
	hMOZ	
	dMof	
	hMOF	
	hTIP60	
	hHBO1	
p300/CBP	hp300	Metazoan-specific, but shows structural homology with yRtt109
	hCBP	Uses a ternary Theorell–Chance (hit-and-run) catalytic mechanism
		Contains a substrate-binding loop that participates in AcCoA and lysine binding
		Contains an autoacetylation loop that requires lysine autoacetylation for maximal catalytic activity
Rtt109	yR11109	Fungal-specific, but shows structural homology with p300
		Contains a substrate-binding loop that participates in AcCoA and probably also lysine binding
		Requires autoacetylation of a lysine residue near the active site for maximal catalytic activity
		Requires one of two histone chaperone cofactors (Asf1 or Vps75) for maximal catalytic activity and histone substrate specificity

y, yeast; h, human; GNAT, Gcn5-related *N*-acetyltransferase.

Figure 1.10 Table listing the main histone acetyltransferase (HATs) families with examples from yeast and human. Key structural and biochemical proprieties are described. From (183). Reprinted with permission of Cold Spring Harbor Laboratory Press.

Given the widespread presence of acetylation throughout the genome, it is conceivable that transcriptional activation/repression by HATs/HDACs arises from local imbalance between the two enzyme classes (e.g. at certain promoters) (189). A special case is the *Drosophila* dosage compensation, in which acetylation of H4K16 regulates the transcriptional output of an entire chromosome (190).

Acetylated residues are usually recognized by special reader classes containing bromodomains.

1.14 *Drosophila* as a model organism to study chromatin regulation

The small fruit fly represents one of the most "versatile" model organisms for studying the *in vivo* functions of chromatin remodelers and modifiers. Since the beginning of the century (191), an extensive characterization of *Drosophila melanogaster* allowed to understand the genetic basis of signaling and development (192, 193). Flies also provided the first examples

of chromatin regulation and epigenetic inheritance, such the homeotic gene regulation by the Polycomb system (194).

D. melanogaster has a relatively compact genome and only 4 chromosomes, yet it includes features (such as enhancers, repetitive centromeric sequences, 3D genome organization) shared with other higher eukaryotes. It is easy to maintain in laboratory and has a relatively short life cycle (around 10-12 days at 25°C from embryo to adult), consisting of four main developmental stages: embryo, larvae, pupae and adult (195). The embryonic development happens outside of the body of the fly and it is most relevant for the current study (196-198) (**Figure 1.11**). Once the egg is fertilized, the zygote undergoes 13 cycles of rapid synchronous nuclear divisions (one division roughly every 8-20 min) to form a syncytium. Between the 8th and 10th cycle, the nuclei migrate at the periphery to form a syncytial blastoderm. The rate of mitotic division is slowed down after the 13th cycle, when cellularization happens and a cellular blastoderm is formed.
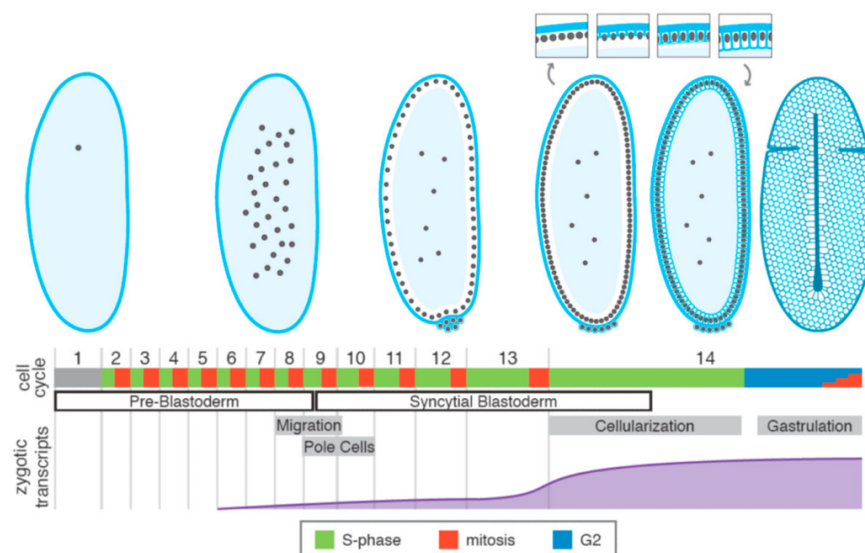
Figure 1.11 Schematic representation of early *Drosophila* embryogenesis. Notable Morphological stages are drawn on top (cellularization shown in the upper panels). Cell cycle phases and onset of zygotic transcription are depicted in the bottom. From (198). Reprinted with permission of Annual Reviews.

Until this point, the zygotic genome is largely silent, with the exception of few genes (199). The major wave of zygotic transcription (also known has maternal-to-zygotic transition, MZT) starts at cycle 14 (200). Subsequently, the embryo undergoes gastrulation and segmentation and ultimately hatching into larvae around 22-24 h after fertilization.

Adult flies can lay many fertilized eggs per day (201), which can be collected in large amounts for biochemical analysis. As an example, many chromatin remodeling enzymes were discovered and purified from large-scale embryo extracts (79, 80, 202-204). These embryonic extracts are also used for *in vitro* chromatin assembly (205-207), transcription

(208, 209), DNA replication (210) and reconstitution of DNA damage response (211). Fly embryos have also been extensively used to study the developmental functions of chromatin regulators (see this dissertation) (207, 212). Furthermore, several cell lines derived from embryos (eg: S2, Kc167) are widely used and well characterized (213). They are well-suited for genomic and biochemical analysis due to simple and inexpensive culturing conditions, short doubling time and very efficient RNAi-mediated knockdown (214).

1.15 Scope of the work

The dynamics of nucleosome and chromatin properties, and its regulation, have proven to be essential for complex living organisms, including *Drosophila*. For technical or historical reasons, perhaps, chromatin regulators have primarily been studied either *in vitro*, through extensive characterization of structure and catalytic mechanisms, or genetically, via analysis and description of phenotypes associated to mutation in genes coding for their components. While in both cases important insight and knowledge were gained, a substantial gap was created, over time, between those fields of chromatin research. In fact, the "conversion" processes of individual remodeling/modifying reaction to the phenotypes observed are often lacking or, even worse, taken for granted as postulates. In this doctoral work I aimed to support and/or challenge some of these postulates, as I think there is still a lot of interesting mechanisms to be discovered hiding behind models and theories accepted but not yet supported by data.

Remodeling by CHRAC/ACF on *in vitro*-reconstituted chromatin appears to have a repressive effect on transcription (215), in agreement with heterochromatin de-repression observed via genetic analysis of *Acf* mutant flies (92). For a long time (since early 2000's), these early studies served to assign an active repressive role to these remodelers - largely undisputed by the scientific community. **I wanted to investigate if and how CHRAC/ACF act as transcriptional repressors, ensuring back-up silencing mechanisms during development.**

Along a similar line, it has been postulated that the *Drosophila* CHRAC/ACF might be involved in response upon DNA breakage as their human orthologs (103-106). How do these nucleosome remodelers participate in this process? Three scenarios, not necessarily mutually exclusive, might be possible: 1) nucleosome sliding by CHRAC/ACF might free the DNA close to the broken ends to allow an easier access of the repair machinery 2) nucleosome assembly by CHRAC/ACF in cooperation with NAP1 might refurbish chromatin after the break is repaired 3) the fly CHRAC/ACF might be somehow involved in γ-H2A.V exchange during the DNA damage response since they appear to participate in H2A.V

deposition under physiological conditions (90). So far, only one study (107) linked CHRAC to DNA damage in flies. **Are CHRAC/ACF generally involved in the DNA damage response of *D. melanogaster*? Do they modulate γH2A.V signaling during this process?**

The DOMINO complex of *D. melanogaster* is considered a rather unique nucleosome remodeling complex due to its combined activities of histone variant exchange and histone acetylation. The yeast orthologous complexes (SWR1.C and NuA4.C), of which the DOM.C appears to be a fusion, are well known and described both biochemically and genetically. The two basics reactions potentially carried out by the fly DOM.C were extrapolated from yeast and never questioned. Only two examples (133, 216), to my knowledge, tried to investigate if the DOM.C activity is different from the sum of its catalytic parts. Surprisingly, in both cases, an intimate link between acetylation and H2A.V deposition was found: one reaction regulates the other and *vice versa*. This dependency, however, was observed only under special circumstances (DNA damage and heat-shock responses). **How does the DOM.C complex function under physiological conditions? How are histone acetylation and H2A.V exchange connected to each other?**

Previous work from our lab showed that splice variants of the central ATPase of DOM.C are non-redundant and associated with distinct phenotypes (160), suggesting a different regulatory potential towards the DOM.C. **How are the two isoforms of DOM, DOM-A and DOM-B, regulating the activity of the complex under physiological conditions?**

2. RESULTS AND DISCUSSION – CHRAC/ACF contribute to the repressive ground state of chromatin

Most of the work contained in this section is published (217) and available at https://www.life-science-alliance.org/content/1/1/e201800024.short. Supplementary tables are all available on the publisher site. Naming and numbering reflect the one available online.

The material reproduced here (figures) is in accordance with the Creative Common License (Attribution 4.0 International) and properly attributed throughout.

Peter B. Becker and I conceived the project and designed the experiments. I performed all the experiments except the Gal4-UAS[Gal] tethering in Kc cells, which was performed by Laura Brueckner. Tamas Schauer analyzed the RNAseq data and, together with me, established the single-embryo RNAseq experimental procedure. Tobias Straub analyzed the MNase-seq data. Dhawal Jain generated the *Acf^C* mutant (in collaboration with Xu Zhang from Frank Schnorrer's lab) and the *Gal4-Acf* fly strains. Peter B. Becker and Bas van Steensel provided supervision.

Clarified the individual contributions, I therefore refer to myself and my collaborators as "we" throughout this section (unless stated otherwise) to highlight a strong team effort.

2.1 Artificial ACF1 tethering shows context-dependent repressive effects

For many nucleosome remodelers, chromatin immunoprecipitation (ChIP) provided insights about their function at specific genomic sites, such as promoters and enhancers. Unfortunately, mapping of chromosomal binding sites for ACF1 by ChIP was never successful, probably due to the proprieties of the interaction between the remodeler and its substrate. In fact, CHRAC/ACF complexes may interact only very dynamically with chromatin, often too transiently to be efficiently trapped by formaldehyde crosslinking (218).

To asses if ACF1 has any effect on transcription, we opted for an experimental approach in which ACF1 is artificially targeted to specific reporter locus via the well-established Gal4/UAS system. To this end, we utilized transgenic flies in which a reporter cassette consisting of five UAS[Gal] sequences upstream of lacZ and mini-white genes (219) is inserted in a defined position of the genome (**Figure 2.1a**). We generated fly strains expressing ACF1 fused (either at the N- or C-terminus) to the DNA binding domain of the yeast transcriptional activator GAL4 (GAL4DBD). These transgenes are expressed under the control of the

endogenous *Acf* promoter. The ACF-GAL4DBD fusions are expressed at levels comparable to the endogenous ACF1 (**Figure 2.1a, b**). In parallel, we generated transgenic flies expressing only the GAL4DBD, also under the control of the endogenous *Acf* promoter, which serve as controls.
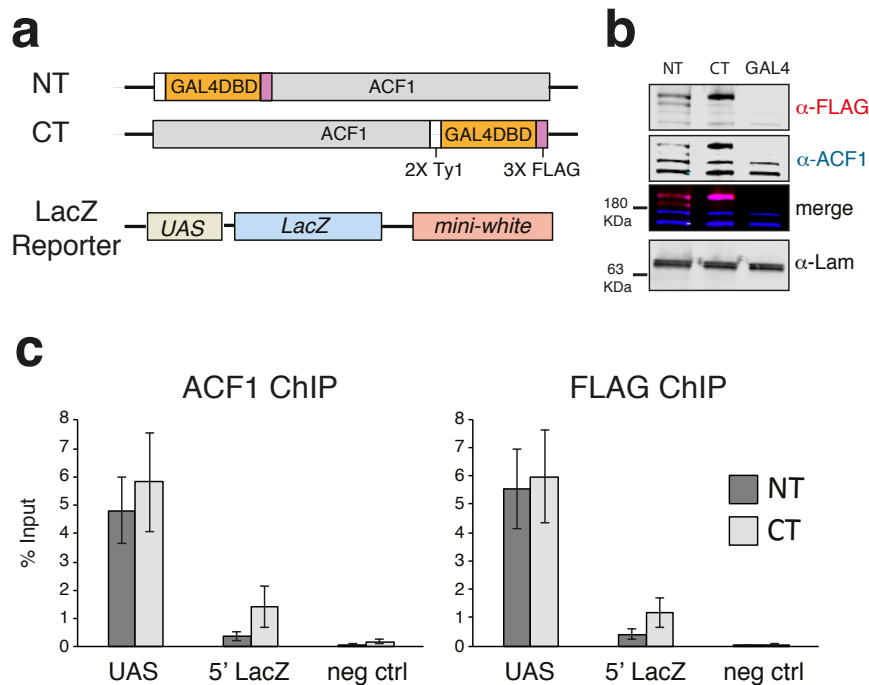
Figure 2.1 a. Schematic of the transgenic constructs designed to artificially recruit ACF1. **b.** Western blot on nuclear extracts from 0-16h old embryos derived from the transgenic ACF1-GAL4DBD lines and control. The transgenes are identified by both the ACF1 specific antibody (which also detect the endogenous ACF) and the FLAG antibody (detects transgene only). Lamin: loading control. **c.** ChIP-qPCR to show ACF1-GAL4DBD recruitment to the reporter in 0-12h old embryos. ACF1 and FLAG antibodies are compared. Bars represent average % Input enrichment (n=3) ± SEM. The negative control ("neg ctrl") region is within the Spt4 gene (on a different chromosome than the reporter). Figure (217). Reprinted as permitted by the Creative Commons Attribution CC-BY 4.0 license.

Crossing the aforementioned fly strains yields a progeny in which ACF1 is recruited to the UAS^{Gal} sequences. The tethering of ACF1-GAL4DBD in early embryos was successfully confirmed by ChIP-qPCR (**Figure 2.1c**). ISWI, the catalytic partner of ACF1, could also be detected at the UAS sites, suggesting the recruitment of at least a full ACF complex (**Figure 2.2a**). Interestingly, ACF1 targeting results in a mild downregulation of *LacZ* reporter expression (average fold-change = 0.58 for GAL4DBD-ACF1 and average fold-change = 0.39 for ACF1-GAL4DBD) (**Figure 2.2b**), although no major changes in nucleosome positioning could be scored by MNase-seq (**Figure 2.2c,d**). These experiments showed that ACF1 can be successfully recruited to a specific genomic locus via the Gal4/UAS system, and this results in a small but consistent repressive effect. Given the limitations of a single-reporter system in flies, we opted for an alternative Gal4/UAS targeting strategy in *D. melanogaster* Kc167 cells, which allows to monitor repression over hundreds of reporters

integrated in different chromatin contexts. This approach was previously used to score how the chromatin environment modulates the well-known heterochromatic protein 1 (HP1) - mediated repression (220). In our case, HP1 provides a reference for any ACF1 effect.
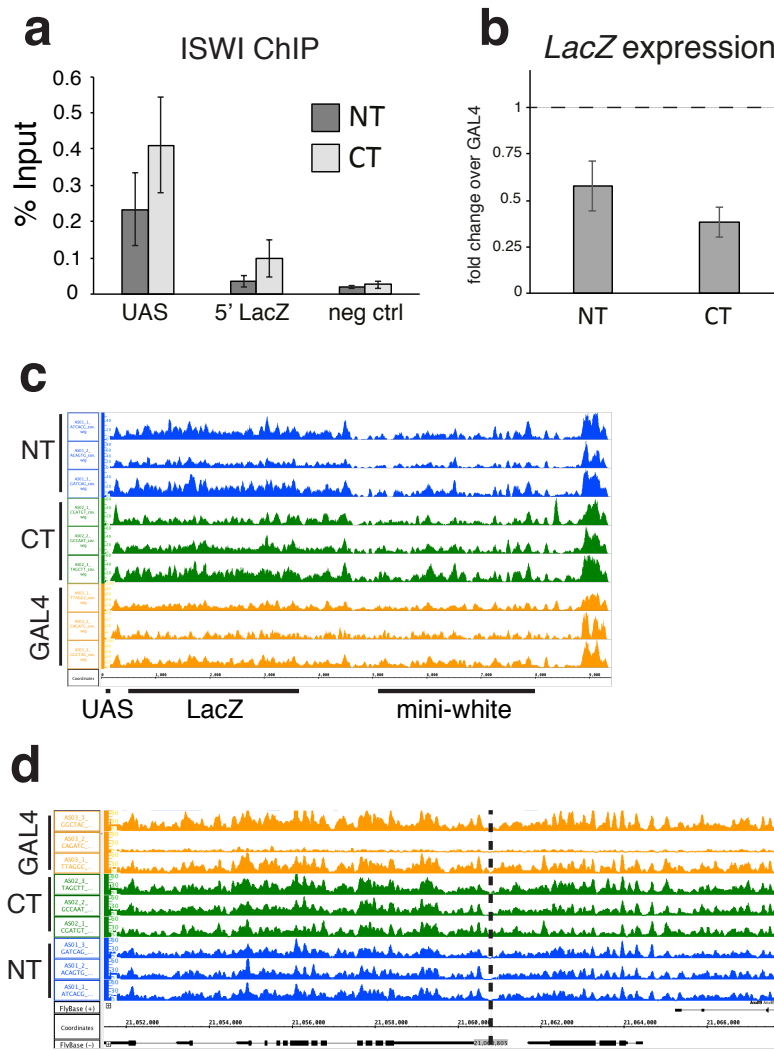
Figure 2.2 a. ChIP-qPCR to show ISWI recruitment to the reporter in 0-12h old embryos. Bars represent average % Input enrichment (n=3 biological replicates) ± SEM. The negative control ("neg ctrl") region is within the Spt4 gene (on a different chromosome than the reporter). **b.** RT-qPCR shows LacZ downregulation in early embryos (2-8 h) upon ACF1-GAL4DBD recruitment. Bars represent average fold-change over the control (n=3) ± SEM. **c.** Genome browser screenshot showing nucleosome dyad coverages at the reporter locus. Individual replicates for each genotype are shown. **d.** Same as (c) but showing nucleosome dyad densities in the genomic regions left and right of the reporter (dashed line). Figure from (217). Reprinted as permitted by the Creative Commons Attribution CC-BY 4.0 license.

Expression of the transfected fusion constructs (V5-GAL4DBD-ACF1, V5-GAL4DBD, V5-ACF1 and ACF1) was confirmed by Western Blot and Immunofluorescence microscopy (**Figure 2.3a,b,c).** Tethering of ACF1, comparably to HP1, resulted in a global down-regulation of reporters (median log2 fold-change = -1.24 and -1.46 respectively) (**Figure 2.4a**). Expression of ACF1 lacking the GAL4DBD caused milder effect but on the same direction of its tethered counterpart (median log2 fold-change = -0.24). Interestingly, the

repressive strength of tethered ACF1 and the mean expression levels of the reporters appeared inversely correlated: GAL4DBD-ACF1 weakly represses reporters with high basal expression (**Figure 2.4b**). A similar correlation appears similarly in the case of the untethered ACF1 (**Figure 2.4c**). GAL4DBD-HP1 showed a small correlation between down-regulation and reporter expression (**Figure 2.4d**), but significantly different from GAL4DBD-ACF1 (**Figure 2.3d**).
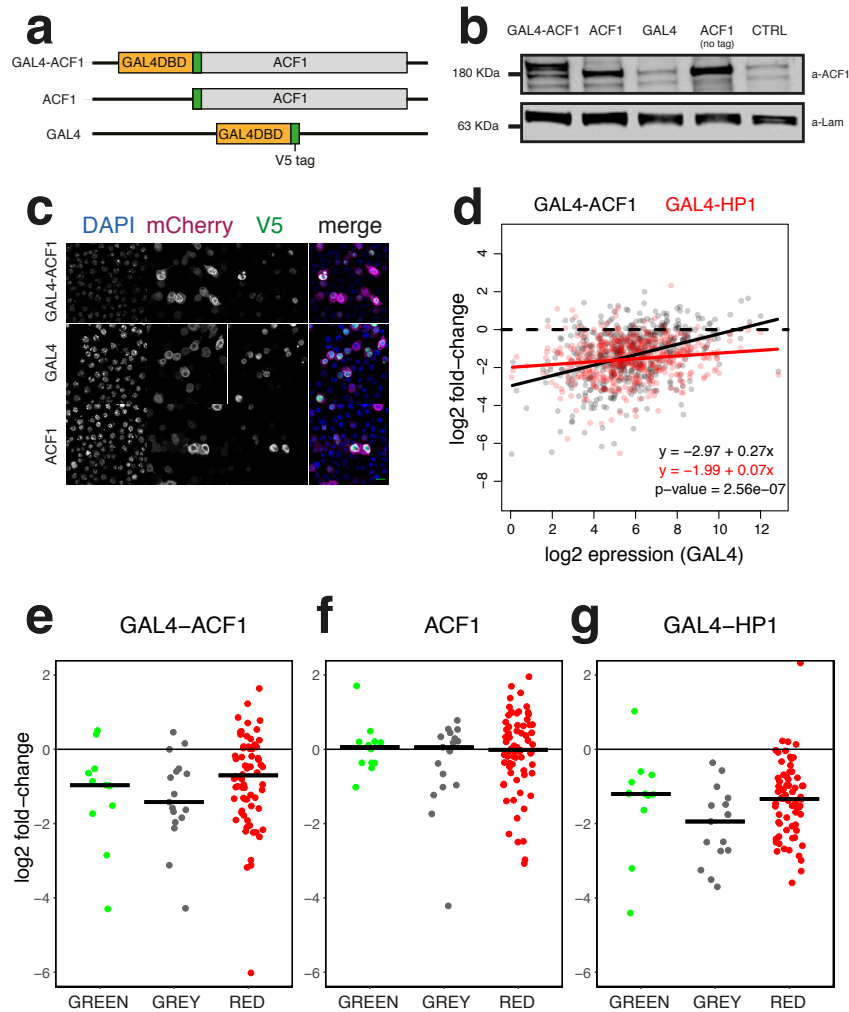
Figure 2.3 a. Schematic of the transgenic constructs designed to artificially recruit ACF1 to multiple reporters in Kc167 cells. All constructs contain a V5-tag. **b.** Western blot on whole cell extracts from Kc167 cells transfected with GAL4DBD-ACF1 transgenes and controls. Expression of transgenes is probed with the ACF1 specific antibody. "CTRL" denotes cells transfected with water. Lamin: loading control **c.** Representative immunofluorescence images of Kc167 cells transfected with the contructs shown in (a). The V5 antibody was stains transgenic proteins. DAPI stains DNA. mCherry antibody was used as control. Scale bar :10 µm. **d.** Correlation between repression strength and basal reporter expression upon GAL4-ACF1 or GAL4-HP1 tethering. Equations and fitted regression lines are shown. p-value derives from testing the slope difference between the two regression lines. **e.** Log2 fold-changes in expression (over GAL4DBD control) for reporters integrated in GREEN (N = 12), GRAY (N = 17) and RED (N = 70) chromatin domains upon recruitment of GAL4-ACF1. Horizontal bars: median. **f.** Same as (b) but for ACF1 lacking GAL4DBD **g.** Same as (b) but for GAL4-HP1. Figure from (217). Reprinted as permitted by the Creative Commons Attribution CC-BY 4.0 license.

To extend our analysis, we investigated if the chromatin environment in which the reporters are integrated affects the repressive potential of ACF1. We referred to the 5-state model of chromatin (221), in which BLACK and BLUE are both inactive but the latter is marked by Polycomb, GREEN is marked by HP1, and YELLOW and RED are both active either constitutively or dynamically during development. For reporters integrated outside these domains, we added the sixth GREY state. We found that reporters located within inactive domains such as BLACK and BLUE are strongly repressed by GAL4DBD-ACF1 (median log2 fold-change = -1.83 and -1.45 respectively), whereas the ones located within YELLOW domains are only modestly down-regulated (median log2 fold-change = -0.39) (**Figure 2.4e).**
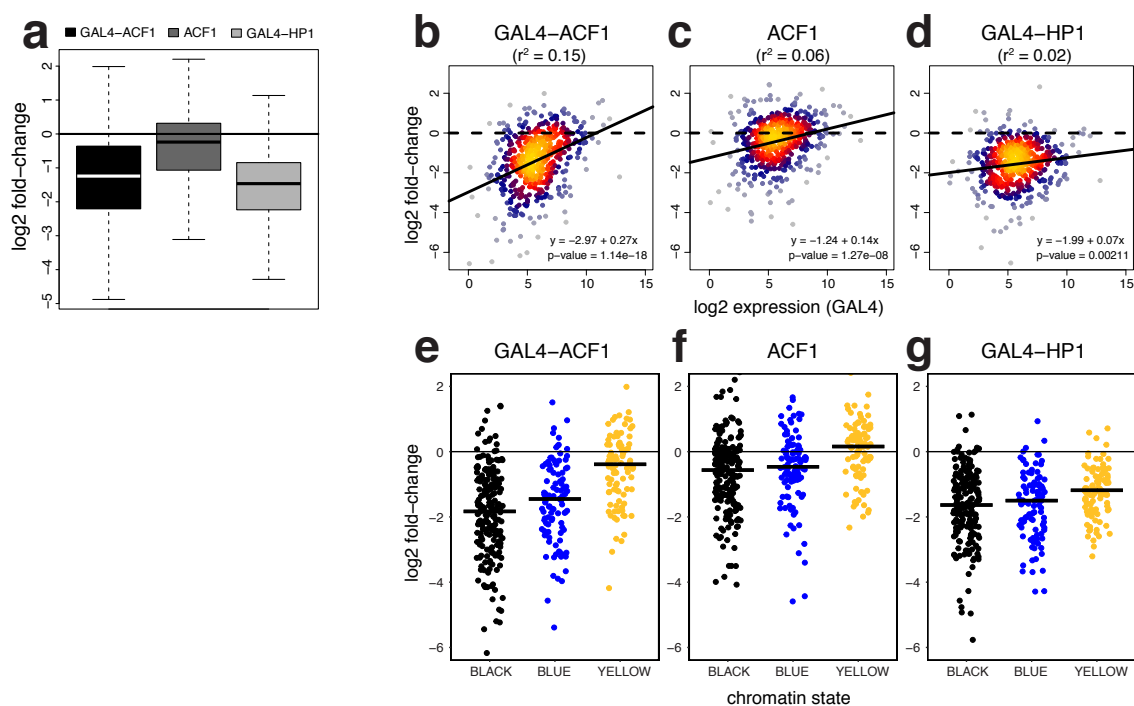
Figure 2.4 a. Boxplot showing the distribution of log$_2$ fold-changes (over GAL4DBD control) in reporter expression upon expression of GAL4-ACF1, GAL4-HP1 or ACF1 alone (ACF1) (N = 492). **b.** Heat-scatterplot comparing log$_2$ fold-change (over GAL4DBD control) for each reporter to its mean log$_2$ expression upon expression of GAL4-ACF1 (N = 492). Linear regression fit and equations are shown in the plot. r^2 values derive from the linear model. p-value derives from testing the slope difference between the regression lines and a y=0 line. **c.** Same as (b) but for expression of ACF1 alone **d.** Same as (b) but for expression of GAL4-HP1. **e.** Log2 fold-changes (over GAL4DBD control) in expression for reporters integrated in BLACK (N = 197), BLUE (N = 102) and YELLOW (N = 94) chromatin states upon expression of GAL4-ACF1. Horizontal bars: median. **f.** Same as (e) but for expression of ACF1 **g.** Same as (e) but for expression of GAL4-HP1. Figure adapted from (217). Reprinted as permitted by the Creative Commons Attribution CC-BY 4.0 license.

Similarly, reporters integrated within RED (median log2 fold-change = -0.70) and GREEN states (median log2 fold-change = -0.70 and -0.97 respectively) are less down-regulated compared to the one lying in BLACK and BLUE states (**Figure 2.3e)**. Tethering of GAL4-HP1 causes, instead, a general and widespread repression of reporters without apparent correlation to any of the 5 chromatin domains in which they are integrated (**Figures 2.3g,**

36

2.4g). Interestingly, the effects caused by expression of ACF1 alone mildly phenocopy the one of GAL4-ACF1 (**Figures 2.3f, 2.4f**).

In summary, these results suggest that CHRAC/ACF may have repressive function that becomes evident through artificial targeting. In contrast to HP1, ACF1-mediated repression depends on the chromatin environment and its strength seems to be inversely correlated with the pre-existing transcriptional activity of the targeted reporters.

2.2 Gene expression is affected in *Drosophila* embryos lacking ACF1

The tethering experiments highlighted a repressive effect for ACF1, consistent with what hypothesized before. However, since the system is very artificial, we wanted to investigate the role of ACF1 in transcription regulation, along with a possible context-dependency, in a more physiological system. To date, no gene expression analysis upon ACF1 loss has not been reported. We chose *D. melanogaster* early embryonic development for two reasons: 1) ACF1 expression is very high 2) both CHRAC and ACF were originally discovered in this developmental stage. Early studies utilizing the *Acf^1* allele scored embryogenesis defects (100). However, this allele does not correspond to a loss-of-function. In fact, the N-terminal deletion of the *Acf^1* allele still allows the expression of part of the C-terminus of ACF1, which contains a PHD and a Bromodomain. This may possibly be considered ad a gain-of-function allele. Another mutant, *Acf^7*, may represents more likely a clean loss of function, as it phenocopies the reduction of ACF1 by RNAi (91). To ensure a traceable and controlled mutation, we engineered a new deletion of the *Acf* gene using a CRISPR/Cas9. We named this new allele *Acf^C*. We confirmed that neither in *Acf^C* or *Acf^7* homozygous embryos ACF1 expression is detected by Western blot (**Figure 2.5a;** (91)). *Acf^C* and *Acf^7* alleles are characterized by a lower larval hatching rate compared to wild-type (**Figure 2.5b;** unpublished observation). In both cases, surviving hatched larvae normally develop into flies with no evident phenotypic defect (unpublished observation). As we are not sure if *Acf^C* mutants develop slower or faster than wild-type, we decided not to rely on timing for stage definition. Instead, we selected single embryos of two early developmental stages based on morphological features, before or after zygotic genome activation (ZGA) (**Figure 2.6a,** see methods). We then determined their gene expression profiles by RNA-seq analysis**.** No strong differences between *Acf^C* and wild-type embryos (before or after ZGA) are evident from Principal Component Analysis (PCA) (**Figure 2.6b**).
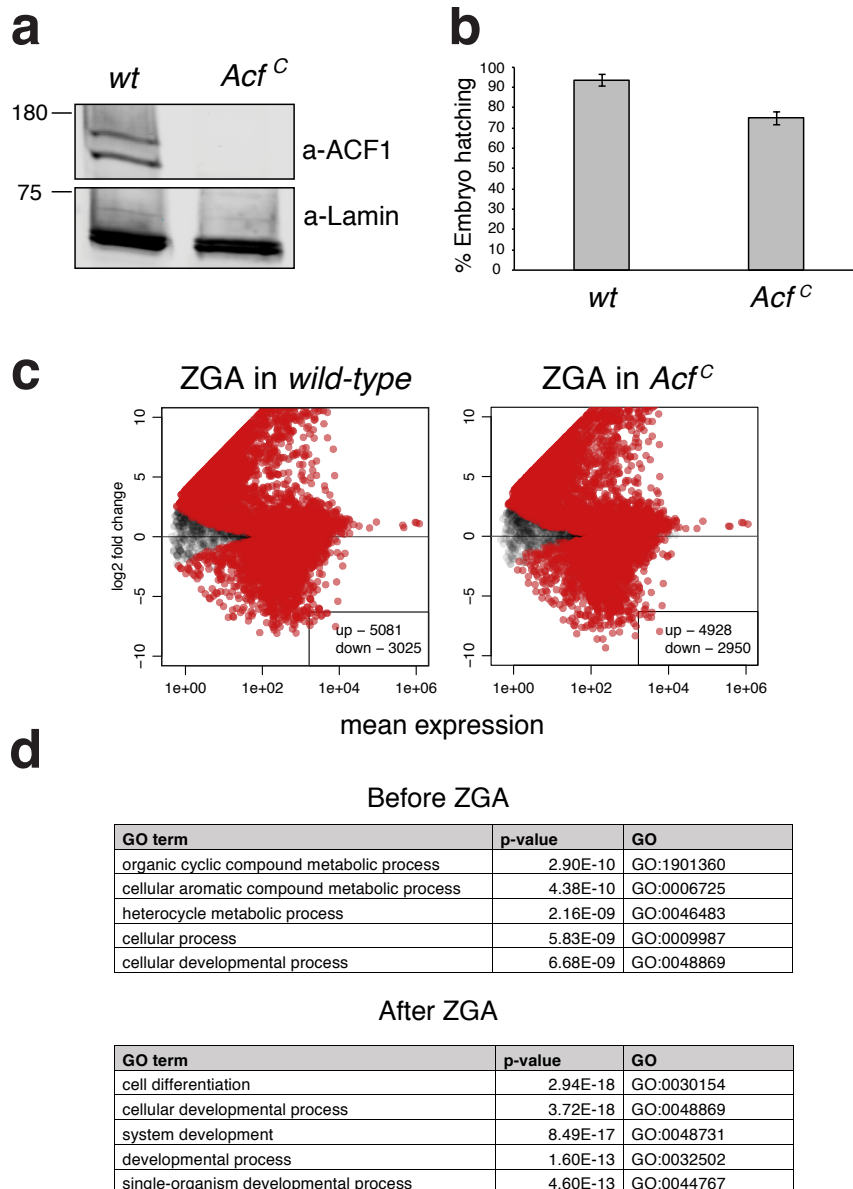
Figure 2.5 a. Nuclear extract from 0-16h old *wild-type (wt)* and ACF1 mutant (*Acf^C*) embryos were probed for ACF1 expression by Western blot. Lamin: loading control. **b.** Barplot comparing *wild-type (wt)* and *Acf^C* larval hatching rates. Bars show average % of larval hatching (n=3, N> 47 embryos /replicate) ± SEM. **c.** Scatterplots showing the results of differential gene expression analysis comparing transcriptomes before and after ZGA, separately for *wild-type and Acf^C*. Each dot represents the $\log_2$ fold-change for each gene in relation to its mean expression (N = 9235 for *wild-type*, N = 9163 for *Acf^C*). Genes significantly mis-regulated (q-value <0.1) are labeled in red. **d.** Gene Ontology analysis on genes significantly mis-regulated (q-value <0.1) in the comparison between *Acf^C* and *wild-type*, separately for before and after ZGA. Top 5 Gene Ontology terms are displayed. Figure from (217). Reprinted as permitted by the Creative Commons Attribution CC-BY 4.0 license.

Maternal-to zygotic-transition appear to be very similar in both strains (**Figure 2.5c;** Supplementary Table 3). Relatively few genes were found to be significantly affected by the depletion of ACF1 in both developmental stages (**Figure 2.6c,d;** Supplementary Table 2), without a bias towards up- or down-regulation and without enrichment for a specific gene ontology term (**Figure 2.5d**).
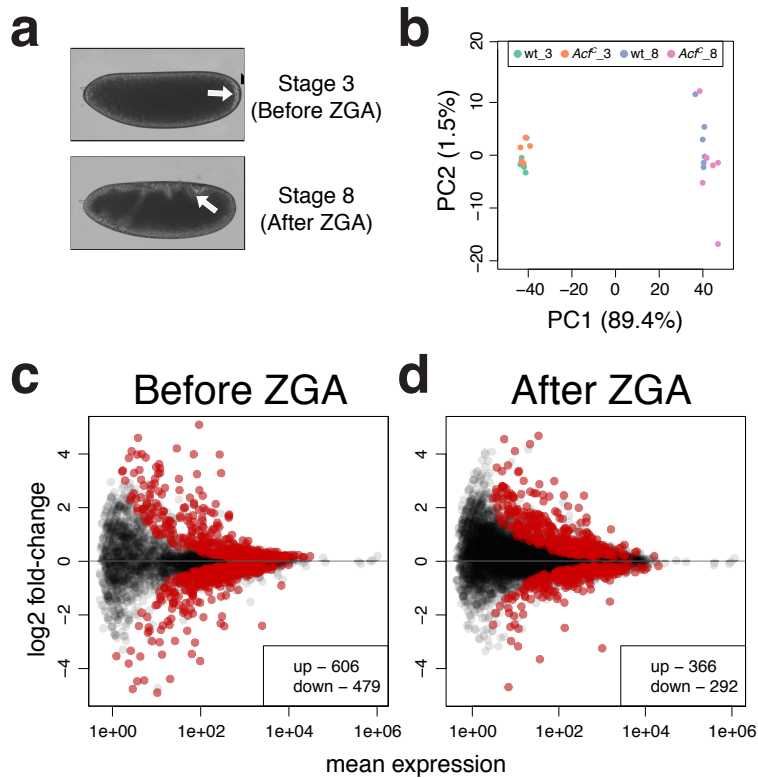
Figure 2.6 a. Representative brightfield images of embryos in Bownes Stage 3 (before ZGA) and 8 (after ZGA). Distinguishing morphological feature of each stage (pole cells formation and germ band elongation for stage 3 and 8 respectively) are indicated by arrows **b.** Principal component analysis (PCA) of single embryos gene expression profiles. Individual replicates are shown. Stages and genotypes are color coded. **c.** Scatterplots showing the results of differential gene expression analysis comparing transcriptomes from *wild-type* and *Acf^C* embryos before ZGA (N = 7585). Each dot represents the log$_2$ fold-change for each gene in relation to its mean expression. Genes significantly mis-regulated (q-value <0.1) are labeled in red. **d.** Same as c. but after ZGA (N = 10088). Figure from (217). Reprinted as permitted by the Creative Commons Attribution CC-BY 4.0 license.

2.3 ACF1 loss affects mostly inactive, ground state chromatin

Given the very small number of differentially expressed genes found in our analysis, we speculated that the role of ACF1 on transcription might be small and visible only on a larger scale than single genes. We could also not exclude functional redundancy with other remodelers. The artificial tethering of ACF1 showed stronger repressive effects on specific chromatin domains, so we investigated whether similar context-dependency also applies in embryos lacking ACF1.

Once again, we investigated transcriptome differences between wild-type and *Acf^C* embryos in the framework of the 5 chromatin states model. While YELLOW, RED and GREEN chromatin domains seem to be mostly unaffected by ACF1 depletion (**Figure 2.7a and 2.8a**), genes found within BLACK and BLUE chromatin domains appear to be slightly but consistently upregulated in *Acf^C* mutants. The comparison between our dataset and publicly available modENCODE histone modifications data (222) from 2-4 h old embryos (similar developmental stages of our study) showed that the transcriptional de-repression in *Acf^C* mutants directly correlates with the lack of defined chromatin marks and with the presence of

39

H3K27me3 (readouts for BLACK and BLUE states respectively) and anti-correlates with the absence of H3K36me3 (readout for YELLOW state) (**Figure 2.8b**, top panels).
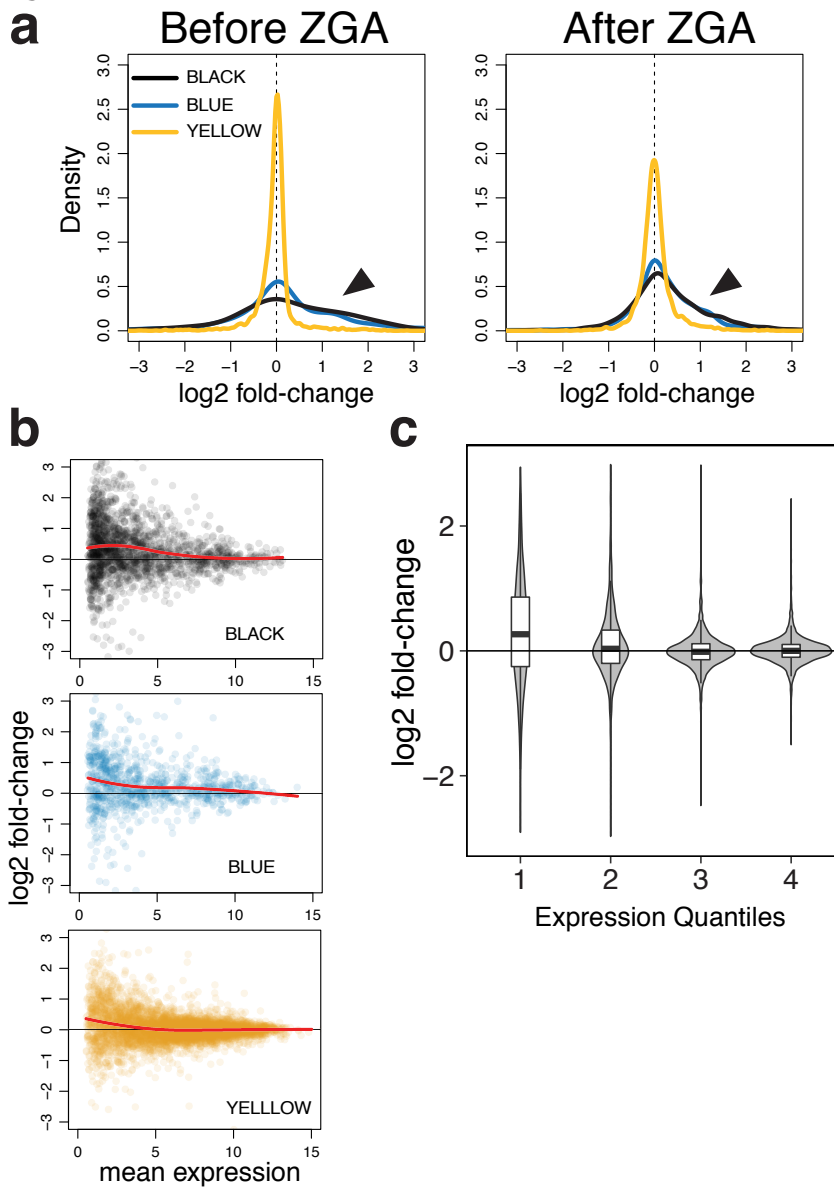
Figure 2.7 a. Density plots showing the distribution of $\log_2$ fold-changes (*Acf^C* vs *wild-type*) for genes within YELLOW, BLUE and BLACK chromatin domains. The two developmental stages are shown separately. Arrows highlight differences between inactive (BLUE/BLACK) and active (YELLOW) domains. **b.** Scatterplots showing the results of differential gene expression analysis in the context of the 5-state model. Each dot represents the $\log_2$ fold-change for each gene in relation to its mean expression (only the stage after ZGA is shown). Local regression fit is represented by red. **c.** Violin-boxplots showing $\log_2$ fold-change distributions for 4 different expression quantiles (only the stage after ZGA is shown) Figure from (217). Reprinted as permitted by the Creative Commons Attribution CC-BY 4.0 license.

Neither direct or anti-correlation could be observed for H3K9me3 or H3K4me3 (readouts for BLACK and BLUE states respectively) (**Figure 2.8b**, bottom panels). With a closer look at the correlation between mean gene expression and fold-change in the context of chromatin

domains, we noted an ACF1-dependent effect on low expressed genes also in the YELLOW active chromatin domain, reminiscent to what observed in similarly expressed genes in BLACK and BLUE domains (**Figure 2.7b**). Indeed, we found that the strength of upregulation determined by the absence of ACF1 is dependent on gene expression, regardless of the chromatin domain (**Figure 2.7c**).

Supported by our tethering experiments, we reason that ACF1 loss releases repression from genes that are generally lowly transcribed.
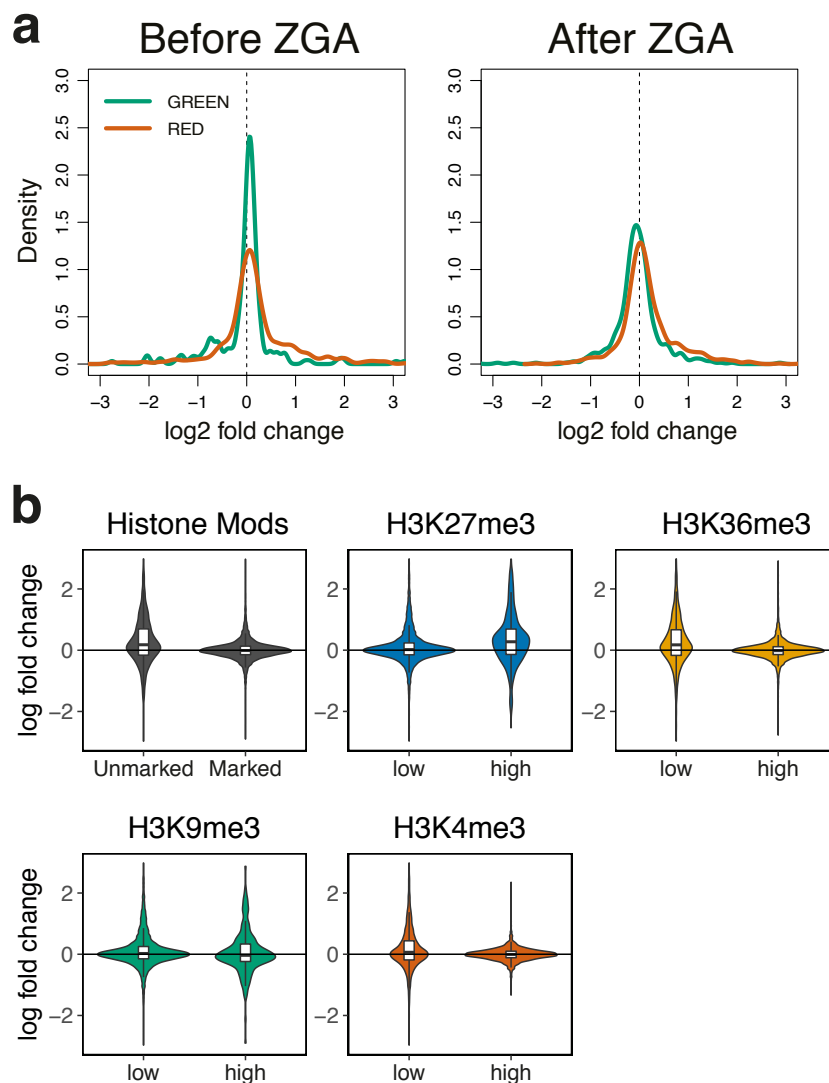

Figure 2.8 a. Density plots showing the distribution of log$_2$ fold-changes (*Acf^C* vs *wild-type*) for genes within GREEN and RED chromatin domains. The two developmental stages are shown separately. **b.** Violin-boxplots showing log$_2$ fold-change (*Acf^C* vs *wild-type*) distributions for genes within domains marked or unmarked by the histone marks analyzed (first panel), or within domains of high or low occupancy of H3K27me3, H3K36me3, H3K9me3, H3K4me3 (other panels). Figure from (217). Reprinted as permitted by the Creative Commons Attribution CC-BY 4.0 license.

2.4 CHRAC/ACF repress inactive chromatin by maintaining nucleosome regularity

Nucleosome sliding by CHRAC/ACF generate chromatin regularity *in vitro,* favoring optimal packing of DNA. We hypothesized that the transcriptional effects seen by ACF1 loss might be a consequence of alteration of such packaging, which can be derived by analysis of nucleosome spacing. To this end, we obtained and analyzed nucleosome maps from wild-type and *Acf[7]* embryos (223), and used an autocorrelation function applied to the nucleosome dyad signal to deduce global nucleosome regularity and spacing. The autocorrelation takes chromosome-wide nucleosome dyad densities and calculates the correlation between this signal and a stepwise-shifted copy of itself. The correlation coefficients calculated by this function are plotted in relation to the stepwise shift (lag) length. This method has been applied before to measure differences in nucleosome architecture at promoters (224) and to estimate nucleosome repeat length (NRL) (225). Genome-wide analysis revealed a significant dampening of autocorrelation amplitude and phasing in *Acf1[7]* embryos, indicating that loss of ACF1 decreases global regularity in nucleosome spacing with a concomitant increase in nucleosome repeat length (NRL = 188.4±0.7 bp and 195.3±1.5 bp for *wild-type* and *Acf[7]* respectively) (**Figure 2.9a**).
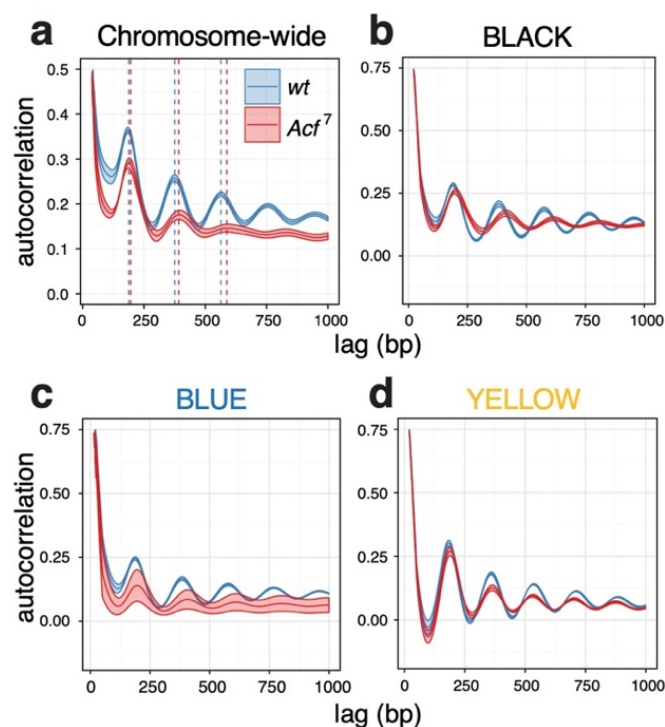
Figure 2.9 a. Plot representing the correlation coefficients for nucleosome dyads signals (chromosomes 2 and 3 combined) in relation to the stepwise shift (lag) as calculated by the autocorrelation function. Each line represents the replicate average SEM (n = 5 for *wild-type* and n=3 for Acf[7]) ± SEM. The centers of nucleosome positions are derived from the autocorrelation peaks and marked by dashed arrows **b., c., d.** Same as (a.) but for BLACK, BLUE and YELLOW chromatin domains. Figure from (217). Reprinted as permitted by the Creative Commons Attribution CC-BY 4.0 license.

Autocorrelation analysis within the context of the 5 chromatin states showed a dampening of the function in Acf^7 embryos within BLACK and BLUE domains but not in YELLOW domains (**Figure 2.9b-d**). We additionally found a chromatin state-specific increase in NRL for BLACK (NRL = 192.6±0.5 bp and 206.0±0.6 bp for wild-type and Acf^7 respectively) and BLUE (*NRL* = 192.2±0.6 bp and 201.0±2.5 bp for wild-type and Acf^7 respectively), but not for YELLOW (*NRL* = 182.0±0.5 bp and 184.0±1.2 bp, for wild-type and Acf^7 respectively) domains.

2.5 The role of CHRAC/ACF in γH2A.V dynamics

As discussed briefly in the introduction, some evidences suggest that the human ACF/CHRAC complexes might be involved in DNA damage response and repair. Initial observation from Dr. N. Steffen, a post-doc in the lab, suggested that also the *D. melanogaster* may be involved in such processes.

To systematically test whether *Acf* mutant embryos are more sensitive to DNA damage, we exposed 2-3.5h old wild-type (*OrR*) and Acf^C embryos to two different X-ray doses and measured how many of them hatched into larvae. At 10Gy only very few embryos survive in both strains. At 1Gy there is not a significant difference in sensitivity between wild-type and mutants (**Figure 2.10A, B**), suggesting a functional embryonic DNA repair pathway in the absence of ACF at a non-lethal X-ray dosage.
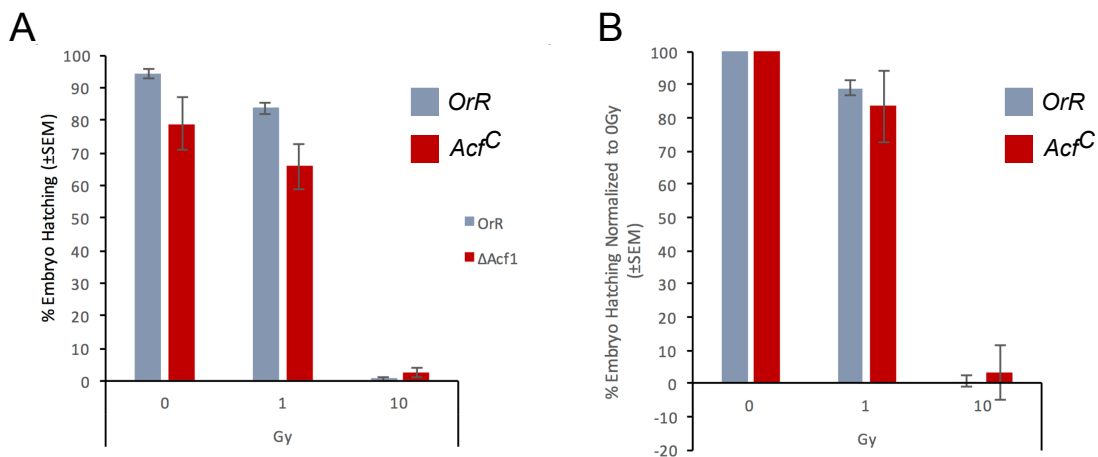
Figure 2.10 A. Hatching rate upon X-ray irradiation (0Gy, 1Gy or 10Gy) of 2-3.5h old embryos from wild-type (*OrR*) or *Acf* mutant (*Acf^C*) strains. Bars represent the average % Hatching (n=3 biological replicates, >50 embryos/replicate) ± SEM. **B.** Same as (A.) but values were normalized to the 0Gy condition.

This, however, doesn't exclude defects in other aspects of DNA damage response or repair, such as phosphorylated H2Av (γH2Av) appearance and turnover that may not result in phenotypic abnormalities. To address this, we monitored γH2Av dynamics is response to irradiation using immunofluorescence (IF). Briefly, 2-3.5h old *OrR* and Acf^C embryos were

exposed to 0Gy and 1Gy and collected 15 min or 3h after X-ray exposure. To ensure equal X-ray exposure, *OrR* and *Acf^C* embryos were exposed and processed at the same time. Upon irradiation with 1Gy there is a significant induction of γH2Av signal with a similar extent in both wild-type and mutant embryos, suggesting a mostly unaffected response to DNA damage in the absence of ACF. 3h after irradiation some of the *Acf^C* embryos retain a bit more γH2Av signal compared to wild-type (**Figure 2.11A**), but careful quantification across many embryos and different biological replicates revealed only a slight and non-significant difference of γH2Av signal between *OrR* and *Acf^C* embryos (**Figure 2.11B**).
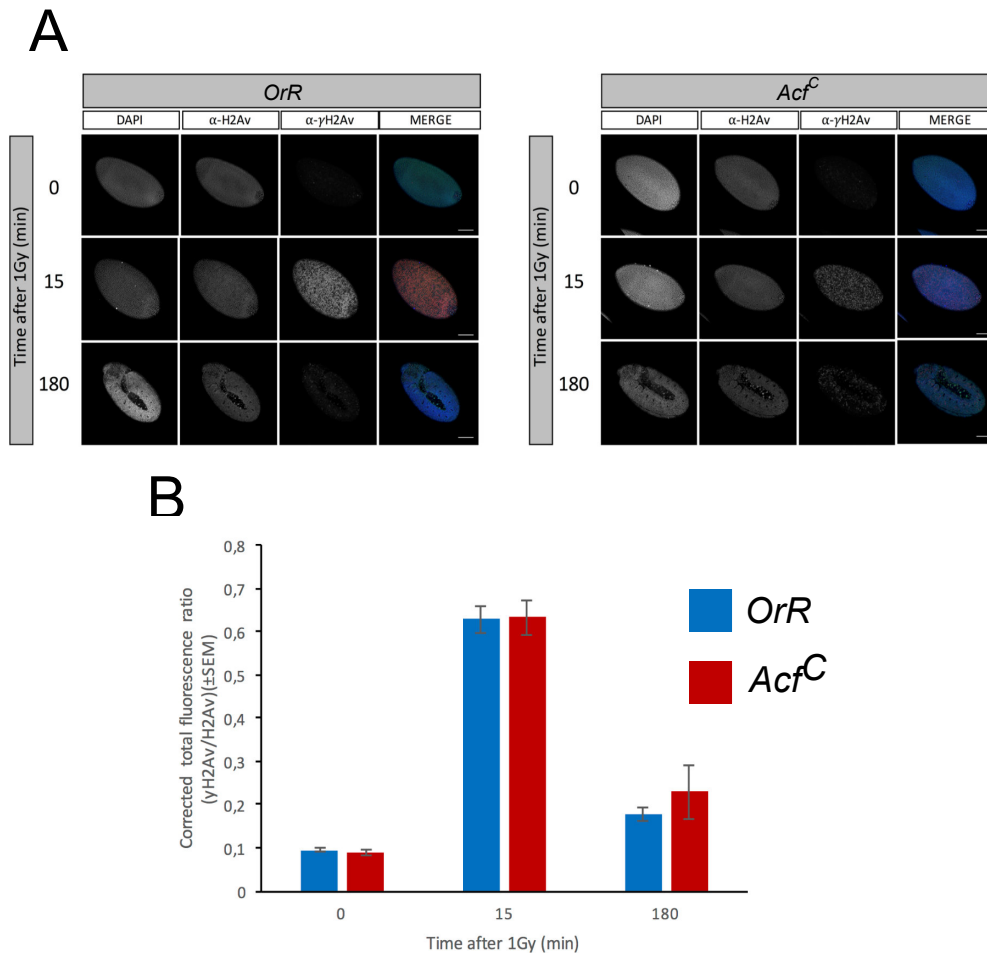
Figure 2.11 A. IF staining for H2Av and yH2Av. 2-3.5h old wild-type (OrR) and *Acf* mutant (*Acf^C*) isogenic embryos were irradiated (0Gy or 1Gy) and collected at 2 different time points after X-ray exposure (15 min and 180 min). **B.** Quantification of IF pictures. Bars represent the average fluorescence ratio between γH2A.V/H2A.V signals (n=3, >10 embryos per condition and replicate) ± SEM.

In conclusion, we weren't able to score any effect of ACF knock-out in terms of x-ray sensitivity and γH2Av dynamics. These results are in contrast with the ones obtained from similar experiments performed previously by Dr. N. Steffen.

2.6 Discussion

Since the concomitant and independent discovery of the nucleosome sliding complexes CHRAC (80) and ACF (84, 99), a main principle emerged from years of *in vitro,* biochemical studies: both remodelers improve the packaging of DNA by promoting the assembly/maintenance of regular chromatin fibers (6). How this concept translates *in vivo*? What is the function of the regularly spaced nucleosome arrays generated by CHRAC/ACF? The first analyses on *Acf* mutant flies showed phenotypic defects that might be attributed to alterations in large, and likely regular (226), chromatin structures such as heterochromatin and Polycomb domains (90, 100). Alteration of gene expression within such domains may follow these global defects in nucleosome organization or, alternatively, be a consequence of local re-arrangement of nucleosomes at specific promoters without a domain-wide alteration of chromatin structure. To this date, a systematic analysis of the contribution of CHRAC/ACF to transcription is lacking and needs to be clarified.

We tried to address this issue by careful experimental design. As the *Acf* mutant utilized in previous studies has later been shown to cause phenotypic effects distinct from loss-of-function (91), we generated a new precise *Acf* gene deletion that results in a complete null phenotype. To avoid confounding effects due to possible developmental delays in *Acf* mutant embryos, we analyzed and compared transcriptomes of single, stage matched wild-type and ACF1 null mutants. Lastly, we triangulated our findings using orthogonal and independent approaches.

We could show that CHRAC/ACF have indeed the potential to act as transcriptional repressors when artificially tethered. While a good symmetry could be observed in the transcription analysis of *Acf* mutant embryos, the extent of gene de-repression is nearly not as strong as anticipated by the tethering studies. This difference might be explained by the presence of other, functionally redundant, remodelers. For example, the RSF remodeling complex (227, 228), which also contains ISWI, can assemble and space nucleosomes similarly to CHRAC/ACF. The artificial targeting of ACF1 may force an increased local concentration of CHRAC/ACF at the tethering sites (229). Magnitude aside, the two different experiments yielded matched, complementary results.

Compared to HP1, our benchmark control for the high-throughput tethering system, ACF1 showed a surprisingly similar repressive strength. But, while the repressive potential of HP1 is rather unaffected by the chromatin context (220), the one of ACF1 is strongly modulated by the chromatin environment. It has been shown that Chd1 nucleosome remodeler can work if tethered (230), and we think this also applies to our case. The interaction of CHRAC/ACF remodelers with nucleosomes, however, is thought to be very transient - with only 1-3% of complexes being engaged with chromatin at any given time in interphase nuclei (231). Given the dynamic nature of this interaction, the repression may arise from local crowding of

CHRAC/ACF around the UAS[Gal] sites and not from allosteric regulation by the GAL4DBD. In other words, The GAL4DBD-UAS[Gal] might increase the residence time of CHRAC/ACF rather than affecting their remodeling rates. In fact, the overexpression of untargeted ACF1 mildly phenocopies its tethered counterpart in terms of selective effect on lowly expressed reporters. Our orthogonal study on *Acf* loss in developing embryos confirmed this context-dependency of CHRAC/ACF repression.

Using autocorrelation function, we measured a global contribution of CHRAC/ACF on genome-wide nucleosome regularity, despite possible redundancies with other ISWI-type remodelers. Once again, the effects of ACF1 depletion are intimately linked to inactive domains, with the correlation between the degree of physiological chromatin regularity and transcriptional repression, which we speculate to be causative.

Notably, we highlighted an important discrimination between two ISWI-type nucleosome sliding factor and their role in transcription. On the one hand, NURF (232, 233) is recruited to promoters by sequence-specific transcription factors to function as a co-activator (234). On the other hand, CHRAC/ACF are most likely not targeted to specific regions of the genome, such as promoters and enhancers (218), and should not be considered as canonical transcription co-factors (specifically co-repressors). These remodelers might, instead, function as general "maintainers" of physiological nucleosome structure, constantly working to ensure optimal compaction of chromatin through the formation of regular arrays during/after replication (90, 235) and DNA repair (103, 106). Their action establishes a repressive ground state of chromatin, with a low degree of accessibility due to efficient DNA packaging. Any additional layer of regulation, for example genes activation by recruitment of histone modifiers and more specific remodelers as well as the targeting of silencing machineries, works on top of the general naïve chromatin infrastructure provided by regular nucleosome arrays.

We weren't able to score any effect of ACF depletion in DNA damage response and repair, at least in terms of x-ray sensitivity and γH2Av dynamics. These results are in contrast with the ones obtained from similar experiments performed previously by Dr. N. Steffen. Two reasons might explain this discrepancy. First, the previous experiments used the *Acf[1]* strain, which is not a null mutant (see earlier discussion) and may generate gain-of-function phenotypes (91). Second, and perhaps more importantly, the experiments were not properly replicated and documented. Despite our negative results, we can still not exclude a role of CHRAC/ACF in DNA damage response or repair. As in the case of transcription, we predict it may likely be just a consequence of the general, non-specific activity of these nucleosome sliders.

3. RESULTS AND DISCUSSION – *Drosophila* SWR1 and NuA4 complexes are defined by DOMINO isoforms

In this work, we systematically characterized the molecular context and function of each DOM splice variant in *D. melanogaster* cell lines and assessed their contribution to the activity of the DOM.C in the context of transcription.

A preprint of the manuscript is available on *biorXiv* at:

https://www.biorxiv.org/content/10.1101/2020.02.10.939793v1.full

Supplementary tables are all available of *biorXiv*. Naming and numbering reflect the one available online.

The material reproduced here (figures) is in accordance with the Creative Common License (Attribution 4.0 International) and properly attributed throughout.

Peter B. Becker and I conceived the project and designed the experiments. I performed all the experiments except the mass-spectrometry of affinity purified DOM-A and DOM-B, which was done by Alexander Reim (sample preparation and measurements). Zivkos Apostolou helped performing some of the experiments. Silke Krause greatly helped in the production of proteins for generation of antibodies (see also the Appendix section). I analyzed all the data except the ones from RNAseq, which was analyzed by Tamas Schauer. Patrick Heun provided help and supervision in establishing the CRISP/Cas9 editing methodology in *Drosophila* cells and Aline Campos helped in clonal isolation and expansion. Peter B. Becker and Michael Wierer provided supervision.

Once again, I refer to myself and my collaborators as "we" throughout this section (unless stated otherwise) to highlight a strong team effort.

3.1 DOM-A and DOM-B, define two distinct DOM complexes

DOM-A and DOM-B, the two protein isoforms originating from the *dom* gene, are identical at their N-termini that contain an HSA domain and an ATPase domain typical of the INO80-like family (**Figure 3.1**). The two splice variants differ in their C-termini. The longer DOM-A isoform is characterized by the presence of a SANT domain and a Poly-glutamine (Poly-Q) enriched domain at its C-terminus. The shorter DOM-B isoforms does not contain, at its C-terminus, domains recognizable by sequence similarity with the ones commonly annotated.
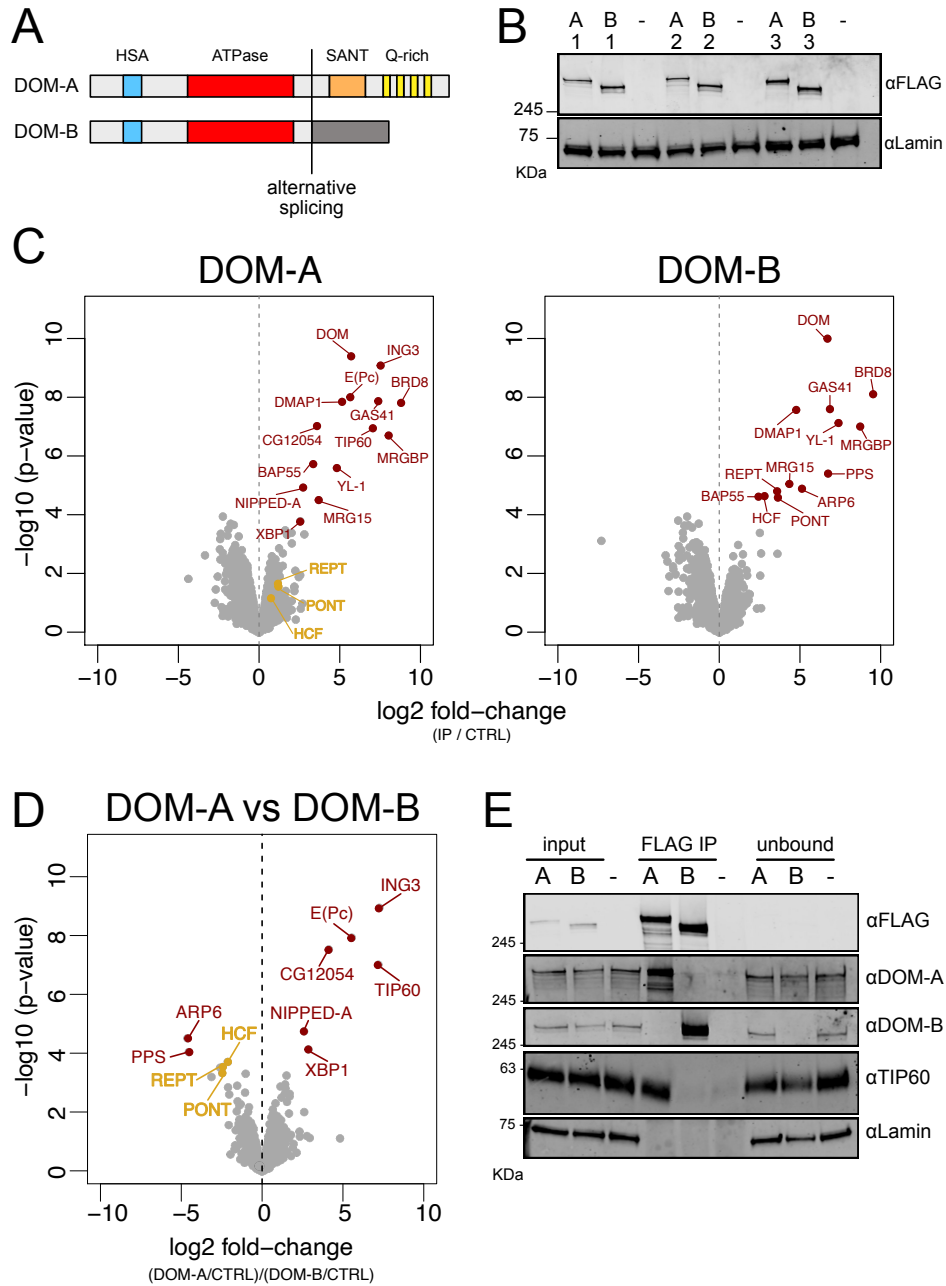
Figure 3.1 A. Protein domain schematic of DOMINO isoforms (DOM-A and DOM-B). **B.** Nuclear fractions from 3 different S2 cell clones edited with CRISPR/Cas9 for the expression of 3XFLAG tagged DOM-A (A) and DOM-B (B). Edited proteins are recognized by Western blot using the FLAG antibody. Nuclear extracts from unedited S2 cells were used as control. Lamin: loading control. **C.** Volcano plot showing the results of the FLAG immunoprecipitation (IP) coupled to mass spectrometry. Each dot represents the -log10 p-value for the given protein measured in relation to its average log2 fold-change (IP/CTRL) (n=3 biological replicates). IP: FLAG pulldowns from 3X FLAG tagged cells (DOM-A or DOM-B). CTRL: FLAG pulldowns from untagged cells. Significantly enriched proteins (FDR < 0.05 and log2 fold-change > 0) are marked by red dots. Yellow dots represent proteins significantly enriched in the DOM-B pulldown but do not meet the criteria for being classified as DOM-B specific interactors (see text). **D.** Same as (C.) but directly comparing DOM-A and DOM-B pulldowns. Log2 fold-change > 0 indicates enrichment in DOM-A pulldown. The opposite indicates enrichment in DOM-B pulldown. Yellow dots represent proteins significantly enriched in the DOM-B pulldown but do not meet the criteria for being classified as DOM-B specific interactors (see text). **E.** Western blot validating the results from the mass spectrometry experiment. The corresponding antibody was used to detect each protein. Figure from (236). Reprinted as permitted by the Creative Commons Attribution CC-BY 4.0 license.

Given these differences, we asked if the two isoforms might interact with different proteins or, more dramatically, form entirely different complexes. Since overexpression of tagged proteins - an approach wildly utilized in *D. melanogaster* (237) - might alter the stoichiometry of interactions, we decided to tag DOM isoforms using CRISPR/Cas9 to ensure purification from endogenous expression levels. We separately edited the C-terminus of DOM-A and DOM-B by inserting a 3XFLAG tag in *D. melanogaster* embryonic S2 cells and obtained 3 distinct clonal populations for each isoform (3 homozygous clones for DOM-A, 2 homozygous and 1 heterozygous clone for DOM-B) (**Figure 3.2**).
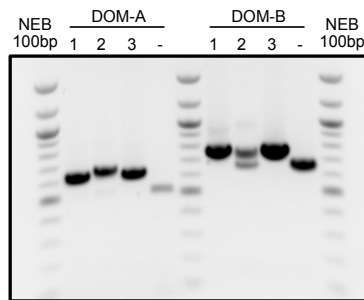
Figure 3.2 The editing of DOM-A and DOM-B C-termini is verified by PCR amplification followed by agarose gel electrophoresis. The insertion of a 3XFLAG tag by CRISPR/Cas9 results in a longer (72bp) PCR product than the control (unedited cells, CTRL). Heterozygous clones show two bands. NEB 100 bp ladder is used as a size marker. Figure from (236). Reprinted as permitted by the Creative Commons Attribution CC-BY 4.0 license.

All clones isolated and verified by PCR show expression of 3XFLAG tagged proteins with correct size and with similar expression levels for both isoforms (**Figure 3.1B**). To reduce the chances of purifying non-specific interactors, and to enrich for the the strongest and most stable ones, we prepared nuclear fractions and performed FLAG immunoprecipitation under stringent conditions. Mass-spectrometry analysis of affinity purified DOM-A and DOM-B identified 13 and 12 significantly enriched interactors (q-value < 0.05 and log2 fold-change > 0) respectively (**Figure 3.1C**, Supplementary Table 1). BAP55, BRD8, DMAP1, GAS41 MRG15, MRGBP and YL-1 are common between DOM-A and DOM-B and were previously characterized as DOM interactors (133). Two interactors expected to be common, PONT and REPT, show a stronger association with DOM-B than with DOM-A (log2 DOM-A IP/ CTRL = 1.19 and 1.16, FDR = 0.373 and 0.338 respectively). A newly identified DOM-B interactor, HCF, also interacts less strongly DOM-A (log2 DOM-A IP/ CTRL = 0.70, FDR = 0.466). Notable differences were found by directly comparing DOM-A and DOM-B pulldowns (**Figure 3.1D**). Amongst the interactors that are enriched only in the DOM-A pulldown, three are particularly interesting: ING3, E(Pc) and TIP60. The yeast orthologs of these proteins constitute the acetyltransferase module of the yeast NuA4.C. The yeast ortholog of NIPPED-A, another interactor specific for DOM-A, is also a component of NuA4.C. Lastly, we found two more proteins that associate only with DOM-A: XBP1 and CG12054. Both are

transcription factors and were not described before as component of DOM complex. DOM-B specific interactors appear to be only two, both of them not identified in previous studies: PPS and ARP6. The function of ARP6 is not known in *Drosophila,* but its yeast ortholog is part of the SWR1.C and it is essential for H2A.Z incorporation (140). We validated the DOM-A/Tip60 interaction by raising new monoclonal antibodies against Tip60 and confirming its interaction with DOM-A by co-immunoprecipitation coupled to Western blot (**Figure 3.1E**). The same experiment indicates that DOM-A and DOM-B might be included in separate complexes, at least under these conditions, as they don't interact with each other. We sought to investigate the functional relevance of this physical separation of isoform-specific DOM complexes.

3.2 DOM-A and DOM-B are not redundant and show specific effects on transcription

Previous observations in flies (147, 238) suggest that the two DOM isoforms are not redundant and may not depend on each other for functionality. Along this line, isoform-specific knock-down of DOM variants by RNAi in *D. melanogaster* embryonic Kc167 cells showed that knock-down of one isoform doesn't cause reduction of the other and *vice versa* (**Figure 3.3A**).
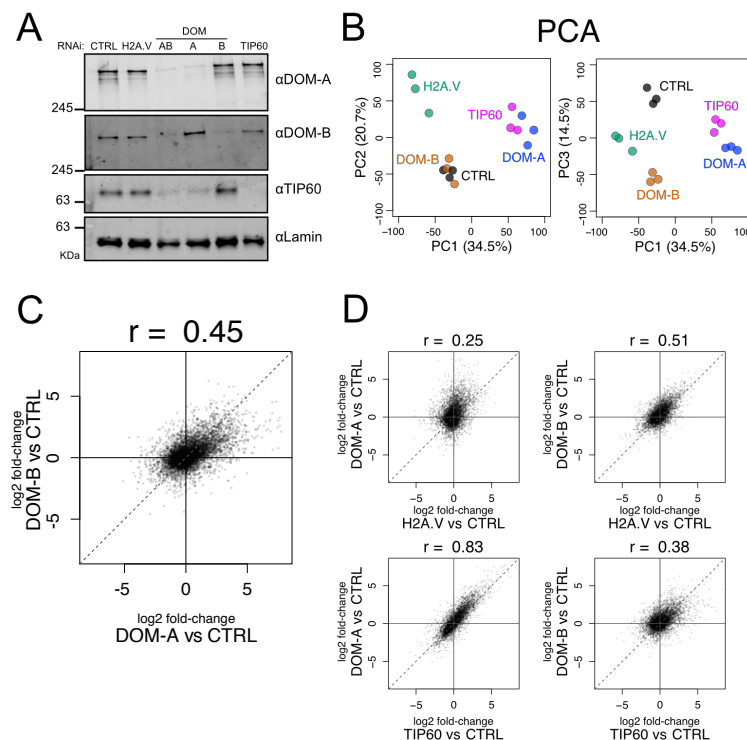
Figure 3.3 A. Nuclear extracts from Kc167 cells treated with the dsRNAs (RNAi) shown in the figure were analyzed by Western blot and proteins were probed using with their corresponding antibodies. Lamin: loading control. **B.** Transcriptomes from Kc167 cells treated with dsRNAs described in the figure were subjected to Principal Component Analysis (PCA). Individual replicates are shown. Three components (PC1, PC2 and PC3) and their percentage of variance (in parenthesis) are shown. **C.** Scatter plot comparing gene expression changes (expressed as log2 fold-changes) between DOM-A and DOM-B knock-down (both relative to control). Individual genes are shown (N=10250). Spearman's correlation coefficient (r) is reported. **D.** Same as (c.) but comparing DOM-A or -B to H2A.V or TIP60 knock-downs (all relative to control). Figure from (236). Reprinted as permitted by the Creative Commons Attribution CC-BY 4.0 license.

Interestingly, an expected functional association between DOM-A and Tip60 could be scored: knock-down of DOM-A strongly reduces Tip60 protein levels but not its mRNA expression (**Figure 3.4A**), suggesting that TIP60 may necessitate of DOM-A for its stability (**Figure 3.3A**). Since both DOM isoforms could potentially be implicated in transcription as their yeast homologs SWR-1 and NuA4 (239, 240), we assessed the transcriptional effects of DOM-A and DOM-B depletion by RNAseq. We also included knock-downs of H2A.V and TIP60. As expected, all the different knock-downs show significant perturbations of gene expression, with notable differences amongst the different proteins (**Figure 3.4B,** Supplementary Table 2). Distinct clustering of transcriptome responses to the loss of DOM-A or DOM-B is observed by Principal Components Analysis (PCA) (**Figure 3.3B**). Differential gene expression analysis also confirmed differences upon isoform-specific loss (**Figure 3.3C**). Interestingly, while transcriptional perturbations caused by knock-down of DOM-A are very similar to the ones caused by depletion of Tip60, a smaller correlation is observed with H2A.V knock-down (**Figure 3.3B,D**).
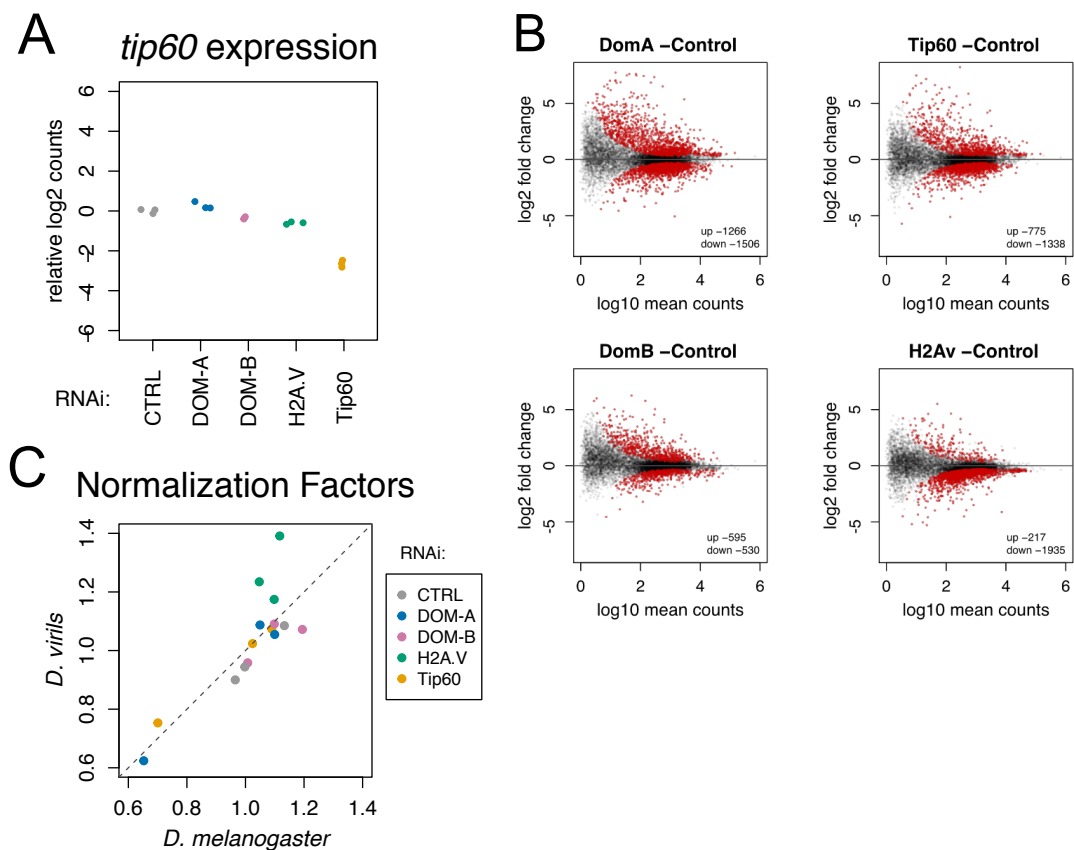
Figure 3.4 A. Plot showing *tip60* mRNA expression, measured by RNAseq, upon dsRNA treatments (RNAi) shown on the x-axis. Individual replicates are shown. **B.** Results of differential gene expression analysis between DOM-A, DOM-B, TIP60 and H2A.V knockdown and control. Each dot represents the log$_2$ fold-change for each gene in relation to its mean expression (log10 mean counts) (N=10250). Genes significantly mis-regulated (adjusted p-value <0.01) are labeled in red. **C.** Comparison of normalization factors calculated from the *D. melanogaster* or the *D. virils* (spike-in) genome used to scale transcriptomes. A deviation from the diagonal line indicates global changes in transcription. Individual replicates are shown. Color coding indicates the dsRNA treatment (RNAi) for each sample. Figure from (236). Reprinted as permitted by the Creative Commons Attribution CC-BY 4.0 license.

The transcriptional response upon knock-down of DOM-B, on the other hand, correlates more with H2A.V than Tip60. Notably, we could observe global transcription down-regulation upon H2A.V knock-down thanks to the use of *D. virilis* spike-ins (higher value of *D. virilis* normalization factors, see methods) (**Figure 3.4C).**

The depletion of one or the other splice variant of DOM causes gene expression perturbations that are, for the most part, specific for each isoform. The partial overlap of gene mis-regulation upon DOM-B and H2A.V depletions drove us to further investigate the relationship between the remodeler and the variant.

3.3 The DOM-B complex is the main ATP-dependent remodeler for H2A.V

Being SWR1-type remodelers, both DOM isoforms are expected to contribute to H2A.V deposition/exchange into chromatin. We decided to look if and how much global H2A.V levels are perturbed upon isoform-specific knock-downs by probing nuclear fractions that contain both soluble nuclear proteins and insoluble chromatin (see methods). We observed that H2A.V was strongly reduced by DOM-B depletion (**Figures 3.5A and 3.6A**), while its mRNA level was unchanged (**Figure 3.6B**).
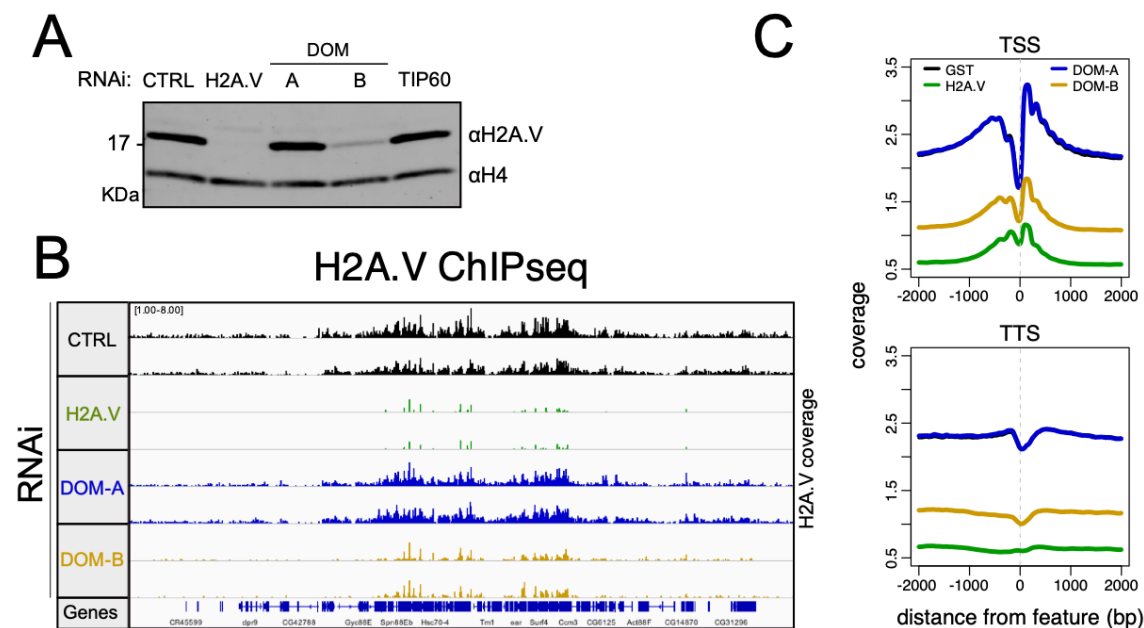
Figure 3.5 A. H2A.V levels in nuclear extracts from Kc167 cells treated with the dsRNAs (RNAi) shown in the figure were analyzed by Western blot using a specific antibody against H2A.V. Histone H4 (H4): loading control. **B.** Snapshot of spike-in and input normalized H2A.V ChIPseq signal along a region of Chromosome 3R. dsRNA treatments are color coded and indicated in the figure. Individual replicates are shown. **C.** Average spike-in and input normalized H2A.V signal around Transcription Start and Termination Sites (TSS and TTS respectively) across all genes analyzed (N=10139 genes, n=2 biological replicates). Figure adapted from (236). Reprinted as permitted by the Creative Commons Attribution CC-BY 4.0 license

We also conducted a small-scale RNAi screen targeting some of the interactors identified by our affinity purification analysis and found that only depletion of ARP6 reduced the levels of H2A.V comparably to DOM-B knock-down (**Figure 3.6C**). H2A.V was surprisingly not

affected by depletion of DOM-A, TIP60 or other DOM-A-specific subunits (**Figure 3.5A**, **Figure 3.6A,C**).
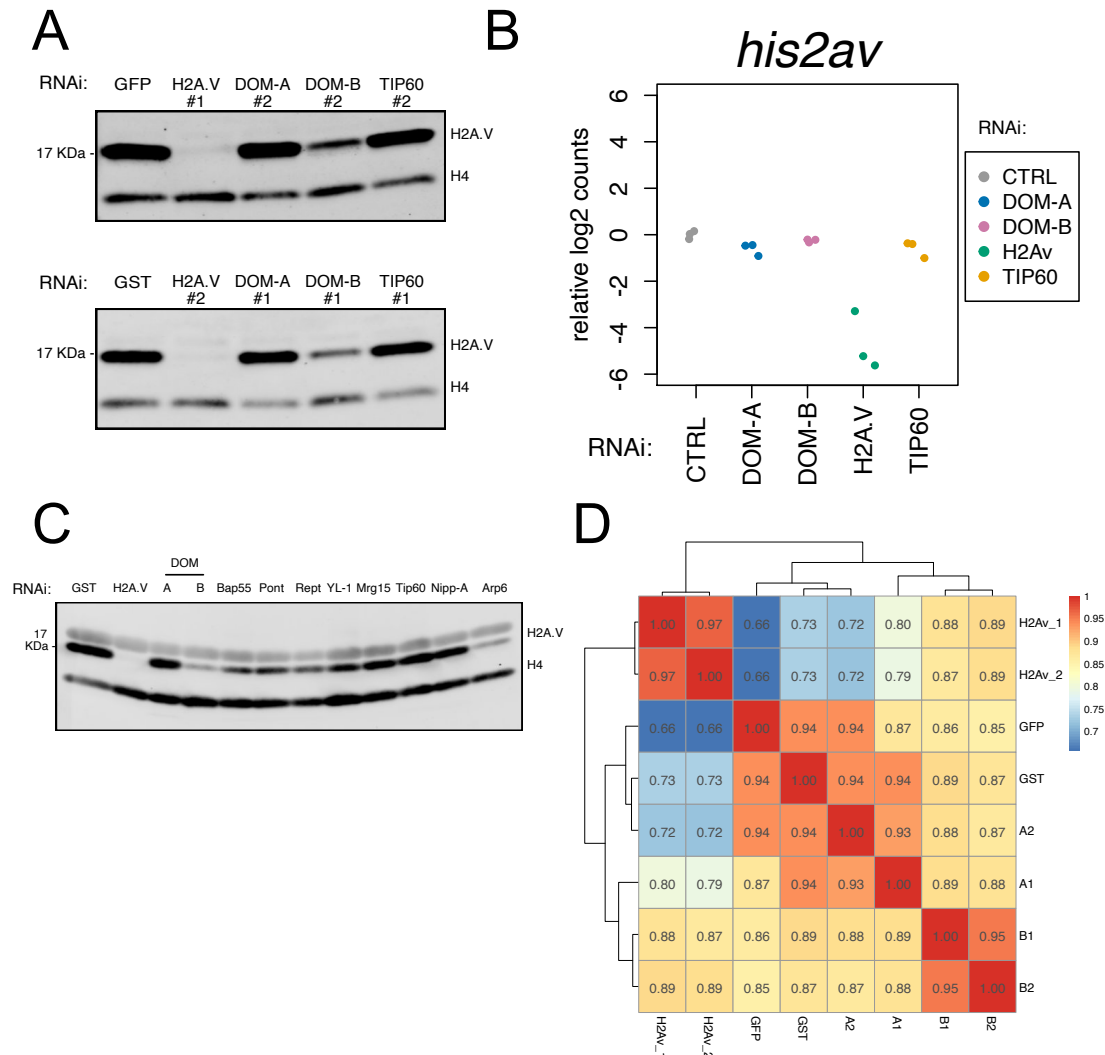
Figure 3.6 A. H2A.V levels in nuclear extracts from Kc167 cells treated with the dsRNAs (RNAi) shown in the figure were analyzed by Western blot using a specific antibody against H2A.V. Replicates of Figure 3.4A Histone H4 (H4): loading control. **B.** Plot showing *his2av* mRNA expression, measured by RNAseq, upon dsRNA treatments (RNAi) shown on the x-axis. Individual replicates are shown. **C.** Same as (A.) but with additional dsRNAs treatments targeting DOM interactors identified by affinity purification and mass spectrometry. **D.** Heatmap showing Spearman's correlation between H2A.V ChIPseq biological replicates and conditions. Correlation values, calculated on normalized average coverage signal around the TSS, are shown. Clustering is based on Euclidean distance. Individual samples are shown. Figure adapted from (236). Reprinted as permitted by the Creative Commons Attribution CC-BY 4.0 license.

We could not, however, exclude small local changes in H2A.V caused by DOM-A depletion, like the ones happening at promoters, which would be difficult to score by western blot. We decided to employ a more sensitive, ChIPseq-based approach to assess H2A.V changes on chromatin (see methods)(241). We measured a significant reduction of H2A.V levels along the whole genome upon knock-down of DOM-B, especially at promoters and transcriptional termination sites (**Figures 3.5B,C and Figure 3.6D**), in line with results obtained before by Western blot. Again surprisingly, RNAi of DOM-A (or Tip60) has only very little effect on

H2A.V, even at Promoters or Transcriptional Termination Sites (**Figure 3.5B,C**). These observations suggested that DOM-B might be indeed the main remodeler for H2A.V. As remodelers like SWR1 require cycles of ATP binding and hydrolysis to incorporate H2A.Z (70, 242), we wanted to test if DOM-B incorporates H2A.V *in vivo* in an ATP-dependent manner. We designed a complementation strategy, based on RNAi, in which we in which we replace the endogenous DOM-B gene with GFP-tagged wild-type or putative ATP-binding deficient (K945G)(138, 242) DOM-B (**Figure 3.7A**).

Condition	Rescue construct	Comparison	p-value
#1	DOM-B_WT	DOM-B vs CTRL RNAi	0.0001
#2	DOM-B_KG	DOM-B vs CTRL RNAi	0.0942
#3		Condition #1 vs #2	0.0025
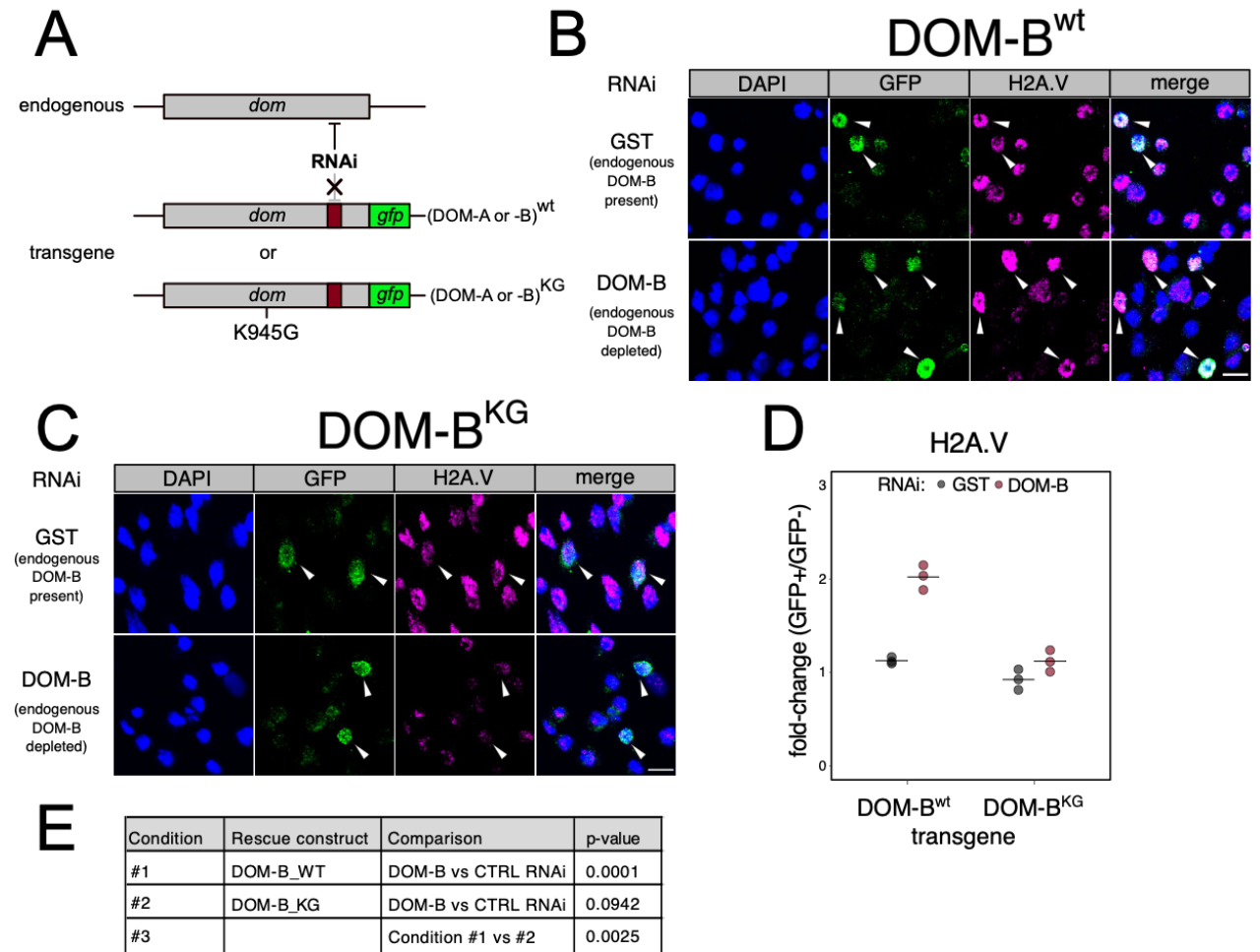
Figure 3.7 A. Experimental design to test if DOM-A or -B require ATP for their function. Description in main text **B.** Representative immunofluorescence image showing the results of DOM-B complementation assay as described in (A.). In cells treated with dsRNA targeting GST, the endogenous copy of DOM-B is present. In cells treated with dsRNA against DOM-B (endogenous DOM-B depleted) only the transgene is expressed. Cells were stained GFP and H2A.V antibodies. DNA was stained with DAPI. Arrows denote cells in which the transgene is expressed and localizes to the nucleus. Scale bar: 10 µm **C.** Same as (B.) but for DOM-B K945G mutant **D.** Quantification of the immunofluorescence-based complementation assay. Individual replicate measures, corresponding to the fold-change of mean H2A.V signal between GFP-positive and GFP-negative cells (> 100 total cells/replicate), are shown as dots. dsRNA treatments are color coded and DOM-B transgenes are compared **E.** Table reporting p-values (linear regression) for the comparisons in (D.). Figure adapted from (236). Reprinted as permitted by the Creative Commons Attribution CC-BY 4.0 license.

We employed immunofluorescence to score the levels of H2A.V in cells in which the transgene is expressed. As a positive control for our experimental strategy, we could score

the expected rescue of H2A.V levels in cells complemented with a wild-type DOM-B transgene (**Figure 3.7B**). However, we didn't observe the same effect with the mutant transgene (**Figure 3.7C**). We quantified our immunofluorescence images and compared the mean H2A.V signal between GFP positive cells (GFP+, expressing the transgene) and GFP negative cells (GFP-, not expressing the transgene). The analysis confirmed that the ATPase mutant DOM-B could not restore H2A.V levels (**Figures 3.7D,E**), indicating that the DOM-B.C is incorporating H2A.V in an ATP-dependent manner.

3.4 The DOM-A complex is the *Drosophila* NuA4 and catalyzes H4K12 acetylation

Despite sharing extensive homology with DOM-B, including the catalytic domain, DOM-A seems not to be involved in H2A.V incorporation. While we couldn't entirely exclude its involvement in H2A.V incorporation/exchange under particular conditions such as DNA damage (133), we had to reconsider a model in which DOM-A acts as an H2A.V remodeler. The transcriptional responses caused by TIP60 and DOM-A knock-downs showed very high correlation, suggests a physical association with functional relevance. Our mass-spectrometry analysis indicates that several components of the DOM-A.C have orthologs in the the yeast NuA4.C. The central subunit of NuA4.C, Eaf1, doesn't contain an ATPase domain but shares homology, in the N-term HSA domain and C-terminal SANT domain, with DOM-A. We wondered if DOM-A.C might be indeed a novel, previously uncharacterized *Drosophila* NuA4 complex. (**Figure 3.8A**). As NuA4.C acetylates histones, we looked if H3 and H4 acetylation state changes upon depletion of DOM-A or TIP60 by targeted mass-spectrometry. We included DOM-B and H2A.V knock-down as controls. We measured a specific reduction of H4K12ac (average 28.9% reduction) and, to a lesser extent, H4K5ac (average 23.1% reduction) (**Figures 3.8B**,**C**) specifically after DOM-A knock-down. Our analysis showed that RNAi against DOM-A, but not against DOM-B, specifically reduces. Importantly, the effect of DOM-A RNAi on H4K12ac and H4K5ac is very similar to Tip60 RNAi (average 36.3% reduction for H4K12ac, average 16.4% reduction for H4K5ac) (**Figures 3.8B**,**C**). Interestingly, we observe some effects on the H3K27me3 mark, of which DOM-A/Tip60 knock-down causes a small but reproducible increase (**Figure 3.8D,E**). No specific perturbation is observed for H4 methylation (**Figure 3.7F).**
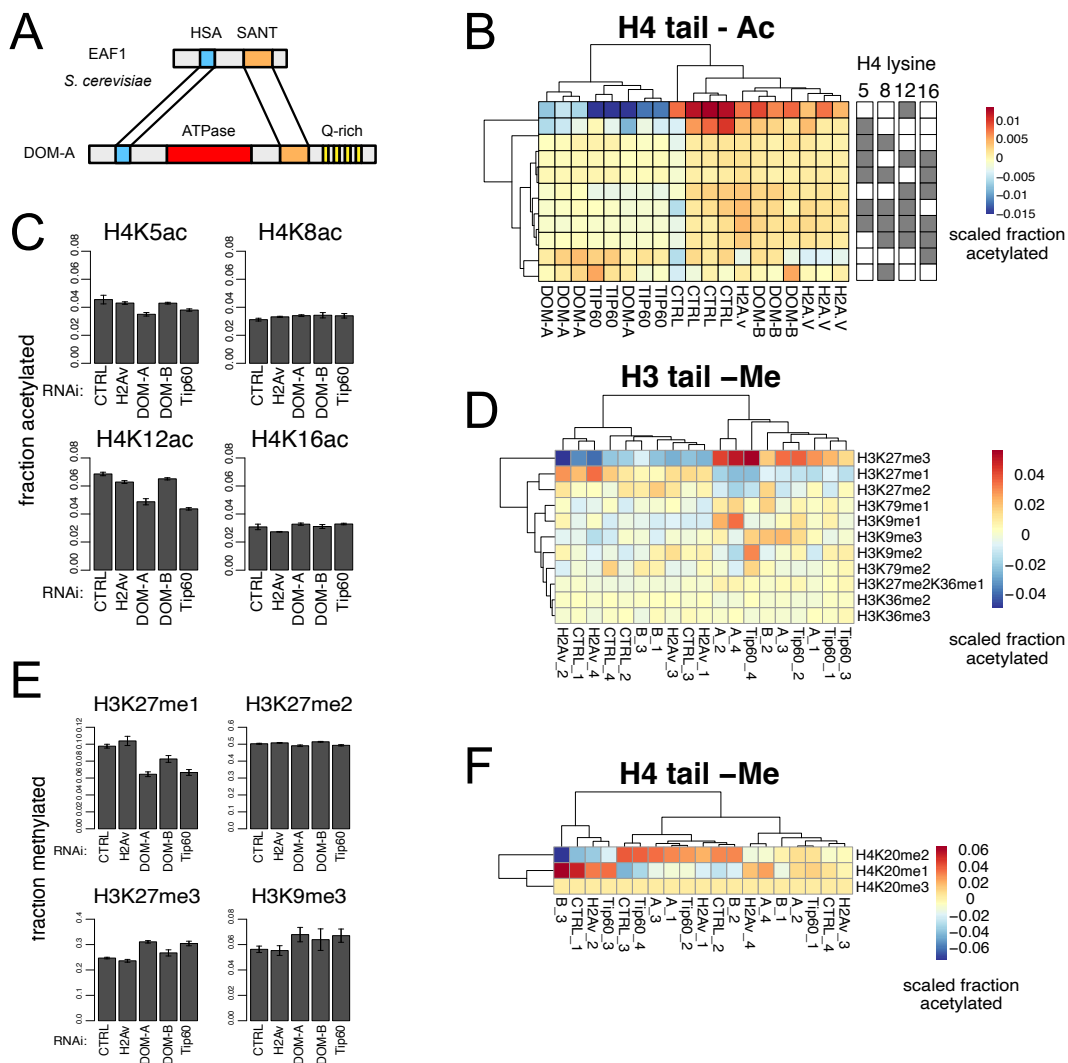
Figure 3.8 A. Comparison of domain organization between of *S. cerevisiae* Eaf1 and *D. melanogaster* DOM-A. **B.** Heatmap showing scaled acetylation levels for H4K5, K8, K12, K16 and combinations of them in Kc167 cells treated with dsRNA (RNAi) shown in the figure. Individual biological replicates are shown. Rows and columns are clustered based on Euclidean distance. **C.** Plots showing changes in acetylation levels for H4K5, K8, K12 and K16 in Kc167 cells treated with dsRNAs (RNAi) shown in the figure. Bars represent average fraction of acetylated peptide (over non-acetylated) (n=3 for B, n=4 for all the others) ± SEM. **D.** Same as (B.) but for methylation of H3K9, K27, K36 and combinations **E.** Same as (C.) but for H3K27me1/2/3 and H3K9me3. **F.** Same as (B.) but for methylation of H4K20. Figure adapted from (236). Reprinted as permitted by the Creative Commons Attribution CC-BY 4.0 license.

As H4K12ac seems to be the residue most prominently affected by DOM-A/Tip60, we decided to look at whether the mark is affected on chromatin using the same ChIPseq-based approach we previously developed for H2A.V. We could see a reduction of H4K12ac signal in many genomic loci upon DOM-A/Tip60 RNAi compared to the control, but in some regions the mark seems to be unaffected by the knock-down (**Figure 3.9A,B,C).** Comparison between H4K12ac and gene expression showed that genes downregulated in DOM-A or TIP60 knock-downs tend to have higher basal H4K12ac at promoters (**Figure 3.9D**). The

reduction of H4K12ac by DOM-A or TIP60 knock-down, however, seems not to be specific for the correspondingly regulated genes (**Figure 3.9E,F**) By contrast, DOM-B and H2A.V RNAi cause an unexpected increase in H4K12ac signal in many of the regions where we observed H4K12ac loss upon DOM-A/Tip60 RNAi (**Figure 3.9A,B**), as if the reduction of DOM-B and/or its substrate H2A.V allowed for more DOM-A activity.
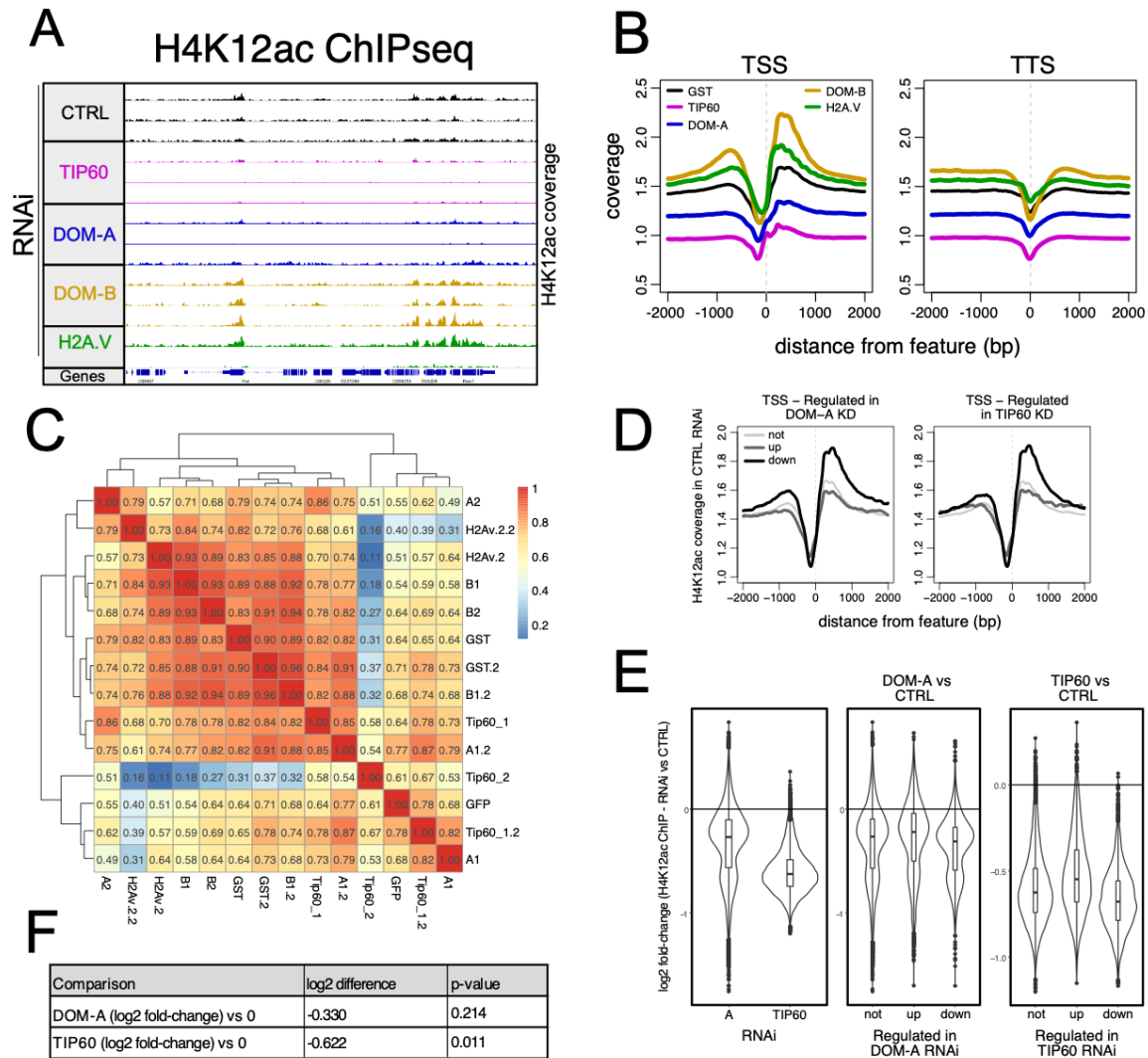
Figure 3.9 A. Snapshot of spike-in and input normalized H4K12ac ChIPseq signal along a region of Chromosome 3R. dsRNA treatments are color coded and indicated in the figure. Individual replicates are shown. **B.** Average spike-in and input normalized H4K12ac signal around Transcription Start and Termination Sites (TSS and TTS respectively) across all genes analyzed (N=10139 genes, n=3 biological replicates except n=2 for H2A.V RNAi). **C.** Heatmap showing Spearman's correlation between H4K12ac ChIPseq biological replicates and conditions. Correlation values, calculated on normalized average coverage signal around the TSS, are shown. Clustering is based on Euclidean distance. Individual samples are shown. **D.** Composite plot showing spike-in and input normalized H4K12ac coverage around Transcription Start Sites (TSS) for genes not-regulated (not), up-regulated (up), downregulated (down) in the knockdown of DOM-A (left panel) or TIP60 (right panel) (N provided in Figure 3.4B). Each line represents the average coverage (n>2 biological replicates) of H4K12ac in Kc167 cells treated with dsRNA against GST. **E.** Violin-boxplot showing log2 fold-change in H4K12ac signal (averaged across a 4000bp window around the TSS) between DOM-A or TIP60 and control RNAi. In the left panel, all genes are considered (N= 10139). In the central and right panels, genes are divided in not-, up- and down-regulated classes as in (G.). **F.** Table listing calculated p-values (one-sample t-test, two sided) for the differences shown in the left panel of (H.). n=3 biological replicates are considered. Each replicate is a single value representing the median of log2 fold-change across all genes analyzed. Figure adapted from (236). Reprinted as permitted by the Creative Commons Attribution CC-BY 4.0 license.

As the yeast NuA4.C doesn't not require ATP to acetylate histones, we wondered if the H4K12ac catalyzed by the DOM-A.C might be also independent of ATP. We utilized again the same experimental strategy for complementation we employed for DOM-B, this time comparing wild-type and putative ATP-binding mutant DOM-A (**Figure 3.7A**) and their ability to restore H4K12ac levels. As for DOM-B, we could score the expected rescue of H4K12ac levels in cells complemented with a wild-type DOM-A transgene (**Figure 3.10A**). Contrary to DOM-B, however, we observe the same rescue with the mutant transgene (**Figure 3.10B**). We quantified once again our immunofluorescence images and compared the mean H4K12ac signal between GFP+ (transgene present) and GFP- (transgene absent). The analysis confirmed that both the wild-type and the mutant transgene could restore H4K12ac levels (**Figures 3.10C,D**), indicating that the DOM-A.C can catalyze H4K12ac without the need for ATP binding.
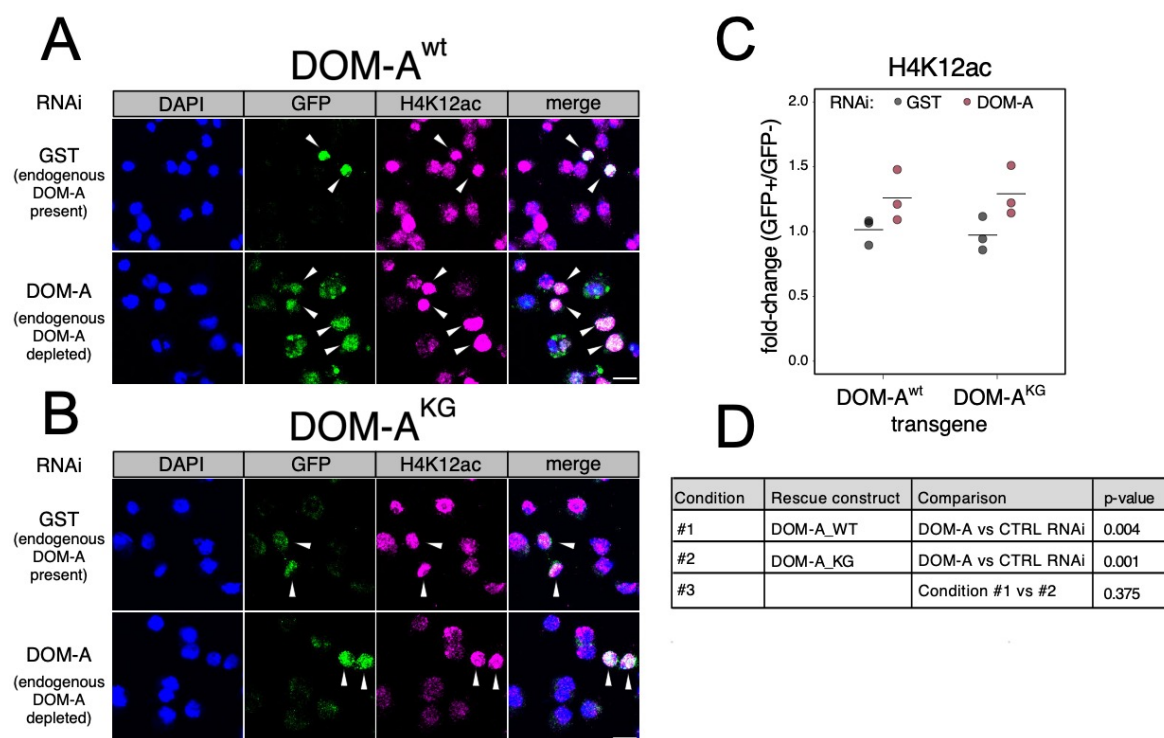
Figure 3.10 **A.** Representative immunofluorescence image showing the results of DOM-A complementation assay as described in (A.). In cells treated with dsRNA targeting GST, the endogenous copy of DOM-A is present. In cells treated with dsRNA against DOM-A (endogenous DOM-A depleted) only the transgene is expressed. Cells were stained with GFP and H4K12ac antibodies. DNA was stained with DAPI. Arrows denote cells in which the transgene is expressed and localizes to the nucleus. Scale bar: 10 μm **B.** Same as (A.) but for DOM-A K945G mutant **C.** Quantification of the immunofluorescence-based complementation assay. Individual replicate measures, corresponding to the fold-change of mean H4K12ac signal between GFP-positive and GFP-negative cells (> 100 total cells/replicate), are shown as dots. dsRNA treatments are color coded and DOM-A transgenes are compared **D.** Table reporting p-values (linear regression) for the comparisons in (C.). Figure adapted from (236). Reprinted as permitted by the Creative Commons Attribution CC-BY 4.0 license.

3.5 Preliminary functional characterization of mammalian EP400 and SRCAP complexes

Our work on the *Drosophila* DOM.C make extensive parallelisms with the yeast SWR1.C and NuA4.C. We wondered whether such a diversification might be extended further to the mammalian complexes EP400 and SRCAP. Based on our prediction, EP400 should be the NuA4.C/DOM-A.C responsible for histone acetylation, while SRCAP should be dedicated to H2A.Z incorporation as SWR1.C/DOM-B.C (see discussion later).

To test this hypothesis, we decided to knock-down EP400, SRCAP, KAT5 (TIP60) and H2A.Z.1 with siRNAs in human osteosarcoma cell lines (U2-OS) and score effects on H2A.Z and H4K16ac by western blot. We chose H4K16 as it is known to be the target of KAT5 acetylation (180). Similar to the Drosophila situation, SRCAP seems to be the major complex responsible for maintaining H2A.Z levels (**Figure 3.11**). H2A.Z levels are not reduced completely by H2A.Z.1 knock-down because the siRNAs used don't target the H2A.Z.2 isoform (same size as H2A.Z.1, recognized by the antibody)
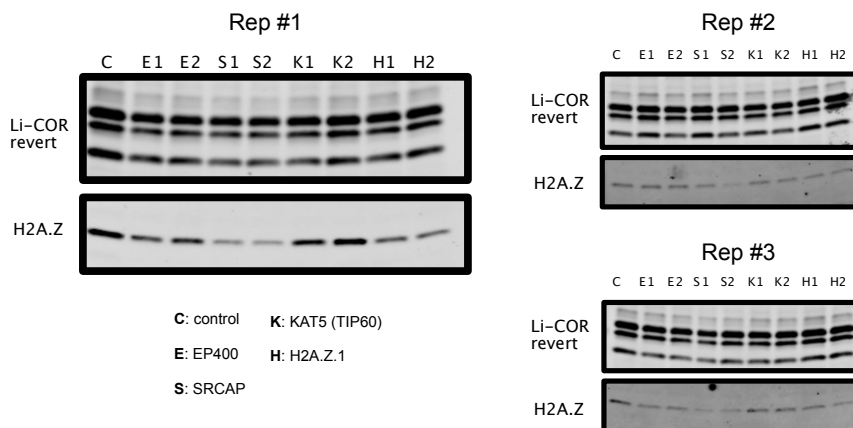
Figure 3.11 Assessing the effects of various knock-down on H2A.Z levels in U2-OS cells. Staining with li-COR revert used as loading control. Nuclear extract was probed with H2A.Z antibody. Blots for replicate experiments are shown.

In the case of H4K16ac, we couldn't score reproducible specific effects of either EP400, SRCAP or KAT5 (**Figure 3.12**). I think this is rather technical problem and a targeted mass-spectrometry approach will likely solve the issue.

In conclusion, our initial prediction seems to be correct for H2A.Z incorporation. We can't speculate too much about H4K16ac as a better experimental approach is needed to confirm, or disprove, our model.
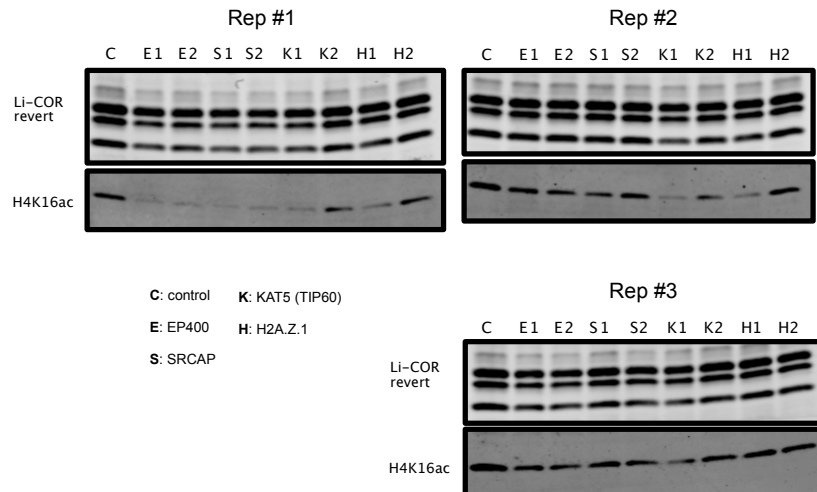
Figure 3.12 Assessing the effects of various knock-down on H4K16ac levels in U2-OS cells. Staining with Li-COR revert used as loading control. Nuclear extract was probed with H4K16ac antibody. Blots for replicate experiments are shown.

3.6 Discussion

Our affinity purification coupled to mass-spectrometry of endogenously tagged DOM isoforms, carried under stringent conditions, strongly suggest the presence of two separate complexes. In the original characterization of the DOM.C (133), the complex was purified by overexpression and purification of tagged PONTIN, which may have yielded a mixture of complexes with both DOM-A.C and DOM-B.C present. Additionally, as PONTIN is also contained in the dINO80 complex (243), the mixture might have been further contaminated. Given these uncertainties, we think the model for H2A.V exchange during DNA damage response proposed in this early work (133) should be re-visited in light of our results, perhaps accounting also for the contribution of dINO80.C. It will be interesting to define the role of each complex on the recognition and restoration of damaged chromatin, especially at the level of H2A.V remodeling and acetylation-based signaling.

With our work, we confirmed earlier reports in which immunofluorescence analysis showed that DOM-B, and not DOM-A, affect H2A.V levels during fly oogenesis (238). We further confirmed that the DOM-B.C is the major, ATP-dependent remodeler for H2A.V in flies, like its yeast ortholog SWR1.C. We also discover that a previously unidentified subunit, ARP6, which appears to be essential to incorporate H2A.V, like its yeast (140) and human (244) homologs. Knock-down of DOM-B has effects on transcription, but these are only partially overlapping with the effects of H2A.V depletion, suggesting either 1) off-target effects of the RNAi or 2) specific roles of DOM-B in transcription that are independent of H2A.V incorporation. Since similar effects have been documented before in yeast, where Swr1 causes transcriptional mis-regulation in the absence of H2A.Z (240), we consider the second hypothesis as the most likely.

The DOM-A.C, surprisingly, doesn't affect H2A.V levels and incorporation in any of our assays. This is again in agreement with earlier reports for specific developmental stages (238). Two possible scenarios might explain these results. In the first case, the lack of a necessary interaction partner might prevent productive H2A.V incorporation. This hypothesis is supported by the finding that ARP6 only interacts with DOM-B and might be a necessary component for H2A.V incorporation, since its depletion causes drastic reduction of H2A.V global levels. In the second case, subunits that associate specifically with DOM-A might have an inhibitory effect on its ATPase activity through allosteric regulation. This hypothesis might be supported by the fact that the human homolog of DOM-A, EP400, is capable of incorporating H2A.Z *in vitro* when purified alone (245) but little effects on H2A.Z are observed upon its depletion *in vivo*, where it is likely "quenched" by being part of a multi-subunit complex (146) and probably ATPase inactive. Regardless, incorporation of H2A.V seems to be unfavored in the DOM-A.C, probably to redirect the complex to other biochemical activity while retaining only some proprieties, such as specific genomic targeting. Our data showed, for the first time, that the DOM-A.C might be in fact the *Drosophila* NuA4, responsible for the specific acetylation of H4K12. Depletion of DOM-A.C causes a global reduction of H4K12ac at a global level, but some regions of the genome covered by H4K12ac seem to be unaffected by the loss of DOM-A.C. This may be explained by the fact the DOM-A.C is not the only enzymatic complex targeting H4K12. In fact, the acetyltransferase CHM (246, 247) has also been shown to acetylate the same residue. To date, H4K12ac has been implicated in *Drosophila* aging (247) but its function is still largely unknown. As both DOM-A and TIP60 loss significantly perturb gene expression in the same manner, we speculate H4K12ac may participate in transcriptional regulation. Genes down-regulated upon DOM-A and TIP60 RNAi show high H4K12ac around their TSS, but the H4K12ac is not specifically reduced at their promoters. We speculate that these genes might rely more on H4K12ac for their expression and might be more sensitive to changes in acetylation. As H4K12ac is the most abundant H4 acetylation (246, 247), we cannot rule out, however, that some of these effects may be due to perturbations of global chromosomal condensation. The increase in H4K12ac at promoter observed upon DOM-B RNAi appears to be partially phenocopied by the knock-down of H2A.V. It is possible that H2A-containing nucleosomes are a better substrate for the DOM-A.C compared to the ones containing only H2A.V. The loss of the variant might therefore result in higher H4K12ac catalyzed by TIP60. Upon loss of DOM-A, TIP60 protein levels drop suggesting that TIP60 might be unstable if not incorporated within the DOM-A.C - at least in *D. melanogaster* cells. This may indicate that, at a certain point during evolution, some components of a SWR1-type complex formed a stable and productive association with an acetyltransferase module - becoming what we now know consider the dNuA4.C. This evolutionary "fusion" has been previously proposed

for the human EP400 complex (248), which we consider the ortholog of the DOM-A.C. Curiously, in *C. albicans*, the otherwise separated NuA4.C and SWR1.C might transiently, and reversibly, associate (249). Our data indicate that the DOM-A.C can acetylate H4K12 without the need of ATP binding/hydrolysis by DOM-A. In agreement with our hypothesis, the introduction of the ATPase domain of the *Drosophila* DOM between the HSA and SANT domain of its yeast ortholog Eaf1, seems to not affect the function of NuA4.C (248), once again suggesting a vestigial role for the DOM ATPase in the context of NuA4. At this point, however, we can't exclude additional functions of DOM-A.C that might require ATP binding/hydrolysis.

Finally, through our affinity purification coupled to mass-spectrometry of DOM complexes, we discovered, uncharacterized interactors for DOM-A. Amongst those, we identified the transcription factor CG12054. Its interaction with DOM complexes was only observed once in a screen (250). The human ortholog of CG12054, called JAZF1 may participate in gene silencing (251) and has been associated to endometrial stromal tumors (252). Its role in flies is, to date, unknown.

The specific regulation of diverse nuclear processes requires division of labor between chromatin modifying enzymes. During evolution, genome duplications and genetic divergence creates the opportunity to expand and separate activities/specificities. In some organisms, however, the need of diversification is achieved through alternative splicing (253, 254). We think this is the case of SWR1 and NuA4 complexes. While in yeast and mammals two genes define the two complexes, the *Drosophila* SWR1.C and NuA4.C are created and functionally separated through alternative splicing (**Figure 3.13**).
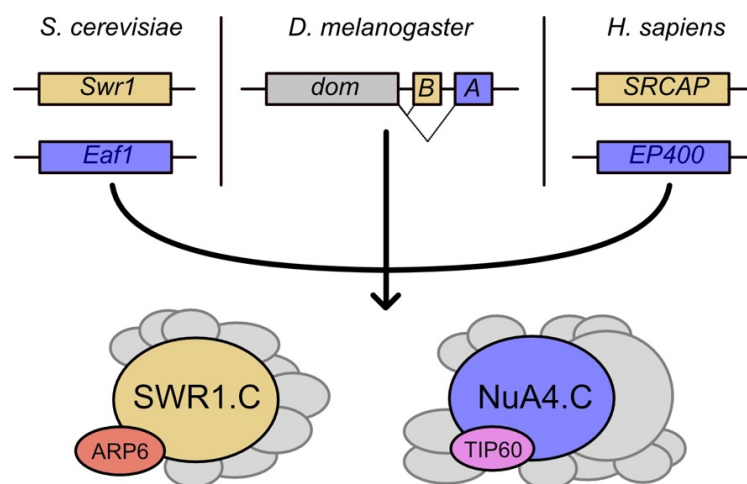
Figure 3.13 Model for SWR1.C and NuA4.C specification in *S. cerevisiae*, *D. melanogaster* and *H. sapiens*. Figure adapted from (236). Reprinted as permitted by the Creative Commons Attribution CC-BY 4.0 license.

Surprisingly, the gene orthologs of *dom* in honeybee (*A. mellifera*, LOC413341), jewel wasp (*N. vitripennis,* LOC100115939), Jerdon's jumpin ant (*H. saltator*, LOC105183375), common house spider (*P. tepidariorum*, LOC107448208) and red flour beetle (*T. castaneum*, LOC656538) undergo alternative splicing to generate at least two isoforms with different C-termini. The mode of specification of SWR1 and NuA4 through splice variants might therefore not be limited to *Drosophila,* but diffused throughout the whole Arthropoda phylum. Since many chromatin remodelers are encoded by alternatively spliced genes, this regulatory mechanism might be a common, functional alternative to gene duplication across evolution.

4. MATERIALS and METHODS – CHRAC/ACF contribute to the repressive ground state of chromatin

4.1 *D. melanogaster* strains and genetics

Constructs expressing ACF1-GAL4 fusions (and control) were generated by recombineering (255). Briefly, the *Acf* gene contained in a fosmid (pflyfos021945) was tagged with 2x-TY1-GAL4DBD(1-147)-3XFLAG (N-terminus or C-terminus) through recombination in *E. coli*. The control was generated by entirely replacing the *Acf* coding sequence with the tag. Fosmids were inserted into chromosome 2L (*yw*; attP40, locus 25C7, chr2L) (Genetic Services Inc., Boston, MA). The expression of ACF1-GAL4 fusions in homozygous embryos was confirmed by Western blot. To tether ACF1-GAL4 to UAS sites, ACF1-GAL4 (and control) flies were crossed to N1 strain (Containing the *UAS-LacZ-mini-white* reporter (219)). The *Acf^7* allele, in which most of the *Acf* coding sequence is deleted, has been described earlier (91).

4.2 Generation of the *Acf^C* mutant allele via CRISPR/Cas9

gRNAs to target the 5' and 3' end of the *Acf gene* were designed using the Zhang lab CRISPR resource (http://crispr.mit.edu/). gRNA sequences were inserted into a primer [5'-TAATACGACTCACTATAG-(targeting sequence)-GTTTTAGAGCTAGAAATAGC-3'] in 5' to 3' direction. The construct was amplified by PCR using a scaffold primer (5'-AAAAGCACCGACTCGGTGCCACTTTTTCAAGTTGATAACGGACTAGCCTTATTTTAACTTGCTATTTCTAGCTCTAAAAC-3') and a universal reverse primer (5'-AAAAGCACCGACTCGGTGCC-3'). The PCR product was purified using GeneElute PCR cleanup kit (Sigma, Cat No NA1020). RNA was generated by *in vitro* transcription using T7 MEGAshortscript kit (Ambion, Cat No AM1354). Purified RNA was assessed on agarose gel elecrophoresis.

gRNA efficiency was tested in SL2 cells stably expressing Cas9 (clone Hgr14; (256)) by transient transfection of 1 µg sgRNA / 1.4 x 10^6 cells. 48 hr later, genomic DNA was extracted and a ~600 bp region surrounding the selected gRNA sequences was amplified by PCR. The product was heated to 95°C for 5 min and then cooled with a ramp rate of 0.1°C/sec (257). Mismatched base pairs (readout for gRNA cleavage) close to the cutting site were detected by T7 endonuclease (M0302S, NEB) cleavage and agarose gel electrophoresis.

Homology arms were constructed by PCR amplification of two genomic regions (1.3 kb upstream and 1.5 kb downstream from the gRNA-targeted sequences). A 3XP3-dsRed fly

selection cassette (obtained from pJet1.2 (257)) was inserted between the homology arms by golden gate cloning.

The plasmid containing the repair construct and *in vitro* transcribed gRNAs were injected into *yw; Cas9; lig^{4169}* blastoderm embryos (258). F0 mosaic males were crossed with *w1118* females and F1 transformants were screened for red fluorescence in the eye. Homozygous flies were backcrossed to *yw* (>4 generations) or to *OrR* (>8 generations) strain. *Acf* deletion was analyzed by PCR and loss of ACF1 was confirmed by Western blot. CRISPR/Cas9 editing of *Acf* resulted in a deletion of about 4Kb, which removed most of the coding sequence but leaves the 5' and 3' UTRs. No ACF1 protein could be detected in the newly generated *Acf^C* mutant, similarly to what observed in the previously analyzed *Acf^7* allele (generated by imprecise p-element excision) (91).

To assay for hatching rates in the *Acf^C* mutant, 0-16 h embryos were collected on apple juice agar plates and incubated at 25°C. 25 h later, hatched larvae were counted.

4.3 Nuclei isolation and Western Blot

Overnight embryos (0-16 h after egg laying) were collected on apple juice agar plates and dechorionated with 25% bleach for 5 min. Embryos were washed several times with PBS (140 mM NaCl, 2.7 mM KCl, 10 mM Na_2HPO_4, 1.8 mM KH_2PO_4) to remove residual bleach. Embryos were transferred in 1.5 ml tubes, resuspended in ice-cold NB-0.3 (15 mM Tris-Cl pH 7.5, 60 mM KCl, 15 mM NaCl, 5 mM $MgCl_2$, 0.1 mM EGTA pH 8, 0.3 M sucrose, 0.2 mM PMSF, 1mM DTT, Roche cOmplete protease inhibitor without EDTA) and homogenized using a metal pestle (LLG Labware, Cat No 9.314.501). The homogenate was layered on top of an ice-cold, bi-phasic sucrose cushion consisting of NB-0.8 (15 mM Tris-Cl pH 7.5, 60 mM KCl, 15 mM NaCl, 5 mM $MgCl_2$, 0.1 mM EGTA pH 8, 0.8 M sucrose) (top) and NB-1.4 (15 mM Tris-Cl pH 7.5, 60 mM KCl, 15 mM NaCl, 5 mM $MgCl_2$, 0.1 mM EGTA pH 8, 1.4 M sucrose) (bottom). Nuclei were pelleted through the sucrose cushion by centrifugation at 13000 rpm for 10 min (4°C) and washed twice with ice-cold NB-0.3.

Nuclei were resuspended in 5X Laemmli Sample Buffer (250 mM Tris-HCl pH 6.8, 10% w/v SDS, 50% v/v Glycerol, 0.1% w/v bromophenol blue, 10% β-mercaptoethanol) and incubated at 96°C for 8 min. Proteins were detected by Western blot using the following antibodies: αACF1 8E3(218) (1:5), αFLAGm2 (1:1000, Sigma, Cat No F1804) and α Lamin T40 (1:1000, kind gift from H. Saumweber).

4.4 ChIP-qPCR

0-12 h AEL embryos were collected, dechorionated and washed as previously described. Embryos were weighted in to 15 ml tubes and divided in 0.5 - 1g aliquots. After three washes

with 50 ml of PBS/0.01% Triton X-100, embryos were resuspended in 9 ml of Fixing Solution (50 mM HEPES pH 7.6, 100 mM NaCl, 1 mM EDTA, 0.5 mM EGTA)/3.7% formaldehyde (Merck, Cat No 1040031000) and n-Heptane (30 ml) was added. Tubes were vigorously agitated for 1 min and then incubated for 13.5 min at 18°C on a rotating wheel. Crosslinking was stopped by pelleting embryos at 3000 rpm for 1 min, resuspending them in 50 ml of PBS/0.01% Triton X-100/125 mM glycine and incubating them for 5 min at room temperature (RT). Embryos were washed twice with PBS/0.01% Triton X-100, flash-frozen in liquid nitrogen and stored at -80°C. Frozen embryos were homogenized in 5 ml of ice-cold RIPA buffer (10 mM Tris-Cl pH 8, 1 mM EDTA, 140 mM NaCl, 1% Triton X-100, 0.1% SDS, 0.1% sodium deoxycholate/1 mM DTT/0.2 mM PMSF/Roche cOmplete Protease inhibitor without EDTA), by douncing 10 times with a loose pestle and 10 times using a tight pestle. Nuclei were pelleted at 170 g for 10 min (4°C), resupended in 5 ml of RIPA/g of embryos and divided into 1 ml aliquots. Nuclei were sonicated using a Covaris S220 system (100W Peak Power, 20% Duty Factor, 200 Cycles/Burst, 15 min total time). Insoluble chromatin was removed by centrifugation at 13000 rpm for 20 min (4°C). The supernatant, containing soluble chromatin, was pre-cleared using RIPA-equilibrated 50% Protein A+G (1:1) sepharose beads slurry for 1h at 4°C. Immunoprecipitation was performed on 200 µl of chromatin by overnight incubation (4°C) after the addition of 4 µl of the following antibodies: αACF1 Rb2(218), αFLAGm2 (Sigma, Cat No F1804) or αISWI Rb1 (Becker Lab, unpublished). The next day, 30 µl of Protein A+G (1:1) 50% slurry was added and the tubes were rotated for 3h at 4°C. Beads were washed 5 times with RIPA buffer. After the final wash, beads were resuspended in 100 ul of RIPA buffer containing 10 µg/100 µl of RNase-A (Sigma, Cat. No. R4875) and incubated at 37°C for 20 min. Proteins were digested using 250 ng/µl Proteinase K (Genaxxon, Cat.no. M3036.0100) and, simultaneously, crosslink was reversed by incubation at 68°C for 2 hr. DNA was purified using 1.8X Agencourt AMPure XP beads (Beckman Coulter, Cat No A63880) following standard protocol and eluted in 50 µl of 5 mM Tris-Cl pH 8. Purified DNA was used for standard qPCR analysis at 1:2 dilution. Primers are listed in Supplementary Table 1.

4.5 RT-qPCR

2-8 h AEL embryos were collected, dechorionated and washed as previously described. Embryos were homogenized in 300 µl of QIAzol (QIAgen, Cat No 79306) using a metal pestle. Additional 700 µl of QIAzol were added, the homogenate the samples were flash-frozen in liquid nitrogen and stored at -80°C. RNA was extracted following the standard protocol provided by QIAgen. cDNA was generated from 1.5 µg of extracted total RNA using Superscript III First Strand Synthesis System (Invitrogen, Cat No 18080051, random

hexamer priming). cDNA was used for standard qPCR analysis at 1:10 dilution. Primers are listed in Supplementary Table 1.

4.6 Immunofluorescence microscopy on Kc167 cells

200 µl of cells (>10^6 cell/ml) were seeded onto poly-lysine coated 3-well depression slides (Thermo Scientific, Cat No 631-0453) and allowed to attach for 1.5 h at 26°C. After two washed with PBS, cells were fixed in PBS/3.7% formaldehyde for 10 min at room temperature. Cells were washed twice with PBS and permeabilized with ice-cold PBS/0.25% Triton X-100 for 6 min. After two washes with PBS, cells were blocked with PBS/0.1% Triton X-100/5% Normal Donkey Serum (NDS, Jackson Immuno Research)/5% non-fat milk for 2 h and then incubated overnight at room temperature with the following primary antibodies: αV5 (1:1000, GenScript, Cat No A00623) and αmCherry (259) (1:20). Cells were washed twice with PBS/0.1% Triton X-100 and incubated for 2h at room temperature with the following secondary antibodies: donkey-αrat-Cy3 (1:500, Jackson Immuno Research) and donkey-αrabbit-Alexa488 (1:300, Jackson Immuno Research). Cells were washed twice with PBS/0.1% Triton X-100 and DNA was stained with 1:500 DAPI in PBS for 10 min at room temperature. Coverslips were mounted using Vectashield Mounting Medium (Vector Laboratories, Cat No H-1000) and sealed with nail polish. Images were taken on a Leica Sp5 confocal microscope maintaining the same settings for all the samples.

4.7 Artificial tethering of ACF1 to multiple reporters in Kc167 cells

The barcoded reporter library integrated in Kc167 cells containing was generated as previously described (220). Plasmids for the expression of GAL4-ACF1 fusion and controls, under the control of Actin5 promoter, were assembled by Gibson cloning in previously described vectors (220). All constructs generated were checked by both DNA sequencing and restriction digestion analysis. The artificial tethering experiment, including sample preparation, high throughput sequencing and data processing/analysis was performed exactly as described in (220). GAL4-HP1 construct was included as positive control. Two biological replicates were analyzed for each condition. Reporters without measured read counts in at least one condition were discarded. Linear models were calculated using the *lm* function in R. To check expression and localization of GAL4-ACF1 fusion and controls, 3x10^6 Kc167 cells were transiently transfected with 1 µg of the corresponding plasmid using X-tremeGENE HP Transfection Reagent (SIGMA, Cat No 6366236001) following standard protocol (4.5:1 transfection reagent:DNA ratio). Three days after transfection, cells were collected for western blot and immunofluorescence analysis as previously described.

4.8 Single-embryo RNA-seq

0-45 min AEL embryos were collected on apple juice agar plates and incubated at 25°C for the time needed to reach the desired developmental stage (around 1 h for Bownes Stage 3 and 4 h for Bownes Stage 8). To see embryonic structures, embryos were submerged in a drop of Voltalef 10s halocarbon oil (Lehman and Voss Co.) placed on a microscope slide. Single embryos of the desired staged were hand-picked with a 26G needle and crushed into 200 μl of Lysis Buffer (with Proteinase K added) from the Agencourt RNAdvance Tissue Kit (Beckman Coulter, Cat No A32645). 10 μl of 1:100 ERCC Spike-in RNA mix (Ambion, Cat No 4456740) were added and the samples were incubated at 37°C for 20 min. Single-embryo homogenetaes were then flash-frozen in liquid nitrogen and stored at -80°C. Total RNA was extracted using Agencourt RNAdvance Tissue Kit (Beckman Coulter, Cat No A32645), following standard protocol with half of the volumes described. Extracted total RNA was analyzed on a Bioanalyzer 2100 (Agilent). Ribosomal RNA was depleted using rRNA Depletion Kit (Human/Mouse/Rat) (New England Biolabs, Cat No E6310). Libraries for RNAseq were prepared using NEBnext Ultra RNA Library Prep Kit for Illumina (New England Biolabs, Cat No E7530S) following standard protocol. Libraries were sequenced on an Illumina HiSeq1500 instrument with 50 bp paired-end reads. 6 embryos (from 3 different collections) per genotype and stage were analyzed. Reads were mapped against the reference *D. melanogaster* genome (FB2016_01 dmel_r6.09 with selected chromosomes) using STAR (version 2.5.0a) with *quantMode GeneCounts* for counting reads per gene (260). Genes without read counts in at least half of the samples were excluded from further analysis. One replicate from the Acf^C genotype (Stage 3) was excluded due to improper staging (data not shown). DESeq2 (261) was used to calculate size factors for normalization. High-variance genes (between 85th and 99th variance percentile) were used for Principal Component Analysis. Differential expression analysis was performed with DEseq2 by fitting negative binomial GLM separately for the two developmental stages(261). Adjusted p-value cut-off for significance was set to 0.1. Results of differential expression analysis are reported in Supplementary Table 2 and Supplementary Table 3. The FlyMine online database was used for gene ontology analysis (262). The *nearest* method from the GenomicRanges Bioconductor packages was utilized to assign genes to the corresponding state of the 5-state chromatin-state model (221). Local polynomial regression fitting (*loess*) was employed to visualize trends on MA-plots. modENCODE histone modification signals (smoothed M-values) (222) were averaged over genes and low/high levels were distinguished by a cutoff based on the local minimum in the density of the H3K36me3 levels. Genes were separated into marked/unmarked based on histone modification levels in all four marks used for analysis.

4.9 Nucleosome mapping and autocorrelation

2-8 h AEL embryos were dechorionated, washed and fixed as described previously. Crosslinked nuclei were also isolated as described in section 4.4, but using ice-cold NX-I buffer (15 mM HEPES pH 7.6, 10 mM KCl, 2 mM MgCl2, 0.5 mM EGTA, 0.1 mM EDTA, 350 mM sucrose, 1 mM DTT, 0.2 mM PMSF, Roche cOmplete Protease inhibitor without EDTA) instead of RIPA for homogenization. Nuclei from 0.2 - 0.5 g of fixed embryos were resuspended in RIPA buffer containing 2 mM $CaCl_2$ and digested with 13 units of MNase / g of starting embryos (Sigma, Cat.no N5386) for 15 min at 37°C, with 500 rpm shaking. MNase digestion was stopped by transferring the tubes on ice and adding 10 mM EDTA (pH 8.0) (final concentration). Non-solubilized material was pelleted by centrifugation at 12500 rpm for 10 min (4°C). The supernatant was collected, RNase-A (50 µg/ml, Sigma, Cat. No. R4875) was added and RNA was digested at 37°C for 30 min. Proteins were digested using 250 ng/µl Proteinase K (Genaxxon, Cat.no. M3036.0100) and, simultaneously, crosslink was reversed by incubation at 68°C for 2 hr. DNA was purified using 1.8X Agencourt AMPure XP beads (Beckman Coulter, Cat No A63880) following standard protocol and eluted in 50 µl of 5 mM Tris-Cl pH 8. Purified DNA was quantified using Qubit® dsDNA HS Assay Kit (Life Technologies, Cat.no.Q32851). Libraries for sequencing were prepared using a custom-made protocol available upon request. Libraries were sequenced on an Illumina HiSeq1500 instrument with 50 bp paired-end reads. Reads were mapped against the reference *D. melanogaster* genome (FB2016_01 dmel_r6.09) using Bowtie v1.1.1 with "-X 750" parameter setting. Fragments were size selected (between 120 and 200 bp) and resized to 50 bp fixed at the fragment center to obtain dyad coverage vectors. The nucleosome dyad maps from *Acf⁷, yw and w1118* were taken from (207). Autocorrelation function (lag length = 1000 bp) was calculated for the dyad coverage vectors for both the whole genome and for the 5 chromatin domains (221). The vectors for the latter case represent head-to-tail concatemerized regions of given annotation. The slope of the linear regression of the first and second autocorrelation peak (intercept = 0) was used to define nucleosomal repeat lengths (NRL). Values reported are average NRL (between biological replicates) ± SEM.

4.10 Accession Codes

Sequencing data are available in the Gene Expression Omnibus under accession numbers GSE106759 and GSE106733.

4.11 Embryo irradiation and fixation

For embryo hatching analysis, 2-3.5h old embryos were manually transferred and aligned in 6cm agar-apple juice plates. Embryos where irradiated with 0Gy, 1Gy or 10Gy using a

Faxitron® CellRad machine (130 kV, 5 mA) and incubated for additional 23h at 25°C. Hatching rate was determined by counting the number of embryos that hatched into larvae. For Immunofluorescence (IF), 2-3.5h old embryos in 10cm collection plates where irradiated with 0Gy or 1Gy using a Faxitron® CellRad machine (130 kV, 5 mA). 15 min after irradiation, approximately half of the embryos were collected from each plate and dechorionated in 25% bleach for 3-5 min, whereas the remaining where kept at 25°C for additional 3h. After extensive washes with water, embryos were transferred in 1.5ml tubes. For heat fixation, 500 ul of boiling Triton-X-salt solution (0.03% Triton-X-100, 68 mM NaCl) was added to the dechorionated embryos. 500 ul of ice-cold Triton-X-salt solution was added immediately after and the tubes were put on ice for 5 min. The Triton-X-salt solution was removed and 500 ul of n-heptane were added, followed by 500 ul of 100% methanol. Tubes were shaken for 15 second and embryos were allowed to settle on ice for 5 min. Embryos were washed two times with 500 ul of 100% methanol and stored at -20°C in 200 ul of 100% methanol. The fixation procedure was repeated for the remaining half of the embryos (3h after irradiation).

4.12 Immunofluorescence of irradiated embryos

Fixed embryos were transferred into 0.2 ml PCR tubes and rehydrated by three 10 min washes with PBS + 0.1% Triton-X-100. Embryos were blocked for 3h in Blocking Solution [PBS + 0.3% Triton-X-100 + 5% Normal Donkey Serum (Jackson Immuno Research) + 5% non-fat milk]. After a brief wash with PBS, embryos were incubated overnight at 4°C with primary antibodies diluted in Blocking Solution (1:100 rabbit α-H2Av, see (160))(1:1000 mouse α-yH2Av, Developmental Studies Hybridoma Bank). Embryos were washed 4 times (15 min each) with PBS + 0.1% Triton-X-100, then incubated for 3h at room temperature with secondary antibodies diluted in Blocking Solution (1:300 donkey α-Rabbit.Alexa488, Jackson Immuno Research)(1:500 donkey α-Mouse.Cy3, Jackson Immuno Research). Embryos were washed 4 times (15 min each) with PBS + 0.1% Triton-X-100, then stained with 1:500 DAPI (in PBS) for 10 min. Embryos were washed 2 times (10 min each) with PBS, then mounted using Vectashield (Vector Laboratories).

Pictures were taken using a Leica Sp5 confocal microscope. For quantification, surface pictures of whole embryos (>10 embryos/condition) were taken using a 20X objective and a 1.27X zoom factor (1024X1024 pixels) maintaining the same settings across all conditions and biological replicates. H2Av and γH2Av signals were quantified using a custom-made macro (made by Dr. Anna Klem, bioimaging Facility LMU Munich) with Fiji (263).

5. MATERIALS and METHODS – *Drosophila* SWR1 and NuA4 complexes are defined by DOMINO isoforms

5.1 Cell lines and culture conditions

Kc167 cells line were purchased from the Drosophila Genomic Resource Center (https://dgrc.bio.indiana.edu/Home). S2 (subclone L2-4) cells were obtained from P. Heun as a kind gift (264). *D. virilis* 79f7Dv3 cells were a kind gift from B.V. Adrianov (241). Cells were cultivated at 26°C in Schneider's *Drosophila* Medium (Thermo-Fischer, Cat. No 21720024) supplemented with 10% FBS (Kc167 and S2) or 5% FBS (79f7Dv3) and 1% Penicillin-Streptomycin solution (Sigma-Aldrich, Cat No P-4333).

5.2 CRISPR/Cas9 tagging

Candidate gRNAs targeting exon 14 or exon 11 of *dom* were designed using GPP sgRNA designer (https://portals.broadinstitute.org/gpp/public/analysis-tools/sgrna-design) (265). The top 5 gRNA candidates were checked for off-targets using flyCRISPR Target Finder (https://flycrispr.org/target-finder/, guide length = 20, Stringency = high, PAM = NGG only) (266). Four gRNAs (2 for exon 14 and 2 for exon 11) were selected (Supplementary Table 3). Constructs containing the gRNA sequence fused to the tracrRNA backbone under the control of *Drosophila* U6 promoter were synthesized as gBlocks (Integrated DNA Technologies) and amplified by PCR using Q5 polymerase (New England Biolabs, Cat No. M0491S). The repair templates, consisting on the sequence encoding for 3XFLAG tag (with an added stop codon) inserted between two homology arms of 200 bp each, were also synthesized as gBlocks (Integrated DNA Technologies) (Supplementary Table 3). These repair templates were cloned in pUC19. For CRISPR editing, 1 x 10^6 S2 (L2-4) cells were transfected with 110 ng of gRNAs mixture (1:1), 200 ng of repair plasmid and 190 ng of pIB_Cas9_Blast (for expression of SpCas9 and selection with Blasticidin, kind gift of P. Heun) using X-tremeGENE HP DNA Transfection Reagent (Roche, Cat. No 6366236001). 24 hours after transfection, selection was started by replacing the medium with fresh one containing 25 µg/ml Blasticidin (Gibco, Cat. No A1113903). Three days after selection, different amounts of cells the cells (1000, 2000 and 5000) were seeded into 6 cm tissue culture dishes and allowed to attach for 1-2 h. After removing the medium, cells were carefully overlaid with 2.5 mL of a 1:1 mix of 2X Schneider's Medium (prepared from powder, Serva, Cat. No 35500) + 20% FBS + 2% Penicillin-Streptomycin and 0.4% low-melting

agarose equilibrated to 37°C. To avoid drying, the 6 cm dishes were sealed with parafilm and enclosed into 15 cm dishes (also sealed with parafilm) together with a piece of wet paper. Colonies originated from single cells were picked after 2-3 weeks using a pipette, resuspended in 100 µL of complete Schneider's *Drosophila* Medium and plated into 96-well plates. Individual clones were allowed to expand for 1-2 weeks and then transferred into 48-well plates. For testing of clones, DNA was extracted from 50 µL of resuspended cells using Nucleospin Gel and PCR Cleanup (Macherey-Nagel, Cat. No 740609.250). DNA was amplified by PCR to check the insertion of the 3XFLAG tag. Selected clones were further expanded and stored in liquid nitrogen in 90% FBS + 10% DMSO.

5.3 Nuclear extraction and FLAG affinity enrichment

0.5-1 billion cells were pelleted at 500 g for 5 min. After one wash with 10 ml of PBS, cells were lysed in 10 ml of ice-cold NBT-10 buffer [15 mM HEPES pH 7.5, 15 mM NaCl, 60 mM KCl, 0.5 mM EGTA pH 8, 10% Sucrose, 0.15% Triton-X-100, 1 mM PMSF, 0.1 mM DTT, 1X cOmplete EDTA-free Protease Inhibitor (Roche, Cat. No 5056489001)] by 10 min rotation at 4°C. To isolate nuclei, the lysate was gently overlaid on a 20 ml sucrose cushion consisting of ice-cold NB-1.2 buffer (15 mM HEPES pH 7.5, 15 mM NaCl, 60 mM KCl, 0.5 mM EGTA pH 8, 1.2 M Sucrose, 1 mM PMSF, 0.1 mM DTT, 1X cOmplete EDTA-free Protease Inhibitor) and centrifuged at 4000 g for 15 min. After one wash with 10 ml of ice-cold NB-10 buffer (15 mM HEPES pH 7.5, 15 mM NaCl, 60 mM KCl, 0.5 mM EGTA pH 8, 10% Sucrose, 1 mM PMSF, 0.1 mM DTT, 1X cOmplete EDTA-free Protease Inhibitor), nuclei were resuspended in ice-cold Protein-RIPA buffer (50 mM Tris-HCl pH 7.5, 150 mM NaCl, 1mM EDTA, 0.5% IGEPAL CA-630, 0.5% Na-Deoxycholate, 0.1% SDS, 1mM PMSF, 0.1 mM DTT, 1X cOmplete EDTA-free Protease Inhibitor) and sonicated in 15 mL Falcons tubes using Bioruptor (Diagenode; 20 cycles, 30 sec ON / 30 sec OFF). To remove insoluble material, the sonicated extract was centrifuged at 16000 g for 15 min at 4°C and the supernatant (soluble fraction) was collected. Total protein concentration was measured with Protein Assay Dye Reagent Concentrate (BIO-RAD, Cat No 5000006), using serial BSA dilutions as standards. The nuclear extract was divided in 2 mg aliquots, flash-frozen in liquid nitrogen and stored at -80°C. For immunoprecipitation (IP), 2 mg of nuclear extract / IP was centrifuged at 16,000 g for 15 min (4°C) to remove aggregates. Nuclear extracts were diluted (1:1) with Benzonase dilution buffer (50 mM Tris-HCl pH 7.5, 150 mM NaCl, 4 mM $MgCl_2$, 0.5% NP-40, 1 mM PMSF, 0.1 mM DTT, 1X cOmplete EDTA-free Protease Inhibitor) and 1 µL of Benzonase (Merck-Millipore, Cat. No 1.01654.0001) was added. Immediately after, 60 µL of Protein-RIPA-equilibrated FLAG-m2 beads (50% slurry) (Sigma-Aldrich, Cat. No A2220) were added and proteins were immunoprecipitated for 3h at 4°C (on a rotating wheel). FLAG beads were washed 3 times with ice-cold Protein-RIPA buffer and 3 times with

ice-cold TBS (5 mM Tris-HCl pH 7.5, 150 mM NaCl) (5 min rotation each, 4°C). For western blot analysis, beads were resuspended in 50 µL of 5X Laemmli Sample buffer (250 mM Tris-HCl pH 6.8, 10% w/v SDS, 50% v/v glycerol, 0.1% w/v bromophenol blue, 10% β-mercaptoethanol) and incubated at 95°C for 5 min. For mass-spectrometry, beads were resuspended in 50 µL of elution buffer (2 M urea, 50 mM Tris-HCl, pH 7.5, 2 mM DTT and 10 µg ml^{-1} trypsin) and incubated at 37°C for 30 min. The supernatant was collected and beads were resuspended in 50 µL of alkylation buffer (2 M urea, 50 mM Tris-HCl, pH 7.5 and 10 mM chloroacetamide) and incubated at 37°C for 5 min. The two supernatants were combined and further incubated at room temperature overnight. The pH of the solution containing digested peptides was adjusted with 1% Trifluoroacetic acid (TFA). Digested peptides were desalted by adding 1 volume of 1% TFA in isopropanol and loading onto Stage Tips containing three layers of SDB-RPS (Polystyrene-divinylbenzene copolymer partially modified with sulfonic acid). Peptides were washed twice with 100 µL 1%TFA in Isopropanol and twice with 100 µl 0.2%TFA in water. Peptides were eluted using 80 µl of 2% (v/v) ammonium hydroxide, 80% (v/v) acetonitrile (ACN) and dried using a speed-vac. Dried peptides were dissolved in 10 µL Buffer A* (2% ACN/0.1% TFA) and separated on 50-cm columns in-house packed with ReproSil-Pur C18-AQ 1.9 µm resin (Dr Maisch). Liquid chromatography was carried on an EASY-nLC 1200 ultra-high-pressure system coupled through a nano-electrospray source to a Q-Exactive HF-X mass spectrometer (Thermo Fisher). Peptides were loaded in buffer A (0.1% formic acid) and separated trough a non-linear gradient of 5–30% buffer B (0.1% formic acid, 80% ACN) using a flow rate of 300 nl min^{-1} over 70 min. For measurements, switches between a full scan and 10 data-dependent MS/MS scans were performed. Full scans were acquired with target values of 3×10^6 charges in the 300–1,650 *m/z* range, with a resolution set to 60,000 (maximum injection time = 20 ms). The 10 most abundant ions were sequentially selected with a target value of 1×10^5 and an isolation window of 1.4 *m/z*. Ions were fragmented by higher energy C-trap dissociation with a normalized collision energy of 27 eV. Resolution for HCD spectra was set to 15,000 (maximum injection time = 60 ms). To minimize the re-sequencing of the same peptide, the selected peptide candidates were excluded for 30 s. In total, 3 biological replicates (nuclear extract prepared on different days from 3 different clones) were analyzed in 3 technical replicates (3 parallel IPs on the same nuclear extract). Raw mass spectrometry measurements were analyzed using MaxQuant (version 1.5.6.7)(267) and Perseus (version 1.5.4.2). Peak lists were searched against the *D. melanogaster* UniProt FASTA database combined with 262 common contaminants using Andromeda search engine (268). For both peptides (>7 amino acids) and proteins, the false discovery rate (FDR) was set to 1%. The parameter 'Match between runs' (MBR) was enabled with a maximum time difference of 0.7 min. Relative protein amounts were determined with the MaxLFQ algorithm (269) (ratio

count > 2). Missing values were imputed from a normal distribution (width of 0.2 and a downshift of 1.8 standard deviations). The Imputed LFQ values for each biological replicate were obtained by averaging of the LFQ values of technical replicates. Differential enrichment analysis was performed in R using the *limma* package as previously described (270, 271). The *p.adjust* function (*method = "fdr"*) was applied to obtain adjusted p-values (FDR).

5.4 RNAi

Primers for dsRNA templates were obtained/designed from the following sources: TRiP (https://fgr.hms.harvard.edu/fly-in-vivo-rnai), SnapDragon (https://www.flyrnai.org/snapdragon), E-RNAi (https://www.dkfz.de/signaling/e-rnai3/) (272, 273), and (133) (Supplementary Table 3). Templates for dsRNA synthesis were generated by PCR-amplification with Q5 Polymerase (New England Biolabs, Cat No. M0491S), using genomic DNA from S2 (L2-4) cells as template.

Templates were *in vitro* transcribed using MEGAScript T7 kit (Invitrogen, Cat. No AMB 13345) following the standard protocol and using 500 ng of DNA as starting material. To generated dsRNAs, *in vitro* transcribed RNAs were heated to 85°C for 5 min and slowly cooled-down to room temperature. For RNAi, Kc167 cells were collected and pelleted at 500 g for 5 min. After one wash with PBS, cells were resuspended in Schneider's Drosophila Medium without serum and Penicillin-Streptomycin to a final concentration of 1.5 million/ml (for RNAi in 12-well and 6-well plates) or 3 million/ml (for RNAi in T-75 flasks). Cells were plated and 10 ug/10 million cells (RNAi in 12-well and 6-well plates) or 5 ug/10 million cells (for RNAi in T-75 flasks) of dsRNAs were added. After incubation for 1h with gentle rocking, 3 volumes of Schneider's Drosophila Medium (supplemented with 10% FBS and 1% Penicillin-Streptomycin solution) was added to the cells. Cells were collected and analyzed after 6 days.

5.5 RNAseq

2 million of Kc167 cells were centrifuged at 500 g for 5 min. Pellets were resuspended in 1mL of PBS and 1 million of *D. virilis* 79f7Dv3 cells were spiked-in. The cell mixture was centrifuged again at 500 g for 5 min and RNA was extracted using RNeasy Mini Kit (QIAgen, Cat No. 74104). The optional DNAse digestion step (QIAgen, Cat No. 79254) was included. mRNA was purified via poly-A purification using Poly(A) RNA selection kit (Lexogen, Cat. No M039100). RNA and mRNA were analyzed on a 2100 Bioanalyzer (Agilent Technologies, Cat. No G2939BA) to assess their quality. Libraries for RNAseq were prepared using NEBnext Ultra II directional RNA library prep kit for Illumina (New England Biolabs, Cat. No E7760L). Libraries were sequenced on an Illumina HiSeq1500 instrument with 50 bp single-end reads (LAFUGA, Gene Center Munich, LMU). Sequencing reads were aligned

separately to the *D. melanogaster* (release 6) or to the *D. virilis* (release 1) genome using STAR (version 2.5.3a) with the GTF annotation *dmel-all-r6.17.gtf* or *dvir-all-r1.07.gtf*, respectively. Reads were filtered from multi-mapping by using the parameter *--outFilterMultimapNmax 1*. Genic read counts were obtained by the parameter *--quantMode GeneCounts*. Genes with low read counts (< 1 read per gene in 6 of the samples) were excluded from further analysis. Normalization factors (*sizeFactors*) were calculated using DESeq2 (version 1.24), separately for *D. melanogaster* or *D. virilis*. Ratio of normalization factors (*D. virilis/D. melanogaster)* > 1 or <1 indicate global transcriptional downregulation or upregulation respectively. For spike-in normalization, normalization factors obtained from *D. virilis* were applied to *D. melanogaster* counts. Differential gene expression analysis was performed using DEseq2, with replicate information as batch covariate. The result function of DEseq2 was used to estimate the log2 fold-change and calculate the adjusted p-values. The threshold for adjusted p-value was set to 0.01. Batch effect was corrected by the *ComBat* function from the sva package (version 3.32) on the log2-transformed normalized read counts. Principal Component analysis (PCA) was carried using batch-adjusted counts. Plots were generated using R graphics. Scripts are available on GitHub (https://github.com/tschauer/Domino_RNAseq_2020).

5.6 Nuclear fractionation and western blot

5-10 million cells were centrifuged at 500 g for 5 min and washed once with PBS. Washed cells were either used directly or flash-frozen for later processing. Cell were lysed in 300 µL of ice-cold NBT-10 buffer by 10 min rotation at 4°C. To isolate nuclei, the lysate was gently overlaid on 500 µL of ice-cold NB-1.2 buffer and centrifuged at 5000 g for 20 min. After 1 wash with 500 µL of ice-cold NB-10 buffer, nuclei were resuspended in 60 µL of 2.5X Laemmli Sample buffer in Protein-RIPA buffer and incubated at 95°C for 5 min. Denatured nuclear extracts were ran on pre-cast 8% (for probing of high molecular weight proteins) or 14% polyacrylamide gels (for probing of histones) (Serva, Cat. No 43260.01 and 43269.01) in 1X Running Buffer (25 mM Tris, 192 mM glycine, 0.1% SDS). Protein separated by electrophoresis were transferred onto nitrocellulose membranes (GE Healthcare Life Sciences, Cat. No 10600002) in ice-cold 1X Transfer Buffer (25 mM Tris, 192 mM glycine) with 20% methanol (for histones) or with 10% methanol + 0.1% SDS (for high molecular weight proteins) at 400 mA for 45-60 min. After 1h of blocking with 5% BSA in TBS buffer for 1 h, membranes were incubated with primary antibodies in TBST buffer (TBS + 0.1% Tween-20) + 5% non-fat milk at 4°C overnight. After three washes (5 min each) with TBST buffer, membranes were incubated with secondary antibodies in TBST buffer for 1 h at room temperature. After three washes (5 min each) with TBST buffer and two washes with TBS

buffer (5 min each), membrane were dried and imaged on a LI-COR Odyssey or a LI-COR Odyssey CLx machine (LI-COR Biosciences).

5.7 ChIPseq

Kc167 cells (70-130 million) were collected in 50 ml tubes and resuspended in complete Schneider's Drosophila Medium to a final volume of 20 ml. For crosslinking, 1:10 of the volume (2.22 ml) of Fixing Solution (100 mM NaCl, 50 mM Hepes pH 8, 1mM EDTA, 0.5 mM EGTA, 10% methanol-free formaldehyde) was added and the tubes were rotated for 8 min (room temperature). The crosslinking reaction was quenched by adding freshly-prepared 2.5 M glycine to a final concentration of 125 mM. Cells were centrifuged at 500 g for 10 min (4°C) and washed once with 10 mL of ice-cold PBS. During this washing step, 3.5 million of crosslinked *D. virilism* 79f7Dv3 cells (with the same procedure as for Kc167 cells) were spiked-in for every 70 million Kc167 cells. For lysis, cells were resuspended in 1 ml of PBS + 0.5% Triton-X-100 + 1X cOmplete EDTA-free Protease Inhibitor / 70 million Kc167 cells and incubated for 15 min at 4°C with constant rotation. Lysate was centrifuged at 2000 g for 10 min to pellet nuclei. After one wash with 10 ml of ice-cold PBS, nuclei were resuspended in 1 ml of RIPA buffer (10 mM Tris-HCl pH 8, 140 mM NaCl, 1mM EDTA, 0.1% Na-deoxycholate, 1% Triton-X-100, 0.1% SDS, 1 mM PMSF, 1X cOmplete EDTA-free Protease Inhibitor) + 2 mM $CaCl_2$ / 70 million Kc167 cells, and flash-frozen in liquid nitrogen in 1ml aliquots. Fixed nuclei were quickly thawed and digested with 1 µL of MNase (to 0.6 units) (Sigma-Aldrich, Cat. No N5386) by incubation at 37°C for 35 min (1000 rpm shaking). Samples were then transferred on ice and 22 µL of 0.5 M EGTA were added to stop the MNase digestion. Digested nuclei were sonicated using a Covaris S220 instrument (50 W peak power, 20% duty factor, 200 cycles/burst, 8 min). Insoluble chromatin was removed by centrifugation at 16000 g for 30 min (4°C). The supernatant, containing soluble chromatin, was pre-cleared using RIPA-equilibrated 50% Protein A+G (1:1) sepharose beads slurry for 1h at 4°C (10 µL slurry / 100 µL of chromatin). An aliquot of of pre-cleared chromatin (100 µL) was kept aside as input fraction and stored overnight at 4°C. For immunoprecipitation, primary antibodies (amounts described later in section 5.12) were added to 300 µL of pre-cleared chromatin and the samplese were incubated overnight at 4°C with constant rotation. The next day, 40 µl of Protein A+G (1:1) 50% slurry was added and the tubes were rotated for 3h at 4°C. After 5 washes with RIPA buffer (5 min rotation at 4°C, pelleted at 3000 g for 1 min between washes), beads were resuspended in 100 µL of TE (10 mM Tris pH 8, 1 mM EDTA) containing 10 µg/100 µl of RNase-A (Sigma, Cat. No. R4875) and incubated at 37°C for 20 min. After addition of 6 µL of 10% SDS, proteins were digested with 250 ng/µl Proteinase K (Genaxxon, Cat.no. M3036.0100) and, simultaneously, crosslink was reversed by incubation at 68°C for 2 hr. DNA was purified using 1.8X Agencourt AMPure XP beads (Beckman

Coulter, Cat No A63880) following standard protocol and eluted in 30 μl of 5 mM Tris-Cl pH 8. Libraries for sequencing were prepared using NEBNext Ultra II DNA library prep kit for Illumina (New England Biolabs, E7465). Libraries were sequenced on an Illumina HiSeq1500 instrument with 50 bp single-end reads (LAFUGA, Gene Center Munich, LMU). Sequencing reads were aligned separately to the *D. melanogaster* (release 6) or to the *D. virilis* (release 1) genome using *bowtie2* (274) (default settings). *Homer* (275) [parameters: *-fragLength 150* and *-totalReads* (reads mapped to *D. virilis* genome)] was utilized to generate tag directories and input-normalized coverage files. The Integrative Genomics Viewer (276) was used to display input-normalized and scaled coverage tracks. Scripts for *D. virilis* scaling and input normalization are available on GitHub (https://github.com/tschauer/Domino_ChIPseq_2020) . Base R graphics and *tsTools* (https://github.com/musikutiv/tsTools) were utilized to generate composite plots. Annotations were obtained from *TxDb.Dmelanogaster.UCSC.dm6.ensGene_3.4.4* (http://bioconductor.org/packages/release/data/annotation/html/TxDb.Dmelanogaster.UCSC. dm6.ensGene.html). Heatmaps were generated using *pheatmap* (https://cran.r-project.org/web/packages/pheatmap/index.html).

5.8 Cloning of DOM constructs

DOM-A and DOM-B cDNAs were assembled by In-Fusion Cloning (Takara Bio, Cat. No 638909) into pENTR3c vector (Thermo Fischer Scientific, Cat. No A10464). The following cDNA templates were used (obtained from the Drosophila Genomic Resource Center): LD35056, LD03212, LD32234. To generate RNAi-resistant DOM-A and DOM-B cDNAs, around 500 bp of the wild-type cDNA sequence were substituted via restriction cloning with a manually mutagenized (sense mutations) and synthesized DNA constructs (gBlock, Integrated DNA Technology). K945G mutants were generated by site-directed mutagenesis (New England Biolabs, Cat. No E0554S). To express GFP-tagged DOM-A and DOM-B (wild-type or K945G) in Kc167 cells, constructs in pENTR3c were recombined in pHWG vector (*D. melanogaster hsp70* promoter – recombination site - GFP – stop codon) (Drosophila Genomic Resource Center) by Gateway cloning (Thermo Fischer Scientific).

5.9 Complementation assays and immunofluorescence

Kc167 cells (1-2 million) were transfected with 500 ng of pHWG plasmid (described in section 5.8) + 25 ng of selection vector (pCoBlast; Thermo Fischer, Cat. No K5150-01) using Effectene Transfection Reagent (QIAgen, Cat. No 301425). 48 h after transfection, cells were transferred in T-25 flasks and selection was started by adding Blasticidin to a final concentration of 50 ng/ul. After 7-8 days of selection the cells were collected and subjected to RNAi as described in section 5.4.

For immunofluorescence, 0.2-0.4 million cells (in 200 µL of complete medium) were seeded directly onto a round 12 mm coverslips (Paul Marienfeld GmbH & Co., Cat No. 0117520). After 2-4 h, coverslips were gently rinsed with 500 µL of PBS. After crosslinking in 500 µL of ice-cold PBS + 2% formaldehyde for 7.5 min, cells were incubated for additional 7.5 min in 500 µL of ice-cold PBS + 0.25% Triton-X-100 + 1% formaldehyde for permeabilization. Following two washes with 1 ml of PBS, coverslips were submerged in PBS + 3% BSA for 1h at room temperature to block cells. To reduce the amount of primary antibody needed, coverslips were carefully placed on a piece of parafilm (inside a wet chamber) and overlaid with 40 µL of primary antibody in PBS + 1.2% normal donkey serum (Jackson Immuno Research). Coverslips were incubated at 4°C overnight. Coverslips were transferred back to 12-well plates and washed two times with 1 ml of PBS. For the incubation with secondary antibodies, the same procedure as for the primary antibody was carried out but the incubation was performed at room temperature for 1h. After transferring the coverslips back to 12-well plates and washing them two times with 1 ml of PBS, DNA was stained with 0.2 µg/ml DAPI (Sigma-Aldrich, Cat. No 10236276001) for 5 min at room temperature. Following one wash with PBS and one with deionized water, coverslips were mounted on glass slides with 8 µL of Vectashield mounting medium (Vector Laboratories, Cat. No H-1000) and sealed with nail polish. Images were taken using a Leica SP5 confocal microscope. Image processing and analysis was performed with Fiji and R-Studio was used for plotting. p-values were calculated using linear regression (*lm* function in R).

5.10 Histone extraction and targeted mass-spectrometry

Kc167 cells were subjected to RNAi as described in section 5.4. Histones were acid-extracted from frozen pellets of 4-12 million cells. Briefly, cells were resuspended in 500 µL of ice-cold 0.2M H_2SO_4 and to acid-extract proteins overnight at 4°C with constant rotation. A centrifugation step at 16,000 g for 10 min at 4°C was carried out to remove insoluble material. The soluble supernatant was collected and acid-extracted proteins were precipitated by adding trichloroacetic acid (final concentration = 26%) followed by an incubation at 4°C for 2 h. Precipitated proteins were pelleted by centrifugation at 16,000 g for 45 min. After two washes with ice-cold 100% acetone (5 min rotation at 4°C, 10 min of 16,000 g spin at 4°C between washes), pellets were air-dried for 30 min (under a chemical hood). Dried pellets were resuspended in 10 µL of 2.5x Laemmli Sample Buffer / million cells and heated at 95°C for 5 min for denaturation. Samples were stored at -20°C until further use. Acid-extracted proteins from 10 million cells were loaded and separated onto a denaturing 4-20% polyacrylamide gels (Serva, Cat. No 43277.01). Gel was stained with Coomassie (Serva, Cat. No 17524.01) and stored at 4°C (in water) until further processing. Bands corresponding to histones were excised from the gel and further fragmentedand

transferred into a PCR tube. After one wash with water, gel pieces were de-stained by two repeated incubations of 30 min at 37°C with 200 μL of 50% acetonitrile (ACN) in 50 mM NH_4HCO_3. After two washes with 200 μL water, gel pieces were dehydrated by two washes with 200 μL of 100% ACN, followed by 5 min of speed-vac to remove residual ACN. 10 μL of deuterated acetic anhydride (Sigma-Aldrich, Cat. No 175641) and 20 μL of 100 mM NH_4HCO_3 were added to the gel pieces to acylate histones in-gel. 70 μL of 1 M NH_4HCO_3 were added to the reaction after about 1 min. Samples were incubated at 37°C for 45 min in a thermomixer. After 5 washes with 200 μL of 100 mM NH_4HCO_3 and 5 with 200 μL of water, gel pieces were washed two times with 200 μL of 100% can and the residual ACN was evaporated using a speed-vac (3 min). To digest peptides, gel pieces were rehydrated in 20 μL of trypsin solution (25 ng/ μL trypsin in 100 mM NH_4HCO_3) (Promega, Cat. No V5111) and incubated at 4°C for 20 min. 100 μL of 50 mM NH_4HCO_3 were then added to the gel pieces and the digestion reaction was further incubated overnight at 37°C. Peptides were sequentially extracted from gel two times with 60 μL of 50% ACN 0.25% trifluoroacetic acid (TFA) (10 minutes incubation, room temperature) and two times 40 μL of 100% can (10 minutes every step, room temperature). Peptides were dried in a speed-vac and stored at -20°C. Dried peptides were resuspended in 100 μL of 0.1% TFA and loaded onto a pre-washed (with ACN) and pre-conditioned (with 0.1% TFA) C18 Stagetip for desalting. Bound peptides were washed 3 times with 20 μL of 0.1% TFA and eluted 3 times with 20 μL of 80% ACN 0.25% TFA. Eluted peptides were dried using a speed-vac, resuspended in 15 μl of 0.1% TFA and stored at -20°C. Peptides were injected in an RSLCnano system (Thermo Fisher Scientific) and separated by high performance liquid chromatography in a 15-cm analytical column (75 μm ID in-house packed with ReproSil-Pur C18-AQ 2.4 μm from Dr. Maisch) using a 50-min gradient from 4 to 40% acetonitrile in 0.1% formic acid (300 nl/min flowrate). The chromatographic eluate was electrosprayed into Q Exactive HF mass spectrometer (Thermo Fisher Scientific). The MS instrument was programmed as described in (246), but the MS3 fragmentation was not performed. Full scan MS spectra (from m/z 270-730) were acquired with resolution R=60,000 at m/z 400 (AGC target of $3x10^6$). Targeted ions were isolated with a window of 0.7 m/z to a target value of $2x10^5$ and fragmented at 27% normalized collision energy. Typical mass spectrometric conditions were: 1) spray voltage = 1.5 kV 2) no sheath and auxiliary gas flow 3) heated capillary temperature = 250°C. The Skyline software (https://skyline.ms/project/home/software/Skyline/begin.view) was used for peak analysis and integration . Further data analysis was performed in R according to the formulas described in (246) (Supplementary Table 4)**.**

5.11 siRNA-mediated knock-down in U2-OS

U2-OS cells were a kind gift from Prof. Dr. Andreas Ladurner (Physiological Chemistry, BMC, LMU Munich). Cells were grown and passaged in standard DMEM media supplemented with 5% FBS and 1% Penicillin-Streptomycin solution (Sigma-Aldrich, Cat No P-4333).

For siRNA-mediated knock-down, the following siRNAs were ordered from Thermo-Fischer (see table below) and transfected at a final concentration of 10nM using Lipofectamine RNAiMAX reagent (Thermo-Fisher, Cat. No 13778030).

Target name	Cat. No
Neg CTRL #1	4390843
EP400 #1	s33487
EP400 #2	s33488
SRCAP #1	s21294
SRCAP #2	s21295
KAT5 #1	s20629
KAT5 #2	s20630
H2A.Z.1 #1	s6414
H2A.Z.1 #2	s6416

Cells were collected 3 days after transfection. Knock-down efficiency was checked by RT-qPCR.

For nuclear extraction, the exact same protocol described in section 5.6 was used. For H2A.Z detection, a rabbit polyclonal antibody was used at 1:1000 dilution (Abcam, ab4174). For H4K16ac detection, a rabbit polyclonal antibody was used at 1:10000 dilution (Merck-Millipore, Cat. No 07-329). Total histones were stained using Li-COR Revert (Li-COR, Cat. No 926-11011).sa

5.12 Antibodies

The detailed procedure for generation of DOM-A and DOM-B polyclonal antisera is described in the appendix (section 6.1). To generate the monoclonal antibody against TIP60, the full length TIP60 was fused with an N-terminal 6xHis tag and expressed in *E. coli*. The protein was purified via Ni-NTA chromatography and eluted with imidazole. Monoclonal antibodies were developed by Dr. Elizabeth Kremmer (BioSysM, LMU Munich). Antibodies were validated by RNAi and western blot.

Antibodies used in this study are described in the following table:

Antigen	Antibody	Species	Type	Application	Dilution/amount
DOM-A	17F4	rat	monoclonal	Western Blot	1/5
	SA-8977	rabbit	polyclonal	Western Blot	1/1000
				ChIP	2 ul / IP

DOM-B	SA-8979	rabbit	polyclonal	Western Blot	1/1000
				ChIP	10 ul / IP
Tip60	11B10	rat	monoclonal	Western Blot	1/20
H2A.V	Rb-H2Av	rabbit	polyclonal	Western Blot	1/1000
				ChIP	25 ul / IP
				Immunofluorescence	1/2500
H4	ab10158	rabbit	polyclonal	Western Blot	1/5000
H4K12ac	07-595	rabbit	polyclonal	ChIP	2 ul / IP
				Immunofluorescence	1/2500
FLAG	m2	mouse	monoclonal	Western Blot	1/1000
GFP	11814460001	mouse	monoclonal	Immunofluorescence	1/500
Lamin	T40	mouse	monoclonal	Western Blot	1/1000

5.13 DATA AND CODE AVAILABILITY

Sequencing data have been deposited at the Gene Expression Omnibus under accession number GSE145738.

Targeted proteomics data have been deposited at ProteomeXchange under accession number PXD017729.

Scripts for *D. virilis* scaling and input normalization for ChIP-seq are available on GitHub (https://github.com/tschauer/Domino_ChIPseq_2020).

Scripts for RNA-seq analysis are available on GitHub (https://github.com/tschauer/Domino_RNAseq_2020).

6. APPENDIX

6.1 Generation of DOM-A and DOM-B rabbit polyclonal antibodies

For DOM-A, residues 2963 to 3188 were expressed as C-terminal Glutathione-S-transferase (GST) fusion by cloning them into pGEX-6-P vector. For DOM-B, residues 2395 to 2497 were expressed as C-terminal Maltose Binding Protein (MBP) fusion by cloning them into pMAL-c2 vector.

For GST-DOM-A expression and purification, 6L of transformed BL21 *E. coli* (OD600 around 0.6-0.8) were induced with 1mM IPTG at 18°C overnight. Bacteria were pelleted and resuspended in 25 ml of ice-cold lysis buffer (25 mM Hepes pH = 7.6, 500 mM NaCl, 0.1% NP-40, 1X Roche cOmplete protease inhibitors) per liter of initial culture and divided in 25 mL aliquots. Cells were sonicated on ice using a Branson digital Sonifier (settings: 20% output, 1s on/ 1s off, 5 minutes total sonication). Sonicated lysates were spun at 15000 rpm (JA 25-50 rotor) for 15 min. Supernatant was transferred in a new tube and 1 ml of equilibrated (in lysis buffer), 50% slurry of glutathione-sepharose 4 Fast Flow Beads (GE Healthcare, Cat. No 17075605) was added. Tubes were rotated for 2h at 4°C. Beads were washed 3 times with 15 ml of ice-cold lysis buffer (5 min rotation at 4°C, spin at 500 g for 2 min in between). Beads were then washed once with 10 ml of elution buffer (25mM Hepes pH = 7.6, 200 mM NaCl, 1mM DTT, 1X Roche cOmplete protease inhibitors), and once with in 1ml of elution buffer after being transferred in 1.5 ml Eppendorf tubes. For elution, beads were resuspended in 500 µl of elution buffer + 20 mM Reduced Glutathione (pH verified) and rotated for 30 min at 4°C. Beads were pelleted at 500 g for 3 min and supernatant was collected. In total, 3 rounds of elution were performed, and supernatants pooled together. Glycerol was added to a final concentration of 10% and samples were frozen in liquid nitrogen.

For MBP-DOM-B expression and purification, 1L of transformed BL21 *E. coli* (OD600 around 0.6-0.8) were induced with 1mM IPTG at 18°C overnight. Bacteria were pelleted and resuspended in 25 ml of ice-cold lysis buffer MBP (25 mM Hepes pH = 7.6, 500 mM NaCl, 0.5 mM EDTA, 1X Roche cOmplete protease inhibitors). Cells were sonicated on ice using a Branson digital Sonifier (settings: 20% output, 1s on/ 1s off, 5 minutes total sonication). Sonicated lysate was spun at 15000 rpm (JA 25-50 rotor) for 15 min. In the meantime, 1.5 mL of amylose resin (New England Biolabs, Cat. No E8121S) were applied to a Poly-Prep Chromatographic column (BIO-RAD, Cat. No 7311550) and washed with 7.5 mL of ice-cold lysis buffer MBP. Clear lysate was passed through the column containing amylose resin at 4°C. Resin was washed once with 10 ml of ice-cold lysis buffer MBP and twice with 10 ml of

elution buffer MBP (20 mM Hepes pH = 7.6, 150 mM NaCl, 0.5 mM EDTA, 1X Roche cOmplete protease inhibitors). Protein was eluted from resin by adding 5 times 1ml of elution buffer MBP + 20 mM maltose. The first 4 elution fractions were pooled together, glycerol was added to a final concentration of 10% and samples were frozen in liquid nitrogen.

Antibody production in rabbit (2 animals each construct) was done by Eurogentec (https://secure.eurogentec.com/eu-home.html).

Antibodies were tested for western blot (**Appendix Figure 1**) (1:1000 dilution), immunoprecipitation (**Appendix Figure 2**) and immunofluorescence (**Appendix Figure 3**) (1:1000 dilution). In IF, DOM-B antibody gives a mix of nuclear and cytosolic signal.
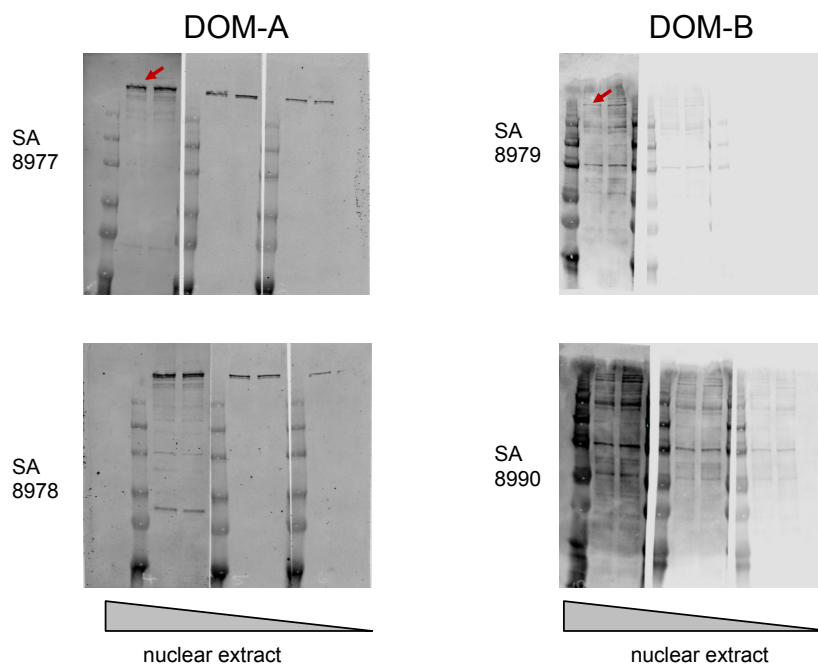
Appendix Figure 1 Testing of DOM-A and DOM-B polyclonal antibodies by Western blot. Nuclear extract from Kc cells was used in serial dilutions (1:5).
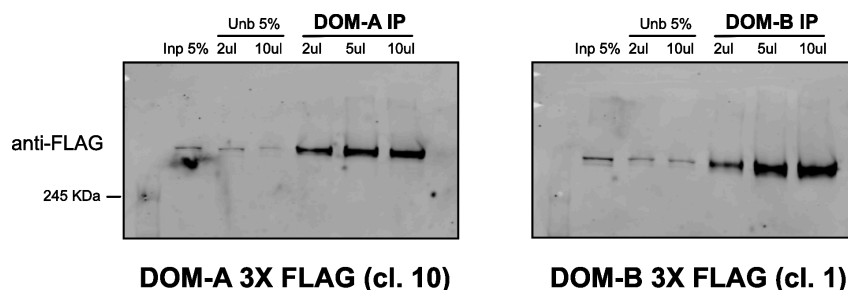
Appendix Figure 2 Testing of DOM-A and DOM-B polyclonal antibodies for immunoprecipitation. Nuclear extract from CRISPR-tagged DOM-A or DOM-B L2-4 cells was used (1 mg of total proteins). IP and washes were in RIPA conditions. 3 different amounts of antibodies were tested
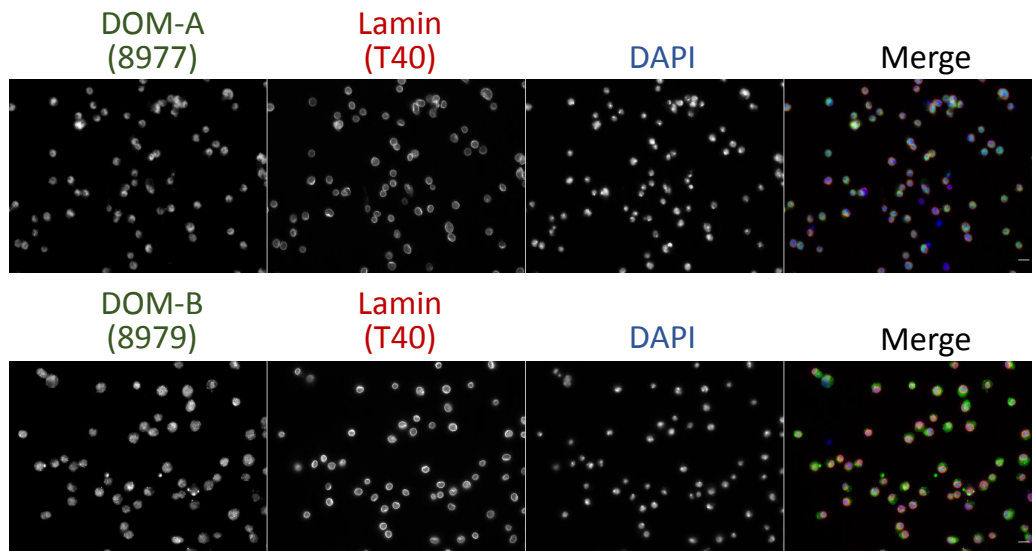
Appendix Figure 3 Testing of DOM-A and DOM-B polyclonal antibodies for immunofluorescence in L2-4 cells. Standard procedures for IF were used.

6.2 Primers utilized in the projects but not published

Name	Sequence	Comments
DomA_qPCR_f1	atcagaccacggctgtaacc	RT-qPCR for DomA, not bad
DomA_qPCR_r1	tctgagtggctggagatgtg	RT-qPCR for DomA, not bad
DomB_qPCR_f2	gcaggaagagcaggagtctg	RT-qPCR for DomB, ok-ish, tm not very good at high diluitions
DomB_qPCR_r2	tcaaccattccctcttcacc	RT-qPCR for DomB, ok-ish, tm not very good at high diluitions
dU6_2_sgRNA_F	gttcgacttgcagcctgaaatacggcacg	For CRISPR in S2 cells, general primer for amplification of gRNAs
dU6_2_sgRNA_R	aaaaaagcaccgactcggtgccacttttttcaagttgataa	For CRISPR in S2 cells, general primer for amplification of gRNAs

CG12054_RNAi _f1	taatacgactcactatagggACCATTCGAAGAAC GGTCAC	RNAi in S2 cells, specific for DCG12054. Designed using SnapDragon, 477bp
CG12054_RNAi _r1	taatacgactcactatagggCGTTGCTAGTGAGA ATGGCA	RNAi in S2 cells, specific for DCG12054. Designed using SnapDragon, 477bp
CG12054_RNAi _f2	taatacgactcactatagggTATGTCCTGCGCTTC ATCAC	RNAi in S2 cells, specific for DCG12054. Designed using SnapDragon, 344bp
CG12054_RNAi _r2	taatacgactcactatagggTAAACTCCTCGGTG GTCCAG	RNAi in S2 cells, specific for DCG12054. Designed using SnapDragon, 344bp
Dom_E1043Q_f 1	CATCCTGGATcaaGCGCAGAACA	For Dom mutagenesis. Walker B mutant. Designed with NEBaseChanger
Dom_E1043Q_r 1	AGATACTTCCACTTTTTGCGG	For Dom mutagenesis. Walker B mutant. Designed with NEBaseChanger
Nup43_f1	GTGCAAGCTTGACCACCTTA	qPCR for Dom ChIP, should amplify both
Nup43_r1	AGCAGAGGATTCGCGATGTA	qPCR for Dom ChIP, should amplify both
Sir2_f1	ACGTGTGCCATCTTGCTTTT	qPCR for Dom ChIP, should amplify both
Sir2_r1	TTTTACGTCGTCAGCTTCGC	qPCR for Dom ChIP, should amplify both

ABBREVIATIONS

ACF	ATP-utilizing Chromatin assembly Factor
ATP	adenosine triphosphate
bp	base pair(s)
ChIP	Chromatin Immunoprecipitation
ChIPseq	ChIP sequencing
CHRAC	Chromatin Accessibility Complex
DBD	DNA binding domain
DOM	DOMINO
GFP	Green Fluorescent Protein
H3K27me3	tri-methylated Lys 27 of histone H3
H3K36me3	tri-methylated Lys 36 of histone H3
H3K4me3	tri-methylated Lys 4 of histone H3
H3K9me2/3	di- or tri-methylated Lys 9 of histone H3
H3S10	Ser 10 of histone H3
H4K5/8/12/16ac	acetylation of Lys 5/8/12/16 of histone H4
HAT	Histone Acetyltransferase
HDAC	Histone Deacetylase
NFR	Nucleosome Free Region
NuA4	Nucleosome Acetyltransferase of H4
PEV	Position-Effect Variegation
PTM	Post Translational Modification
qPCR	quantitative PCR
RNAi	RNA interference
RNAseq	RNA sequencing
RT	retrotranscription
SWR1	Swi2/Snf2-Related 1
UAS	Upstream Activating Sequence
ZGA	Zigotyc Genome Activation

ACKNOWLEDGMENTS

The near 5-year journey of my PhD has been an incredible one. When I look back and reflect on what this "ride" did to me, I'd like to think that it turned me from a student to (almost) a real scientist. It has been a difficult path, though, and I would not have made it without the help and support of many around me.

First and foremost, I'd like to thank Peter - my mentor and supervisor. He is not just an excellent scientist, but also an incredible human being. He guided me well through the initial phases of my doctorate and, later on towards the end, fully supported my independence. He put a lot of trust in me, even when perhaps I did not fully deserve it, and always treated me as a peer - rather than just a student working for him. I think this kind of respect is not easy to come by these days in academia. In many occasions we had different opinions, but he never dismissed my ideas or point of views without considering them first. I know I am often stubborn and he dealt with this with incredible kindness. Honestly, I learned a lot from him. I hope I lived up to his expectations.

I'd like to thank the whole Becker lab, past and present, for the constant support and for creating and maintaining a great scientific environment, where PhD students can flourish. In particular, I want to thank Raffi, as I consider her my "unofficial" second mentor. She is one of the best scientists I've ever met and she's always been a source of inspiration. I'd like to thank Tamas and his scientific rigor, which made a huge impact in the way I see and do science. I want to thank Kenneth for his help and advices when I started in the lab, as well as for his excitement and seminal work on the ACF and DOMINO projects. I'd like to thank Zisis, my teammate in the DOMINO project. He is one of the nicest and hard-working people in the lab – always to look up to. I also want to thank Sandro for his never-ending collection of bold and smart ideas and Marisa for her advice and help in anything regarding hard-core biochemistry. I want to thank Silke, by far the best technician I've had the privilege to work with, and Aline for her help in the tissue culture. Along this line, I also want to thank Angie for her help in ChIP protocols and libraries. Finally, I'd like to thank Lisa, Dhawal, Catherine, Nadia, Christian, Nikolas, Sarah, Anna, Natascha, Arturo and Ömer for feedback, discussions and ideas. I'd like to extend my thanks to the whole Molecular Biology department ("The lab") and especially Andrea, who became a dear friend over the years, and Tobias for his criticism, integrity and inspiration.

I'd like to thank my TAC members, Jürg Müller and Klaus Förstemann for their interest and excitement about my work and for their commitment to guarantee a smooth PhD for me.

REFERENCES

1. M. S. Luijsterburg, M. F. White, R. van Driel, R. T. Dame, The major architects of chromatin: architectural proteins in bacteria, archaea and eukaryotes. *Crit Rev Biochem Mol Biol* **43**, 393-418 (2008).
2. M. Joyeux, Compaction of bacterial genomic DNA: clarifying the concepts. *J Phys Condens Matter* **27**, 383001 (2015).
3. J. Makela, D. J. Sherratt, Organization of the Escherichia coli Chromosome by a MukBEF Axial Core. *Mol Cell* 10.1016/j.molcel.2020.02.003 (2020).
4. F. Mattiroli *et al.*, Structure of histone-based chromatin in Archaea. *Science* **357**, 609-612 (2017).
5. M. Rojec, A. Hocher, K. M. Stevens, M. Merkenschlager, T. Warnecke, Chromatinization of Escherichia coli with archaeal histones. *Elife* **8** (2019).
6. S. Baldi, P. Korber, P. B. Becker, Beads on a string-nucleosome array arrangements and folding of the chromatin fiber. *Nat Struct Mol Biol* **27**, 109-118 (2020).
7. K. Luger, A. W. Mader, R. K. Richmond, D. F. Sargent, T. J. Richmond, Crystal structure of the nucleosome core particle at 2.8 A resolution. *Nature* **389**, 251-260 (1997).
8. J. S. Godde, A. P. Wolffe, Disruption of reconstituted nucleosomes. The effect of particle concentration, MgCl2 and KCl concentration, the histone tails, and temperature. *J Biol Chem* **270**, 27399-27402 (1995).
9. H. Taguchi, N. Horikoshi, Y. Arimura, H. Kurumizaka, A method for evaluating nucleosome stability with a protein-binding fluorescent dye. *Methods* **70**, 119-126 (2014).
10. J. Widom, Role of DNA sequence in nucleosome stability and dynamics. *Q Rev Biophys* **34**, 269-324 (2001).
11. E. Oberbeckmann *et al.*, Absolute nucleosome occupancy map for the Saccharomyces cerevisiae genome. *Genome Res* **29**, 1996-2009 (2019).
12. D. V. Fyodorov, B. R. Zhou, A. I. Skoultchi, Y. Bai, Emerging roles of linker histones in regulating chromatin structure and function. *Nat Rev Mol Cell Biol* **19**, 192-206 (2018).
13. V. Ramakrishnan, J. T. Finch, V. Graziano, P. L. Lee, R. M. Sweet, Crystal structure of globular domain of histone H5 and its implications for nucleosome binding. *Nature* **362**, 219-223 (1993).
14. J. Bednar *et al.*, Structure and Dynamics of a 197 bp Nucleosome in Complex with Linker Histone H1. *Mol Cell* **66**, 384-397 e388 (2017).
15. E. H. Bresnick, M. Bustin, V. Marsaud, H. Richard-Foy, G. L. Hager, The transcriptionally-active MMTV promoter is depleted of histone H1. *Nucleic Acids Res* **20**, 273-278 (1992).
16. X. Shen, M. A. Gorovsky, Linker Histone H1 Regulates Specific Gene Expression but Not Global Transcription In Vivo. *Cell* **86**, 475-483 (1996).
17. K. Hellauer, E. Sirard, B. Turcotte, Decreased expression of specific genes in yeast cells lacking histone H1. *J Biol Chem* **276**, 13587-13592 (2001).

18.   A. Izzo, R. Schneider, The role of linker histone H1 modifications in the regulation of gene expression and chromatin dynamics. *Biochim Biophys Acta* **1859**, 486-495 (2016).

19.   S. Krishnan, A. H. Smits, M. Vermeulen, D. Reinberg, Phospho-H1 Decorates the Inter-chromatid Axis and Is Evicted along with Shugoshin by SET during Mitosis. *Mol Cell* **67**, 579-593 e576 (2017).

20.   E. N. Andreyeva *et al.*, Regulatory functions and chromatin loading dynamics of linker histone H1 during endoreplication in Drosophila. *Genes Dev* **31**, 603-616 (2017).

21.   L. Halmer, C. Gruss, Effects of cell cycle dependent histone H1 phosphorylation on chromatin structure and chromatin replication. *Nucleic Acids Res* **24**, 1420-1427 (1996).

22.   P. J. Robinson, L. Fairall, V. A. Huynh, D. Rhodes, EM measurements define the dimensions of the "30-nm" chromatin fiber: evidence for a compact, interdigitated structure. *Proc Natl Acad Sci U S A* **103**, 6506-6511 (2006).

23.   V. A. Huynh, P. J. Robinson, D. Rhodes, A method for the in vitro reconstitution of a defined "30 nm" chromatin fibre containing stoichiometric amounts of the linker histone. *J Mol Biol* **345**, 957-968 (2005).

24.   K. Maeshima, S. Ide, M. Babokhov, Dynamic chromatin organization without the 30-nm fiber. *Curr Opin Cell Biol* **58**, 95-104 (2019).

25.   M. Ohno *et al.*, Sub-nucleosomal Genome Structure Reveals Distinct Nucleosome Folding Motifs. *Cell* **176**, 520-534 e525 (2019).

26.   V. I. Risca, S. K. Denny, A. F. Straight, W. J. Greenleaf, Variable chromatin structure revealed by in situ spatially correlated DNA cleavage mapping. *Nature* **541**, 237-241 (2017).

27.   H. D. Ou *et al.*, ChromEMT: Visualizing 3D chromatin structure and compaction in interphase and mitotic cells. *Science* **357** (2017).

28.   E. Passarge, Emil Heitz and the concept of heterochromatin: longitudinal chromosome differentiation was recognized fifty years ago. *Am J Hum Genet* **31**, 106-115 (1979).

29.   H. G. Davies, A. B. Murray, M. E. Walmsley, Electron-microscope observations on the organization of the nucleus in chicken erythrocytes and a superunit thread hypothesis for chromosome structure. *J Cell Sci* **16**, 261-299 (1974).

30.   G. Yasuzumi, R. Sugihara, The fine structure of nuclei as revealed by electron microscopy. *Experimental Cell Research* **40**, 45-55 (1965).

31.   R. H. Goodman, D. Spiro, Electron microscopic studies of giant salivary gland chromosomes. *Experimental Cell Research* **27**, 359-363 (1962).

32.   M. M. Rae, W. W. Franke, The interphase distribution of satellite DNA-containing heterochromatin in mouse nuclei. *Chromosoma* **39**, 443-456 (1972).

33.   W. G. Flamm, P. M. B. Walker, M. McCallum, Some properties of the single strands isolated from the DNA of the nuclear satellite of the mouse (Mus musculus). *Journal of Molecular Biology* **40**, 423-443 (1969).

34.   N. Saksouk, E. Simboeck, J. Dejardin, Constitutive heterochromatin formation and transcription in mammals. *Epigenetics Chromatin* **8**, 3 (2015).

35.   T. Jenuwein, Re-SET-ting heterochromatin by histone methyltransferases. *Trends in Cell Biology* **11**, 266-273 (2001).

36.   R. A. Martienssen, M. Zaratiegui, D. B. Goto, RNA interference and heterochromatin in the fission yeast Schizosaccharomyces pombe. *Trends Genet* **21**, 450-456 (2005).

37. S. C. Elgin, G. Reuter, Position-effect variegation, heterochromatin formation, and gene silencing in Drosophila. *Cold Spring Harb Perspect Biol* **5**, a017780 (2013).

38. P. Trojer, D. Reinberg, Facultative heterochromatin: is there a distinctive molecular signature? *Mol Cell* **28**, 1-13 (2007).

39. B. Schuettengruber, H. M. Bourbon, L. Di Croce, G. Cavalli, Genome Regulation by Polycomb and Trithorax: 70 Years and Counting. *Cell* **171**, 34-57 (2017).

40. S. L. Klemm, Z. Shipony, W. J. Greenleaf, Chromatin accessibility and the regulatory epigenome. *Nat Rev Genet* **20**, 207-220 (2019).

41. K. S. Zaret, J. S. Carroll, Pioneer transcription factors: establishing competence for gene expression. *Genes Dev* **25**, 2227-2241 (2011).

42. M. Iwafuchi-Doi, K. S. Zaret, Cell fate control by pioneer transcription factors. *Development* **143**, 1833-1837 (2016).

43. A. Mayran, J. Drouin, Pioneer transcription factors shape the epigenetic landscape. *J Biol Chem* **293**, 13795-13804 (2018).

44. Y. Liu *et al.*, Transcriptional landscape of the human cell cycle. *Proc Natl Acad Sci U S A* **114**, 3473-3478 (2017).

45. H. Niwa, The principles that govern transcription factor network functions in stem cells. *Development* **145** (2018).

46. A. Vihervaara, F. M. Duarte, J. T. Lis, Molecular mechanisms driving transcriptional stress responses. *Nat Rev Genet* **19**, 385-397 (2018).

47. F. Spitz, E. E. Furlong, Transcription factors: from enhancer binding to developmental control. *Nat Rev Genet* **13**, 613-626 (2012).

48. F. Payvar *et al.*, Purified glucocorticoid receptors bind selectively in vitro to a cloned DNA fragment whose transcription is regulated by glucocorticoids in vivo. *Proc Natl Acad Sci U S A* **78**, 6628-6632 (1981).

49. W. S. Dynan, R. Tjian, The promoter-specific transcription factor Sp1 binds to upstream sequences in the SV40 early promoter. *Cell* **35**, 79-87 (1983).

50. D. Engelke, S. Ng, B. Shastry, R. Roeder, Specific interaction of a purified transcription factor with an internal control region of 5S RNA genes. *Cell* **19**, 717-728 (1980).

51. N. J. Fuda, M. B. Ardehali, J. T. Lis, Defining mechanisms that regulate RNA polymerase II transcription in vivo. *Nature* **461**, 186-192 (2009).

52. C. O. Pabo, R. T. Sauer, Transcription factors: structural families and principles of DNA recognition. *Annu Rev Biochem* **61**, 1053-1095 (1992).

53. I. Whitehouse, O. J. Rando, J. Delrow, T. Tsukiyama, Chromatin remodelling at promoters suppresses antisense transcription. *Nature* **450**, 1031-1035 (2007).

54. P. Korber, P. B. Becker, Nucleosome dynamics and epigenetic stability. *Essays Biochem* **48**, 63-74 (2010).

55. E. E. Swinstead, V. Paakinaho, D. M. Presman, G. L. Hager, Pioneer factors and ATP-dependent chromatin remodeling factors interact dynamically: A new perspective: Multiple transcription factors can effect chromatin pioneer functions through dynamic interactions with ATP-dependent chromatin remodeling factors. *Bioessays* **38**, 1150-1157 (2016).

56. B. Li, M. Carey, J. L. Workman, The role of chromatin during transcription. *Cell* **128**, 707-719 (2007).

57. C. Ballare *et al.*, Nucleosome-driven transcription factor binding and gene regulation. *Mol Cell* **49**, 67-79 (2013).

58.   M. Iwafuchi *et al.*, Gene network transitions in embryos depend upon interactions between a pioneer transcription factor and core histones. *Nat Genet* **52**, 418-427 (2020).

59.   M. Fernandez Garcia *et al.*, Structural Features of Transcription Factors Associating with Nucleosome Binding. *Mol Cell* **75**, 921-932 e926 (2019).

60.   S. O. Dodonova, F. Zhu, C. Dienemann, J. Taipale, P. Cramer, Nucleosome-bound SOX2 and SOX11 structures elucidate pioneer factor function. *Nature* 10.1038/s41586-020-2195-y (2020).

61.   A. K. Michael *et al.*, Mechanisms of OCT4-SOX2 motif readout on nucleosomes. *Science* 10.1126/science.abb0074 (2020).

62.   P. B. Becker, J. L. Workman, Nucleosome remodeling and epigenetics. *Cold Spring Harbor perspectives in biology* **5** (2013).

63.   A. Saha, J. Wittmeyer, B. R. Cairns, Chromatin remodelling: the industrial revolution of DNA around histones. *Nat Rev Mol Cell Biol* **7**, 437-447 (2006).

64.   S. He *et al.*, Structure of nucleosome-bound human BAF complex. *Science* **367**, 875-881 (2020).

65.   G. D. Bowman, S. Deindl, Remodeling the genome with DNA twists. *Science* **366**, 35-36 (2019).

66.   C. R. Clapier, J. Iwasa, B. R. Cairns, C. L. Peterson, Mechanisms of action and regulation of ATP-dependent chromatin-remodelling complexes. *Nat Rev Mol Cell Biol* **18**, 407-422 (2017).

67.   L. Farnung, S. M. Vos, C. Wigge, P. Cramer, Nucleosome-Chd1 structure and implications for chromatin remodelling. *Nature* **550**, 539-542 (2017).

68.   F. Mueller-Planitz, H. Klinker, P. B. Becker, Nucleosome sliding mechanisms: new twists in a looped history. *Nat Struct Mol Biol* **20**, 1026-1032 (2013).

69.   K. K. Sinha, J. D. Gross, G. J. Narlikar, Distortion of histone octamer core promotes nucleosome mobilization by a chromatin remodeler. *Science* **355** (2017).

70.   O. Willhoft *et al.*, Structure and dynamics of the yeast SWR1-nucleosome complex. *Science* **362** (2018).

71.   O. Willhoft, D. B. Wigley, INO80 and SWR1 complexes: the non-identical twins of chromatin remodelling. *Curr Opin Struct Biol* **61**, 50-58 (2019).

72.   T. Nakagawa, M. Bulger, M. Muramatsu, T. Ito, Multistep chromatin assembly on supercoiled plasmid DNA by nucleosome assembly protein-1 and ATP-utilizing chromatin assembly and remodeling factor. *J Biol Chem* **276**, 27384-27391 (2001).

73.   D. V. Fyodorov, J. T. Kadonaga, Chromatin assembly in vitro with purified recombinant ACF and NAP-1. *Methods Enzymol* **371**, 499-515 (2003).

74.   A. Hamiche, R. Sandaltzopoulos, D. A. Gdula, C. Wu, ATP-Dependent Histone Octamer Sliding Mediated by the Chromatin Remodeling Complex NURF. *Cell* **97**, 833-842 (1999).

75.   A. Eberharter *et al.*, Acf1, the largest subunit of CHRAC, regulates ISWI-induced nucleosome remodelling. *EMBO J* **20**, 3781-3788 (2001).

76.   D. F. V. Corona *et al.*, ISWI Is an ATP-Dependent Nucleosome Remodeling Factor. *Molecular Cell* **3**, 239-245 (1999).

77.   G. Längst, E. J. Bonte, D. F. V. Corona, P. B. Becker, Nucleosome Movement by CHRAC and ISWI without Disruption or trans-Displacement of the Histone Octamer. *Cell* **97**, 843-852 (1999).

78.   V. K. Maier, M. Chioda, D. Rhodes, P. B. Becker, ACF catalyses chromatosome movements in chromatin fibres. *EMBO J* **27**, 817-826 (2008).

79.   T. Ito, M. Bulger, M. J. Pazin, R. Kobayashi, J. T. Kadonaga, ACF, an ISWI-Containing and ATP-Utilizing Chromatin Assembly and Remodeling Factor. *Cell* **90**, 145-155 (1997).

80.   P. D. Varga-Weisz *et al.*, Chromatin-remodeling factor CHRAC contains the ATPases ISWI and topoisomerase II. *Nature* **388**, 598-602 (1997).

81.   T. Ito *et al.*, ACF consists of two subunits, Acf1 and ISWI, that function cooperatively in the ATP-dependent catalysis of chromatin assembly. *Genes & Dev* **13**, 1529-1539 (1999).

82.   D. F. V. Corona *et al.*, Two histone fold proteins, CHRAC-14 and CHRAC-16, are developmentally regulated subunits of chromatin accessibility complex (CHRAC). *The EMBO journal* **19**, 3049-3059 (2000).

83.   K. F. Hartlepp *et al.*, The histone fold subunits of Drosophila CHRAC facilitate nucleosome sliding through dynamic DNA interactions. *Molecular and cellular biology* **25**, 9886-9896 (2005).

84.   Längst G, Bonte EJ, Corona DFV, Becker PB, Nucleosome Movement by CHRAC and ISWI without Disruption or trans-Displacement of the Histone Octamer. *Cell* **97**, 843-852 (1999).

85.   Eberharter A. *et al.*, Acf1, the largest subunit of CHRAC, regulates ISWI-induced nucleosome remodelling. *The EMBO journal* **20**, 3781-3788 (2001).

86.   X. He, H. Y. Fan, G. J. Narlikar, R. E. Kingston, Human ACF1 alters the remodeling strategy of SNF2h. *The Journal of biological chemistry* **281**, 28636-28647 (2006).

87.   T. R. Blosser, J. G. Yang, M. D. Stone, G. J. Narlikar, X. Zhuang, Dynamics of nucleosome remodelling by individual ACF complexes. *Nature* **462**, 1022-1027 (2009).

88.   J. D. Leonard, G. J. Narlikar, A nucleotide-driven switch regulates flanking DNA length sensing by a dimeric chromatin remodeler. *Molecular cell* **57**, 850-859 (2015).

89.   L. R. Racki *et al.*, The chromatin remodeller ACF acts as a dimeric motor to space nucleosomes. *Nature* **462**, 1016-1021 (2009).

90.   M. Chioda, S. Vengadasalam, E. Kremmer, A. Eberharter, P. B. Becker, Developmental role for ACF1-containing nucleosome remodellers in chromatin organisation. *Development* **137**, 3513-3522 (2010).

91.   K. Boerner *et al.*, A role for tuned levels of nucleosome remodeler subunit ACF1 during Drosophila oogenesis. *Developmental biology* **411**, 217-230 (2016).

92.   D. V. Fyodorov, M. D. Blower, G. H. Karpen, J. T. Kadonaga, Acf1 confers unique activities to ACF/CHRAC and promotes the formation rather than disruption of chromatin in vivo. *Genes Dev* **18**, 170-183 (2004).

93.   J. A. Dowdle *et al.*, Mouse BAZ1A (ACF1) is dispensable for double-strand break repair but is essential for averting improper gene expression during spermatogenesis. *PLoS Genet* **9**, e1003945 (2013).

94.   A. Zaghlool *et al.*, A Role for the Chromatin-Remodeling Factor BAZ1A in Neurodevelopment. *Hum Mutat* **37**, 964-975 (2016).

95.   H. Sun *et al.*, ACF chromatin-remodeling complex mediates stress-induced depressive-like behavior. *Nat Med* **21**, 1146-1153 (2015).

96.   T. G. Fazzio, T. Tsukiyama, Chromatin Remodeling In Vivo: Evidence for a Nucleosome Sliding Mechanism. *Molecular cell* **12**, 1333-1340 (2003).

97. K. Yen, V. Vinayachandran, K. Batta, R. T. Koerber, B. F. Pugh, Genome-wide nucleosome specificity and directionality of chromatin remodelers. *Cell* **149**, 1461-1473 (2012).

98. Y. I. Liu *et al.*, The chromatin remodelers ISWI and ACF1 directly repress Wingless transcriptional targets. *Developmental biology* **323**, 41-52 (2008).

99. T. Ito, B. Michael, M. J. Pazin, R. Kobayashi, J. T. Kadonaga, ACF, an ISWI-Containing and ATP-Utilizing Chromatin Assembly and Remodeling Factor. *Cell* **90**, 145-155 (1997).

100. D. V. Fyodorov, M. D. Blower, G. H. Karpen, J. T. Kadonaga, Acf1 confers unique activities to ACF/CHRAC and promotes the formation rather than disruption of chromatin in vivo. *Genes & Dev* 10.1101/, 170-183 (2004).

101. P. A. Jeggo, J. A. Downs, S. M. Gasser, Chromatin modifiers and remodellers in DNA repair and signalling. *Philos Trans R Soc Lond B Biol Sci* **372** (2017).

102. M. B. Rother, H. van Attikum, DNA repair goes hip-hop: SMARCA and CHD chromatin remodellers join the break dance. *Philos Trans R Soc Lond B Biol Sci* **372** (2017).

103. L. Lan *et al.*, The ACF1 complex is required for DNA double-strand break repair in human cells. *Molecular cell* **40**, 976-987 (2010).

104. O. Z. Aydin, W. Vermeulen, H. Lans, ISWI chromatin remodeling complexes in the DNA damage response. *Cell Cycle* **13**, 3016-3025 (2014).

105. K. Klement *et al.*, Opposing ISWI- and CHD-class chromatin remodeling activities orchestrate heterochromatic DNA repair. *J Cell Biol* **207**, 717-733 (2014).

106. S. Sanchez-Molina *et al.*, Role for hACF1 in the G2/M damage checkpoint. *Nucleic Acids Res* **39**, 8445-8456 (2011).

107. V. Mathew *et al.*, The histone-fold protein CHRAC14 influences chromatin composition in response to DNA damage. *Cell Rep* **7**, 321-330 (2014).

108. P. B. Talbert, S. Henikoff, Histone variants on the move: substrates for chromatin dynamics. *Nat Rev Mol Cell Biol* **18**, 115-126 (2017).

109. C. F. Kurat *et al.*, Regulation of histone gene transcription in yeast. *Cell Mol Life Sci* **71**, 599-613 (2014).

110. A. Gunjan, A. Verreault, A Rad53 Kinase-Dependent Surveillance Mechanism that Regulates Histone Protein Levels in S. cerevisiae. *Cell* **115**, 537-549 (2003).

111. M. Berloco, L. Fanti, A. Breiling, V. Orlando, S. Pimpinelli, The maternal effect gene, abnormal oocyte (abo), of Drosophila melanogaster encodes a specific negative regulator of histones. *Proc Natl Acad Sci U S A* **98**, 12126-12131 (2001).

112. J. H. Waterborg, A. J. Robertson, Common features of analogous replacement histone H3 genes in animals and plants. *J Mol Evol* **43**, 194-206 (1996).

113. P. B. Talbert, S. Henikoff, Histone variants--ancient wrap artists of the epigenome. *Nat Rev Mol Cell Biol* **11**, 264-275 (2010).

114. S. Pentakota *et al.*, Decoding the centromeric nucleosome through CENP-N. *Elife* **6** (2017).

115. T. Fukagawa, W. C. Earnshaw, The centromere: chromatin foundation for the kinetochore machinery. *Dev Cell* **30**, 496-508 (2014).

116. C. Jin, G. Felsenfeld, Nucleosome stability mediated by histone variants H3.3 and H2A.Z. *Genes Dev* **21**, 1519-1529 (2007).

117. S. J. Elsaesser, A. D. Goldberg, C. D. Allis, New functions for an old variant: no substitute for histone H3.3. *Curr Opin Genet Dev* **20**, 110-117 (2010).

118. E. Szenker, D. Ray-Gallet, G. Almouzni, The double face of the histone variant H3.3. *Cell Res* **21**, 421-434 (2011).

119. B. E. Schwartz, K. Ahmad, Transcriptional activation triggers deposition and removal of the histone variant H3.3. *Genes Dev* **19**, 804-814 (2005).

120. M. Buschbeck, S. B. Hake, Variants of core histones and their roles in cell fate decisions, development and cancer. *Nat Rev Mol Cell Biol* **18**, 299-314 (2017).

121. V. Turinetto, C. Giachino, Multiple facets of histone variant H2AX: a DNA double-strand-break marker with several biological functions. *Nucleic Acids Res* **43**, 2489-2498 (2015).

122. T. T. Paull *et al.*, A critical role for histone H2AX in recruitment of repair factors to nuclear foci after DNA damage. *Current Biology* **10**, 886-895 (2000).

123. C. Redon *et al.*, Histone H2A variants H2AX and H2AZ. *Current Opinion in Genetics & Development* **12**, 162-169 (2002).

124. T. H. Thatcher, M. A. Gorovsky, Phylogenetic analysis of the core histones H2A, H2B, H3, and H4. *Nucleic Acids Res* **22**, 174-179 (1994).

125. J. Bonnet *et al.*, Quantification of Proteins and Histone Marks in Drosophila Embryos Reveals Stoichiometric Relationships Impacting Chromatin Regulation. *Dev Cell* **51**, 632-644 e636 (2019).

126. A. van Daal, S. C. Elgin, A histone variant, H2AvD, is essential in Drosophila melanogaster. *Mol Biol Cell* **3**, 593-602 (1992).

127. S. Baldi, P. B. Becker, The variant histone H2A.V of Drosophila--three roles, two guises. *Chromosoma* **122**, 245-258 (2013).

128. M. Adam, F. Robert, M. Larochelle, L. Gaudreau, H2A.Z is required for global chromatin integrity and for recruitment of RNA polymerase II under specific conditions. *Mol Cell Biol* **21**, 6270-6279 (2001).

129. C. M. Weber, J. G. Henikoff, S. Henikoff, H2A.Z nucleosomes enriched over active genes are homotypic. *Nat Struct Mol Biol* **17**, 1500-1507 (2010).

130. C. M. Weber, S. Ramachandran, S. Henikoff, Nucleosomes are context-specific, H2A.Z-modulated barriers to RNA polymerase. *Mol Cell* **53**, 819-830 (2014).

131. T. N. Mavrich *et al.*, Nucleosome organization in the Drosophila genome. *Nature* **453**, 358-362 (2008).

132. B. D. Giaimo, F. Ferrante, A. Herchenrother, S. B. Hake, T. Borggrefe, The histone variant H2A.Z in gene regulation. *Epigenetics Chromatin* **12**, 37 (2019).

133. T. Kusch *et al.*, Acetylation by Tip60 is required for selective histone variant exchange at DNA lesions. *Science* **306**, 2084-2087 (2004).

134. C. M. Lake, J. K. Holsclaw, S. P. Bellendir, J. Sekelsky, R. S. Hawley, The development of a monoclonal antibody recognizing the Drosophila melanogaster phosphorylated histone H2A variant (gamma-H2AV). *G3 (Bethesda)* **3**, 1539-1543 (2013).

135. M. J. Clarkson, J. R. Wells, F. Gibson, R. Saint, D. J. Tremethick, Regions of variant histone His2AvD required for Drosophila development. *Nature* **399**, 694-697 (1999).

136. J. P. Madigan, H. L. Chotkowski, R. L. Glaser, DNA double-strand break-induced phosphorylation of Drosophila histone variant H2Av helps prevent radiation-induced apoptosis. *Nucleic Acids Res* **30**, 3698-3705 (2002).

137. J. Swaminathan, E. M. Baxter, V. G. Corces, The role of histone H2Av variant replacement and histone H4 acetylation in the establishment of Drosophila heterochromatin. *Genes Dev* **19**, 65-76 (2005).

138. G. Mizuguchi *et al.*, ATP-driven exchange of histone H2AZ variant catalyzed by SWR1 chromatin remodeling complex. *Science* **303**, 343-348 (2004).
139. X. Wang, S. Ahmad, Z. Zhang, J. Cote, G. Cai, Architecture of the Saccharomyces cerevisiae NuA4/TIP60 complex. *Nat Commun* **9**, 1147 (2018).
140. W. H. Wu *et al.*, Swc2 is a widely conserved H2AZ-binding module essential for ATP-dependent histone exchange. *Nat Struct Mol Biol* **12**, 1064-1071 (2005).
141. A. Ranjan *et al.*, Nucleosome-free region dominates histone acetylation in targeting SWR1 to promoters for H2A.Z replacement. *Cell* **154**, 1232-1245 (2013).
142. A. J. Morrison, X. Shen, Chromatin remodelling beyond transcription: the INO80 and SWR1 complexes. *Nat Rev Mol Cell Biol* **10**, 373-384 (2009).
143. E. Luk *et al.*, Stepwise histone replacement by SWR1 requires dual activation with histone H2A.Z and canonical nucleosome. *Cell* **143**, 725-736 (2010).
144. X. Liang *et al.*, Structural basis of H2A.Z recognition by SRCAP chromatin-remodeling subunit YL1. *Nat Struct Mol Biol* **23**, 317-323 (2016).
145. R. S. Greenberg, H. K. Long, T. Swigut, J. Wysocka, Single Amino Acid Change Underlies Distinct Roles of H2A.Z Subtypes in Human Syndrome. *Cell* **178**, 1421-1436 e1424 (2019).
146. S. K. Pradhan *et al.*, EP400 Deposits H3.3 into Promoters and Enhancers during Gene Activation. *Mol Cell* **61**, 27-38 (2016).
147. M. L. Ruhf *et al.*, The domino gene of Drosophila encodes novel members of the SWI2/SNF2 family of DNA-dependent ATPases, which contribute to the silencing of homeotic genes. *Development*, 1429-1441 (2001).
148. A. Braun, B. Lemaitre, R. Lanot, D. Zachary, M. Meister, Drosophila immunity: analysis of larval hemocytes by P-element-mediated enhancer trap. *Genetics* **147**, 623-634 (1997).
149. S. Allard *et al.*, NuA4, an essential transcription adaptor/histone H4 acetyltransferase complex containing Esa1p and the ATM-related cofactor Tra1p. *EMBO J* **18**, 5108-5119 (1999).
150. Y. Doyon, W. Selleck, W. S. Lane, S. Tan, J. Cote, Structural and functional conservation of the NuA4 histone acetyltransferase complex from yeast to humans. *Mol Cell Biol* **24**, 1884-1896 (2004).
151. P. Xu *et al.*, The NuA4 Core Complex Acetylates Nucleosomal Histone H4 through a Double Recognition Mechanism. *Mol Cell* **63**, 965-975 (2016).
152. D. Chowdhury *et al.*, gamma-H2AX dephosphorylation by protein phosphatase 2A facilitates DNA double-strand break repair. *Mol Cell* **20**, 801-809 (2005).
153. I. B. Nazarov *et al.*, Dephosphorylation of Histone γ-H2AX during Repair of DNA Double-Strand Breaks in Mammalian Cells and its Inhibition by Calyculin A. *Radiation Research* **160**, 309-317 (2003).
154. S. H. Moon *et al.*, Wild-type p53-induced phosphatase 1 dephosphorylates histone variant gamma-H2AX and suppresses DNA double strand break repair. *J Biol Chem* **285**, 12935-12947 (2010).
155. H. Cha *et al.*, Wip1 directly dephosphorylates gamma-H2AX and attenuates the DNA damage response. *Cancer Res* **70**, 4112-4122 (2010).
156. K. Rust, M. D. Tiwari, V. K. Mishra, F. Grawe, A. Wodarz, Myc and the Tip60 chromatin remodeling complex control neuroblast maintenance and polarity in Drosophila. *EMBO J* **37** (2018).

157. J. Lu, M. L. Ruhf, N. Perrimon, P. Leder, A genome-wide RNA interference screen identifies putative chromatin regulators essential for E2F repression. *Proc Natl Acad Sci U S A* **104**, 9381-9386 (2007).

158. M. H. Kwon, H. Callaway, J. Zhong, B. Yedvobnick, A targeted genetic modifier screen links the SWI2/SNF2 protein domino to growth and autophagy genes in Drosophila melanogaster. *G3 (Bethesda)* **3**, 815-825 (2013).

159. D. Qi, H. Jin, T. Lilja, M. Mannervik, Drosophila Reptin and other TIP60 complex components promote generation of silent chromatin. *Genetics* **174**, 241-251 (2006).

160. K. Börner, P. B. Becker, Splice variants of the SWR1-type nucleosome remodeling factor Domino have distinct functions during Drosophila melanogaster oogenesis. *Development* **143**, 3154-3167 (2016).

161. J. R. Guyon, G. J. Narlikar, S. Sif, R. E. Kingston, Stable remodeling of tailless nucleosomes by the human SWI-SNF complex. *Mol Cell Biol* **19**, 2088-2097 (1999).

162. A. Hamiche, J. G. Kang, C. Dennis, H. Xiao, C. Wu, Histone tails modulate nucleosome mobility and regulate ATP-dependent nucleosome sliding by NURF. *Proc Natl Acad Sci U S A* **98**, 14316-14321 (2001).

163. W. Iwasaki *et al.*, Contribution of histone N-terminal tails to the structure and stability of nucleosomes. *FEBS Open Bio* **3**, 363-369 (2013).

164. L. K. Durrin, R. K. Mann, P. S. Kayne, M. Grunstein, Yeast histone H4 N-terminal sequence is required for promoter activation in vivo. *Cell* **65**, 1023-1031 (1991).

165. V. G. Allfrey, R. Faulkner, A. E. Mirsky, Acetylation and Methylation of Histones and Their Possible Role in the Regulation of Rna Synthesis. *Proc Natl Acad Sci U S A* **51**, 786-794 (1964).

166. G. Felsenfeld, A brief history of epigenetics. *Cold Spring Harb Perspect Biol* **6** (2014).

167. T. R. Hebbes, A. W. Thorne, C. Crane-Robinson, A direct link between core histone acetylation and transcriptionally active chromatin. *The EMBO Journal* **7**, 1395-1402 (1988).

168. J. E. Brownell *et al.*, Tetrahymena Histone Acetyltransferase A: A Homolog to Yeast Gcn5p Linking Histone Acetylation to Gene Activation. *Cell* **84**, 843-851 (1996).

169. A. J. Bannister, T. Kouzarides, The CBP co-activator is a histone acetyltransferase. *Nature* **384**, 641-643 (1996).

170. M.-H. Kuo *et al.*, Transcription-linked acetylation by Gcn5p of histones H3 and H4 at specific lysines. *Nature* **383**, 269-272 (1996).

171. Y. Zhao, B. A. Garcia, Comprehensive Catalog of Currently Documented Histone Modifications. *Cold Spring Harb Perspect Biol* **7**, a025064 (2015).

172. M. Rodriguez-Paredes, M. Esteller, Cancer epigenetics reaches mainstream oncology. *Nat Med* **17**, 330-339 (2011).

173. C. D. Allis, T. Jenuwein, The molecular hallmarks of epigenetic control. *Nat Rev Genet* **17**, 487-500 (2016).

174. B. D. Strahl, C. D. Allis, The language of covalent histone modifications. *Nature* **403**, 41-45 (2000).

175. T. Zhang, S. Cooper, N. Brockdorff, The interplay of histone modifications - writers that read. *EMBO Rep* **16**, 1467-1481 (2015).

176. M. Lawrence, S. Daujat, R. Schneider, Lateral Thinking: How Histone Modifications Regulate Gene Expression. *Trends Genet* **32**, 42-56 (2016).

177. H. van Attikum, S. M. Gasser, The histone code at DNA breaks: a guide to repair? *Nat Rev Mol Cell Biol* **6**, 757-765 (2005).

178. R. C. Allshire, H. D. Madhani, Ten principles of heterochromatin formation and function. *Nat Rev Mol Cell Biol* **19**, 229-244 (2018).

179. M. Zofall, S. I. Grewal, RNAi-mediated heterochromatin assembly in fission yeast. *Cold Spring Harb Symp Quant Biol* **71**, 487-496 (2006).

180. Y. Xu *et al.*, WERAM: a database of writers, erasers and readers of histone acetylation and methylation in eukaryotes. *Nucleic Acids Res* **45**, D264-D270 (2017).

181. W. A. Krajewski, P. B. Becker, Reconstitution of hyperacetylated, DNase I-sensitive chromatin characterized by high conformational flexibility of nucleosomal DNA. *Proc Natl Acad Sci U S A* **95**, 1540-1545 (1998).

182. T. R. Hebbes, A. L. Clayton, A. W. Thorne, C. Crane-Robinson, Core histone hyperacetylation co-maps with generalized DNase I sensitivity in the chicken beta-globin chromosomal domain. *EMBO J* **13**, 1823-1830 (1994).

183. R. Marmorstein, M. M. Zhou, Writers and readers of histone acetylation: structure, mechanism, and inhibition. *Cold Spring Harb Perspect Biol* **6**, a018762 (2014).

184. E. Seto, M. Yoshida, Erasers of histone acetylation: the histone deacetylase enzymes. *Cold Spring Harb Perspect Biol* **6**, a018713 (2014).

185. M. Vogelauer, J. Wu, N. Suka, M. Grunstein, Global histone acetylation and deacetylation in yeast. *Nature* **408**, 495-498 (2000).

186. T. Georgakopoulos, G. Thireos, Two distinct yeast transcriptional activators require the function of the GCN5 protein to promote normal levels of transcription. *The EMBO Journal* **11**, 4145-4152 (1992).

187. M. Vidal, R. F. Gaber, RPD3 encodes a second factor required to achieve maximum positive and negative transcriptional states in Saccharomyces cerevisiae. *Mol Cell Biol* **11**, 6317-6327 (1991).

188. M. Vidal, R. Strich, R. E. Esposito, R. F. Gaber, RPD1 (SIN3/UME4) is required for maximal activation and repression of diverse yeast genes. *Mol Cell Biol* **11**, 6306-6316 (1991).

189. A. Eberharter, P. B. Becker, Histone acetylation: a switch between repressive and permissive chromatin. Second in review series on chromatin dynamics. *EMBO Rep* **3**, 224-229 (2002).

190. M. I. Kuroda, A. Hilfiker, J. C. Lucchesi, Dosage Compensation in Drosophila-a Model for the Coordinate Regulation of Transcription. *Genetics* **204**, 435-450 (2016).

191. T. H. Morgan, Sex Limited Inheritance in Drosophila. *Science* **32**, 120-122 (1910).

192. C. Nusslein-Volhard, E. Wieschaus, Mutations affecting segment number and polarity in Drosophila. *Nature* **287**, 795-801 (1980).

193. T. A. Markow, The secret lives of Drosophila flies. *Elife* **4** (2015).

194. J. A. Kassis, J. A. Kennison, J. W. Tamkun, Polycomb and Trithorax Group Genes in Drosophila. *Genetics* **206**, 1699-1725 (2017).

195. M. A. Fernandez-Moreno, C. L. Farr, L. S. Kaguni, R. Garesse, Drosophila melanogaster as a model system to study mitochondrial biology. *Methods Mol Biol* **372**, 33-49 (2007).

196. P. L. Ferree, V. E. Deneke, S. Di Talia, Measuring time during early embryonic development. *Semin Cell Dev Biol* **55**, 80-88 (2016).

197. V. Hartenstein, A. Lee, A. W. Toga, A graphic digital database of drosophila embryogenesis. *Trends in Genetics* **11**, 51-58 (1995).

198. J. A. Farrell, P. H. O'Farrell, From egg to gastrula: how the cell cycle is remodeled during the Drosophila mid-blastula transition. *Annu Rev Genet* **48**, 269-294 (2014).

199. D. K. Pritchard, G. Schubiger, Activation of transcription in Drosophila embryos is a gradual process mediated by the nucleocytoplasmic ratio. *Genes Dev* **10**, 1131-1142 (1996).
200. S. E. Lott *et al.*, Noncanonical compensation of zygotic X transcription in early Drosophila melanogaster development revealed through single-embryo RNA-seq. *PLoS Biol* **9**, e1000590 (2011).
201. M. T, S. Hari Dass, V. K. Sharma, Egg-laying rhythm in Drosophila melanogaster. *J Genet* **87**, 495-504 (2008).
202. M. A. Martinez-Balbas, T. Tsukiyama, D. Gdula, C. Wu, Drosophila NURF-55, a WD repeat protein involved in histone metabolism. *Proc Natl Acad Sci U S A* **95**, 132-137 (1998).
203. L. Mohrmann *et al.*, Differential targeting of two distinct SWI/SNF-related Drosophila chromatin-remodeling complexes. *Mol Cell Biol* **24**, 3077-3088 (2004).
204. O. Papoulas *et al.*, The Drosophila trithorax group proteins BRM, ASH1 and ASH2 are subunits of distinct protein complexes. *Development* **125**, 3955-3966 (1998).
205. P. B. Becker, T. Tsukiyama, C. Wu, "Chapter 12 Chromatin Assembly Extracts from Drosophila Embryos". (1994), 10.1016/s0091-679x(08)60915-2, pp. 207-223.
206. P. B. Becker, C. Wu, Cell-free system for assembly of transcriptionally repressed chromatin from Drosophila embryos. *Mol Cell Biol* **12**, 2241-2249 (1992).
207. S. Baldi *et al.*, Genome-wide Rules of Nucleosome Phasing in Drosophila. *Mol Cell* **72**, 661-672 e664 (2018).
208. P. B. Becker, S. K. Rabindran, C. Wu, Heat shock-regulated transcription in vitro from a reconstituted chromatin template. *Proc Natl Acad Sci U S A* **88**, 4109-4113 (1991).
209. R. T. Kamakaka, J. T. Kadonaga, "Chapter 13 The Soluble Nuclear Fraction, a Highly Efficient Transcription Extract from Drosophila Embryos". (1994), 10.1016/s0091-679x(08)60916-4, pp. 225-235.
210. G. Crevel, S. Cotterill, DNA replication in cell-free extracts from Drosophila melanogaster. *The EMBO Journal* **10**, 4361-4369 (1991).
211. L. Harpprecht *et al.*, A Drosophila cell-free system that senses DNA breaks and triggers phosphorylation signalling. *Nucleic Acids Res* **47**, 7444-7459 (2019).
212. K. Prayitno, T. Schauer, C. Regnard, P. B. Becker, Progressive dosage compensation during Drosophila embryogenesis is reflected by gene arrangement. *EMBO Rep* **20**, e48138 (2019).
213. A. Luhur, K. M. Klueg, A. C. Zelhof, Generating and working with Drosophila cell cultures: Current challenges and opportunities. *Wiley Interdiscip Rev Dev Biol* **8**, e339 (2019).
214. L. R. Kao, T. L. Megraw, RNAi in cultured Drosophila cells. *Methods Mol Biol* **247**, 443-457 (2004).
215. W. Jiang, S. K. Nordeen, J. T. Kadonaga, Transcriptional analysis of chromatin assembled with purified ACF and dNAP1 reveals that acetyl-CoA is required for preinitiation complex assembly. *J Biol Chem* **275**, 39819-39822 (2000).
216. T. Kusch, A. Mei, C. Nguyen, Histone H3 lysine 4 trimethylation regulates cotranscriptional H2A variant exchange by Tip60 complexes to maximize gene expression. *Proc Natl Acad Sci U S A* **111**, 4850-4855 (2014).
217. A. Scacchetti *et al.*, CHRAC/ACF contribute to the repressive ground state of chromatin. *Life Sci Alliance* **1**, e201800024 (2018).

218. D. Jain, S. Baldi, A. Zabel, T. Straub, P. B. Becker, Active promoters give rise to false positive 'Phantom Peaks' in ChIP-seq experiments. *Nucleic acids research* **43**, 6959-6968 (2015).

219. M. Prestel, C. Feller, T. Straub, H. Mitlohner, P. B. Becker, The activation potential of MOF is constrained for dosage compensation. *Molecular cell* **38**, 815-826 (2010).

220. L. Brueckner, J. van Arensbergen, W. Akhtar, L. Pagie, B. van Steensel, High-throughput assessment of context-dependent effects of chromatin proteins. *Epigenetics Chromatin* **9**, 43 (2016).

221. G. J. Filion *et al.*, Systematic protein location mapping reveals five principal chromatin types in Drosophila cells. *Cell* **143**, 212-224 (2010).

222. S. E. Celniker *et al.*, Unlocking the secrets of the genome. *Nature* **459**, 927-930 (2009).

223. D. Jain, S. Baldi, A. Zabel, T. Straub, P. B. Becker, Genome-wide analysis of phased nucleosomal arrays revals the functional characteristic of the nucleosome remodeler ACF. *biorXiv doi: 10.1101/093666* 10.1101/093666 (2016).

224. J. Wan, J. Lin, D. J. Zack, J. Qian, Relating periodicity of nucleosome organization and gene regulation. *Bioinformatics* **25**, 1782-1788 (2009).

225. U. Braunschweig, G. J. Hogan, L. Pagie, B. van Steensel, Histone H1 binding is inhibited by histone variant H3.3. *The EMBO journal* **28**, 3635-3645 (2009).

226. S. Baldi, S. Krebs, H. Blum, P. B. Becker, Genome-wide measurement of local nucleosome array regularity and spacing by nanopore sequencing. *Nat Struct Mol Biol* **25**, 894-901 (2018).

227. G. LeRoy, G. Orphanides, W. Lane, D. Reinberg, Requirement of RSF and FACT for transcription of chromatin templates in vitro. *Science* **282**, 1900-1904 (1998).

228. K. Hanai, H. Furuhashi, T. Yamamoto, K. Akasaka, S. Hirose, RSF governs silent chromatin formation via histone H2Av replacement. *PLoS genetics* **4**, e1000011 (2008).

229. S. M. G. Braun *et al.*, Rapid and reversible epigenome editing by endogenous chromatin regulators. *Nat Commun* **8**, 560 (2017).

230. J. N. McKnight, K. R. Jenkins, I. M. Nodelman, T. Escobar, G. D. Bowman, Extranucleosomal DNA binding directs nucleosome sliding by Chd1. *Molecular and cellular biology* **31**, 4746-4759 (2011).

231. F. Erdel, T. Schubert, C. Marth, G. Langst, K. Rippe, Human ISWI chromatin-remodeling complexes sample nucleosomes via transient binding reactions and become immobilized at active sites. *Proc Natl Acad Sci U S A* **107**, 19873-19878 (2010).

232. Hamiche A., Sandaltzopoulo R., D. A. Gdula, C. Wu, ATP-Dependent Histone Octamer Sliding Mediated by the Chromatin Remodeling Complex NURF. *Cell* **97**, 833-842 (1999).

233. P. Badenhorst, M. Voas, I. Rebay, C. Wu, Biological functions of the ISWI chromatin remodeling complex NURF. *Genes & Dev* **16**, 3186-3198 (2002).

234. S. Y. Kwon, V. Grisan, B. Jang, J. Herbert, P. Badenhorst, Genome-Wide Mapping Targets of the Metazoan Chromatin Remodeling Factor NURF Reveals Nucleosome Remodeling at Enhancers, Core Promoters and Gene Insulators. *PLoS genetics* **12**, e1005969 (2016).

235. N. Collins *et al.*, An ACF1-ISWI chromatin-remodeling complex is required for DNA replication through heterochromatin. *Nature genetics* **32**, 627-632 (2002).

236. A. Scacchetti *et al.*, Drosophila SWR1 and NuA4 complexes are defined by DOMINO isoforms. *biorXiv* 10.1101/2020.02.10.939793 (2020).
237. K. Johanson *et al.*, Binding interactions of human interleukin 5 with its receptor alpha subunit. Large scale production, structural, and functional studies of Drosophila-expressed recombinant proteins. *J Biol Chem* **270**, 9459-9471 (1995).
238. K. Borner, P. B. Becker, Splice variants of the SWR1-type nucleosome remodeling factor Domino have distinct functions during Drosophila melanogaster oogenesis. *Development* **143**, 3154-3167 (2016).
239. N. E. Searle, A. L. Torres-Machorro, L. Pillus, Chromatin Regulation by the NuA4 Acetyltransferase Complex Is Mediated by Essential Interactions Between Enhancer of Polycomb (Epl1) and Esa1. *Genetics* **205**, 1125-1137 (2017).
240. M. Morillo-Huesca, M. Clemente-Ruiz, E. Andujar, F. Prado, The SWR1 histone replacement complex causes genetic instability and genome-wide transcription misregulation in the absence of H2A.Z. *PLoS One* **5**, e12143 (2010).
241. C. Albig *et al.*, JASPer controls interphase histone H3S10 phosphorylation by chromosomal kinase JIL-1 in Drosophila. *Nat Commun* **10**, 5343 (2019).
242. J. Hong *et al.*, The catalytic subunit of the SWR1 remodeler is a histone chaperone for the H2A.Z-H2B dimer. *Mol Cell* **53**, 498-505 (2014).
243. T. Klymenko *et al.*, A Polycomb group protein complex with sequence-specific DNA-binding and selective methyl-lysine-binding activities. *Genes Dev* **20**, 1110-1122 (2006).
244. R. Matsuda *et al.*, Identification and characterization of the two isoforms of the vertebrate H2A.Z histone variant. *Nucleic Acids Res* **38**, 4263-4273 (2010).
245. J. H. Park, X. J. Sun, R. G. Roeder, The SANT domain of p400 ATPase represses acetyltransferase activity and coactivator function of TIP60 in basal p21 gene expression. *Mol Cell Biol* **30**, 2750-2761 (2010).
246. C. Feller, I. Forne, A. Imhof, P. B. Becker, Global and specific responses of the histone acetylome to systematic perturbation. *Mol Cell* **57**, 559-571 (2015).
247. S. Peleg *et al.*, Life span extension by targeting a link between metabolism and histone acetylation in Drosophila. *EMBO Rep* **17**, 455-469 (2016).
248. A. Auger *et al.*, Eaf1 is the platform for NuA4 molecular assembly that evolutionarily links chromatin acetylation to ATP-dependent exchange of histone H2A variants. *Mol Cell Biol* **28**, 2257-2270 (2008).
249. X. Wang *et al.*, Merge and separation of NuA4 and SWR1 complexes control cell fate plasticity in Candida albicans. *Cell Discov* **4**, 45 (2018).
250. D. Y. Rhee *et al.*, Transcription factor networks in Drosophila melanogaster. *Cell Rep* **8**, 2031-2043 (2014).
251. T. Nakajima, S. Fujino, G. Nakanishi, Y. S. Kim, A. M. Jetten, TIP27: a novel repressor of the nuclear orphan receptor TAK1/TR4. *Nucleic Acids Res* **32**, 4194-4204 (2004).
252. J. I. Koontz *et al.*, Frequent fusion of the JAZF1 and JJAZ1 genes in endometrial stromal tumors. *Proc Natl Acad Sci U S A* **98**, 6348-6353 (2001).
253. I. Macinkovic *et al.*, Distinct CoREST complexes act in a cell-type-specific manner. *Nucleic Acids Res* **47**, 11649-11666 (2019).
254. W. Xu *et al.*, Evolution of Yin and Yang isoforms of a chromatin remodeling subunit precedes the creation of two genes. *Elife* **8** (2019).

255. R. K. Ejsmont, M. Sarov, S. Winkler, K. A. Lipinski, P. Tomancak, A toolkit for high-throughput, cross-species gene engineering in Drosophila. *Nat Methods* **6**, 435-437 (2009).

256. R. Bottcher *et al.*, Efficient chromosomal gene modification with CRISPR/cas9 and PCR-based homologous recombination donors in cultured Drosophila cells. *Nucleic acids research* **42**, e89 (2014).

257. X. Zhang, I. R. Ferreira, F. Schnorrer, A simple TALEN-based protocol for efficient genome-editing in Drosophila. *Methods* **69**, 32-37 (2014).

258. X. Zhang, W. H. Koolhaas, F. Schnorrer, A versatile two-step CRISPR- and RMCE-based strategy for efficient genome engineering in Drosophila. *G3* **4**, 2409-2418 (2014).

259. A. Rottach, E. Kremmer, D. Nowak, H. Leonhardt, M. C. Cardoso, Generation and characterization of a rat monoclonal antibody specific for multiple red fluorescent proteins. *Hybridoma* **27**, 337-343 (2008).

260. A. Dobin *et al.*, STAR: ultrafast universal RNA-seq aligner. *Bioinformatics* **29**, 15-21 (2013).

261. M. I. Love, W. Huber, S. Anders, Moderated estimation of fold change and dispersion for RNA-seq data with DESeq2. *Genome biology* **15**, 550 (2014).

262. R. Lyne *et al.*, FlyMine: an integrated database for Drosophila and Anopheles genomics. *Genome biology* **8**, R129 (2007).

263. J. Schindelin *et al.*, Fiji: an open-source platform for biological-image analysis. *Nat Methods* **9**, 676-682 (2012).

264. R. Villa, T. Schauer, P. Smialowski, T. Straub, P. B. Becker, PionX sites mark the X chromosome for dosage compensation. *Nature* **537**, 244-248 (2016).

265. J. G. Doench *et al.*, Optimized sgRNA design to maximize activity and minimize off-target effects of CRISPR-Cas9. *Nat Biotechnol* **34**, 184-191 (2016).

266. S. J. Gratz *et al.*, Highly specific and efficient CRISPR/Cas9-catalyzed homology-directed repair in Drosophila. *Genetics* **196**, 961-971 (2014).

267. J. Cox, M. Mann, MaxQuant enables high peptide identification rates, individualized p.p.b.-range mass accuracies and proteome-wide protein quantification. *Nat Biotechnol* **26**, 1367-1372 (2008).

268. J. Cox *et al.*, Andromeda: a peptide search engine integrated into the MaxQuant environment. *J Proteome Res* **10**, 1794-1805 (2011).

269. J. Cox *et al.*, Accurate proteome-wide label-free quantification by delayed normalization and maximal peptide ratio extraction, termed MaxLFQ. *Mol Cell Proteomics* **13**, 2513-2526 (2014).

270. K. Kammers, R. N. Cole, C. Tiengwe, I. Ruczinski, Detecting Significant Changes in Protein Abundance. *EuPA Open Proteom* **7**, 11-19 (2015).

271. M. E. Ritchie *et al.*, limma powers differential expression analyses for RNA-sequencing and microarray studies. *Nucleic Acids Res* **43**, e47 (2015).

272. L. A. Perkins *et al.*, The Transgenic RNAi Project at Harvard Medical School: Resources and Validation. *Genetics* **201**, 843-852 (2015).

273. T. Horn, M. Boutros, E-RNAi: a web application for the multi-species design of RNAi reagents--2010 update. *Nucleic Acids Res* **38**, W332-339 (2010).

274. B. Langmead, S. L. Salzberg, Fast gapped-read alignment with Bowtie 2. *Nat Methods* **9**, 357-359 (2012).

275. S. Heinz *et al.*, Simple combinations of lineage-determining transcription factors prime cis-regulatory elements required for macrophage and B cell identities. *Mol Cell* **38**, 576-589 (2010).
276. J. T. Robinson *et al.*, Integrative genomics viewer. *Nat Biotechnol* **29**, 24-26 (2011).